Palaeomagnetic and Structural Investigations in Unbeknown Areas of Central Tibet: A Study on Block Rotations and Crustal Shortening

Dissertation

zur Erlangung des Grades eines Doktors

der Naturwissenschaften

der Geowissenschaftlichen Fakultät

der Eberhard-Karls-Universität Tübingen

vorgelegt von

Martin Staiger

aus Stuttgart

2004

Tag der mündlichen Prüfung: 24. Februar 2004

Dekan: Prof. Dr. Dr. h.c. M. Satir

1. Berichterstatter: Prof. Dr. E. Appel

2. Berichterstatter: Prof. Dr. L. Ratschbacher

Contents

How many years can a mountain exist
Before it's washed to the sea?
Yes, 'n' how many years can some people exist
Before they're allowed to be free?
Yes, 'n' how many times can a man turn his head,
Pretending he just doesn't see?
The answer, my friend, is blowin' in the wind,
The answer is blowin' in the wind.

Bob Dylan (1962)

Abstract

Palaeomagnetic and structural investigations were carried out in Central Tibet along a ~600 km NS-extending stretch between N30°30'-35°30' and E88°30'-90°30'. During two expeditions in the framework of INDEPTH 3/GeoDepth sampling of mainly Tertiary red beds was accomplished at 73 palaeomagnetic drilling sites.

The Dogai Coring Tso fold-and-thrust belt (DGC) in the northern Qiangtang block (~N34°45', E89°00') is build up by a deformed succession of probably Tertiary red beds. The results of field mapping, cross-section and fault-slip analyses, and high-resolution remote sensing lead to a model that explains the DGC as an (a) sinistral transpressional belt formed in response to NE-SW compression in which (b) fault-bound blocks rotated counterclockwise in domino-style, delimited (c) by sinistral oblique thrusts trending subparallel to the Kun Lun belt. Estimations of N-S shortening enforced by folding range from 25 to 58 % while counterclockwise rotation of 35° can account for about 20 %. Palaeomagnetic investigations on 11 sites identified a stable ChRM with well-grouped site means carried by hematite. The fold test is significantly positive and calculation of stepwise unfolding reveals best grouping of directions at 82 % of unfolding. Remagnetisation is assumed during an early stage of the tectonic development. The overall mean direction of 332.6°/40.9° is consistent with the structural findings and verifies a minimum of 28° counterclockwise rotation of blocks. The deformation in the DGC gives evidence that NE-SW compression and northeastward growth of the plateau occurs already in the Tertiary.

The Zagaya section in the northernmost Lhasa block (~N32°15', E89°30') is situated within the Bangong-Nujiang suture zone and comprises folded Tertiary red beds and ophiolitic material. Steeply west-dipping normal faults building the western boundary of two characteristic blocks and a left-lateral EW-trending strike-slip fault to the north are main structural features. About 60 % shortening is represented by the large governing fold. Fault-slip data show ENE-WSW- and NNE-SSW-trending compression and EW-trending extension. Palaeomagnetic investigations on 15 sites of mostly Eocene red beds identified a stable ChRM with well-grouped site means carried by hematite. Remanence acquisition prior to folding (positive fold test) and best grouping of directions at 93 % of unfolding is revealed. Measured declinations deviate in a linear trend from the expected values: Counterclockwise rotation increases when proceeding to the northern fault zone (8.1 °/km, maximum relative rotation of 55°). In the most likely explanation model folding predates a two-phase block rotation where (a) internal small-scaled left-lateral brittle shear is followed by (b) normal faulting with the break-up of blocks. Pre-existing structures within the Bangong-Nujiang suture zone are reactivated in left-lateral style and allow eastward lateral extrusion due to frontal compression enforced by the India-Asia collision.

Kurzfassung

Paläomagnetische und strukturgeologische Untersuchungen wurden in Zentraltibet entlang einer N-S-Strecke von ~600 km zwischen N30°30'-35°30' und E88°30'-90°30' durchgeführt. Während zweier Expeditionen im Rahmen von INDEPTH 3/GeoDepth konnten dabei 73 Lokalitäten in hauptsächlich tertiären Rotsedimenten paläomagnetisch beprobt werden.

Der Dogai Coring Tso Falten- und Überschiebungsgürtel (DGC) im nördlichen Qiangtang-Block (~N34°45', E89°00') besteht aus einer deformierten Folge von wahrscheinlich tertiären Rotsedimenten. Die Ergebnisse von Geländeaufnahme, Profil- und Störungsdatenanalyse und hochaufgelöster Fernerkundung führen zu einem Modell, das den DGC als einen (a) sinsitral-transpressiven Gürtel erklärt, der sich als Reaktion auf NE-SW-gerichtete Einengung bildete und wo (b) von Störungen begrenzte Blöcke zwischen (c) subparallel zum Kun-Lun-System verlaufenden sinistralen Schrägaufschiebungen gegen den Uhrzeigersinns rotiert sind. Die durch Faltung verursachte N-S-Verkürzung wird auf 25 bis 58 % geschätzt, während die Rotation gegen den Uhrzeigersinn ungefähr 20 % bewirkt. Durch paläomagnetische Untersuchungen an Proben von 11 Lokalitäten wurde eine von Hämatit getragene stabile ChRM mit gut gruppierenden Mittelwerten der Einzellokalitäten identifiziert. Der Faltentest ist signifiant positiv und die Berechnung der schrittweisen Entfaltung ergibt die beste Gruppierung bei 82 % Entfaltung. In einem frühen Stadium der tektonischen Entwicklung wird Remagnetisierung vermutet. Die mittlere Gesamtrichtung aller Lokalitäten von 332,6°/40,9° ist in Übereinstimmung mit den strukturellen Erkenntnissen und bestätigt eine Blockrotation von mindestens 28° gegen den Uhrzeigersinn. Die Deformation im DGC liefert Belege dafür, dass NE-SW-gerichtete Einengung und nordostwärts fortschreitendes Anwachsen des Tibetplateaus bereits im Tertiär auftritt.

Das Zagaya-Profil im nördlichsten Lhasa-Block (~N32°15', E89°30') liegt innerhalb der Bangong-Nujiang Suturzone und enthält gefaltete tertiäre Rotsedimente und ophiolitisches Material. Steil nach Westen einfallende Abschiebungen, die zwei charakteristische Blöcke westlich begrenzen, und EW-streichende Linksseitenverschiebungen im Norden sind strukturell prägend. Ungefähr 60 % Verkürzung wird durch die vorherrschende Großfaltung bewirkt. Störungsflächendaten zeigen ENE-WSW- und NNE-SSW-gerichtete Einengung und EW-orientierte Dehnung. Durch paläomagnetische Untersuchungen an Proben von 15 Lokalitäten - hauptsächlich in eozänen Rotsedimenten - wurde eine von Hämatit getragene stabile ChRM mit gut gruppierenden Mittelwerten der Einzellokalitäten identifiziert. Der Remanenzerwerb erfolgte vor der Faltung (positiver Faltentest) und die Richtungen gruppieren am besten bei 93 % Entfaltung. Die gemessenen Deklinationen weichen mit einem auffälligen linearen Trend von den Erwartungswerten ab: Die Rotationen gegen den Uhrzeigersinn wachsen mit der Annäherung an die nördliche Störungszone (8,1 °/km, größte relative Rotation 55°). Im wahrscheinlichsten Erklärungsmodell folgt der Faltung eine zweiphasige Blockrotation mit (a) interner kleinskaliger linksseitiger spröder Scherung mit anschließender (b) Abschiebungstektonik und Aufbrechen von Blöcken. Präexistente Strukturen innerhalb der Bangong-Nujiang Suturzone werden in linksseitigem Bewegungssinn reaktiviert und ermöglichen laterales Ausweichen infolge frontaler, von der Kollision zwischen Indien und Asien erzwungener Einengung.

Prologue

Tibet – what a privilege to investigate a region which is one of the most grandiose and mysterious on earth. It is the place where geologists can study the response to the youngest continent-continent collision, a key area for the understanding of mountain building processes. A land inspiring visitors with breathtaking vastness and almighty peaks, near to the gods.

That is what people may think. On the one hand, they are completely right – pushing forward into "terra incognita" is scientific excitement at its best. On the other hand, a good portion of excitement is needed – and consumed – to overcome obstacles which one would never be faced with in less remote areas.

Tibet represents the most extensive high plateau region in the world, with an area of about 2.5 million square kilometres and an average height of over 4500 meters lying between the Kunlun Mountains in the north and the Great Himalayan range in the south. The latter, of course, dominated by Mt. Everest (Chomolungma, Sagarmatha) and its neighbouring peaks exceeding 8000 meters while highest peaks on the tableland are below 7000 meters. Characteristically one finds salt lakes scattered about the plateau, the largest being Nam Tso. Some of Asia's greatest rivers have their source in Southern Tibet, with the Indus and Yarlong (Brahmaputra) being the most important. The climate, with long cold winters and short summers is unusually rigorous. Shaded against from the monsoon by the Himalayan belt the annual rainfall on the inner plateau is considerably less than on the south side of the Himalayan range. The temperatures vary greatly with altitude and, in addition to the strong influence of permanent winds there are marked differences between day and night and between sun and shade temperature. Most of the land is treeless and a scanty grass is the most widespread type of natural vegetation in these areas.

The known history of Tibet commences in the 7th century AD when Buddhism was introduced. The lamas of Tibetan Buddhism attained political power in the 13th century and the subsequent disunity was brought to an end in 1642, when the fifth Dalai Lama became ruler of all Tibet. In 1720 the Chinese Qing dynasty established control over Tibet. In the 19th century foreigners were systematically excluded and Lhasa became the "forbidden city". After the Qing's overthrow in 1911 independence was declared, but in 1950 Chinese forces invaded Tibet. An uprising in 1959 was suppressed and the Dalai Lama, with thousands of refugees, fled to India. The Dalai Lama (Tensing Gyatso, born 1935) was awarded the Nobel Peace Prize in 1989, in recognition of his appeals for the non-violent liberation of his homeland. China has been widely accused of violating Tibetans' human and religious rights. In 1997 the International Commission of Jurists denounced Chinese rule as an alien occupation and called for an UN-monitored referendum to decide Tibet's future.

Although we were able to reach spots that haven't been visited for tens of years – most likely not visited since Hedin's expeditions in the late 19th century – it turned out that even satellite phones and GPS cannot change significantly the great demands the central Tibetan plateau makes on people living and working there. During field work a significant number of working days were lost to bad weather with extreme precipitation, which caused the flood disaster in central China in 1998. Above-average rainfall or snow and attendant mud made it much more difficult to reach areas of interest or drive off road. Apart from these natural realities the experience brought to light a number of deficiencies in planning as well as some misunderstandings between the western and Chinese team members who arrived in the field with differing perceptions about what the priorities for the field work would be. But overall the positive experience of the Tibetan challenge has been more lasting than any setbacks or frustrations which compromised the effort.

And compared to our arduous but temporary stays it is astonishing how people can live in central Tibet permanently, far from being supported by high-end outdoor gear, which we think we could not live without. The Tibetan people won our great respect for how they live their lives – friendly and peacefully.

1 Introduction

1.1 Geological overview and previous work

1.1.1 Geological overview

The Tibetan-Himalayan orogen shows up with the classic inventory of a continent-continent collision and – compared to the e.g. alpine situation and in a first approximation – it seems to be easy to understand: The Indian plate indented into the Eurasian plate and subsequently the Himalayan range was created by mountain building processes. But despite the lack of a complicating ancient orogenic history as the Variscan event pictures for the Alps the Indian-Asian case is still complex enough. Looking on the northern hinterland of the collisional front, on what is the "Tibetan Plateau" nowadays, we recognize a horizontal stack of crustal blocks – terranes, which were separated from Gondwana and successively accreted to the Asian plate (Fig. 1.1-1). Therefore the buffer that takes up India's drift energy is somehow more inhomogeneous than it is implied by the term "Eurasian Plate". It consists – from north to south – of Kunlun terrane, Qiangtang terrane, and Lhasa terrane. Suture zones, representing former oceanic areas and marked by ophiolitic material alongside the terrane boundaries, divide these former micro-continents. These sutures, mainly named after rivers, are – again from north to south – Jinsha suture, Bangong-Nujiang suture, and Yarlong Zangpo suture.

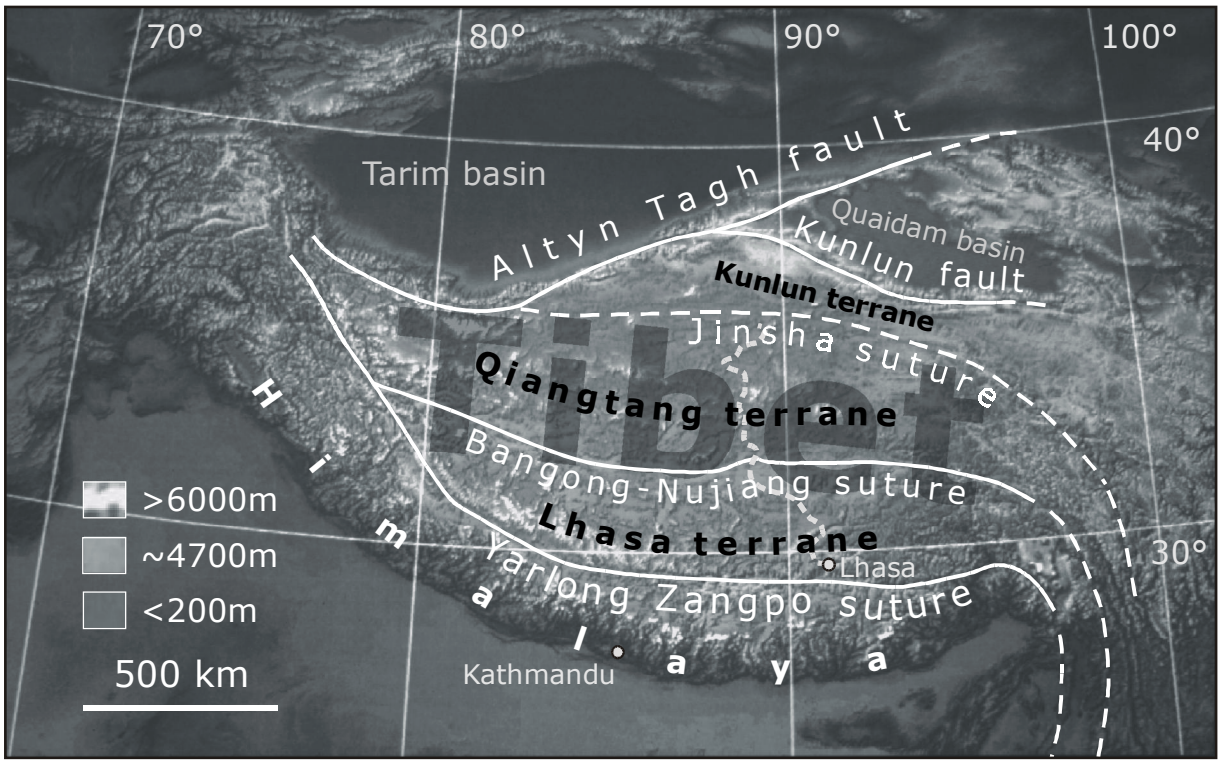

Fig. 1.1-1: *Tibet and the adjacent areas. Terrane pattern and suture traces shown on the base of a digital elevation model (DEM) . Dashed line - expedition route.*

The drift history of the Tibetan terranes is deduced from sedimentological, palaeontological, and palaeomagnetic information. The evolution of the terrane pattern is derived from an interpretation of changes of latitude of the Tibetan terranes and India relative to stable Eurasia (Fig. 1.1-2, modified after Dewey et al., 1988). Being detached from Gondwana in Mid Permian times by the opening of the Tethys Ocean (Sengör, 1984; Scotese and McKerrow, 1990) the Tibetan terranes successively drifted

to the north. While the timing of accretion of the Kunlun terrane is still under debate (Enkin et al., 1992) or even while it is not clear, whether the Kunlun area could be considered as an independent block (Lin and Watts, 1988; Van der Voo, 1993), there is good control of the other terranes. The Lhasa terrane and the Qiangtang terrane clearly belonged to Gondwana during Late Carboniferous to Early Permian as shown by glacial features and palaeontological findings (Metcalfe, 1988; Smith and Xu, 1988). In the Mid Permian the central Tibetan terranes were separated from Gondwana (Sengör, 1984) and drifted to the north, finally forming the southern Eurasian continental margin at the time when the Tethys reached its maximum width in Late Jurassic times (Scotese and McKerrow, 1990; Chen et al, 1993a).

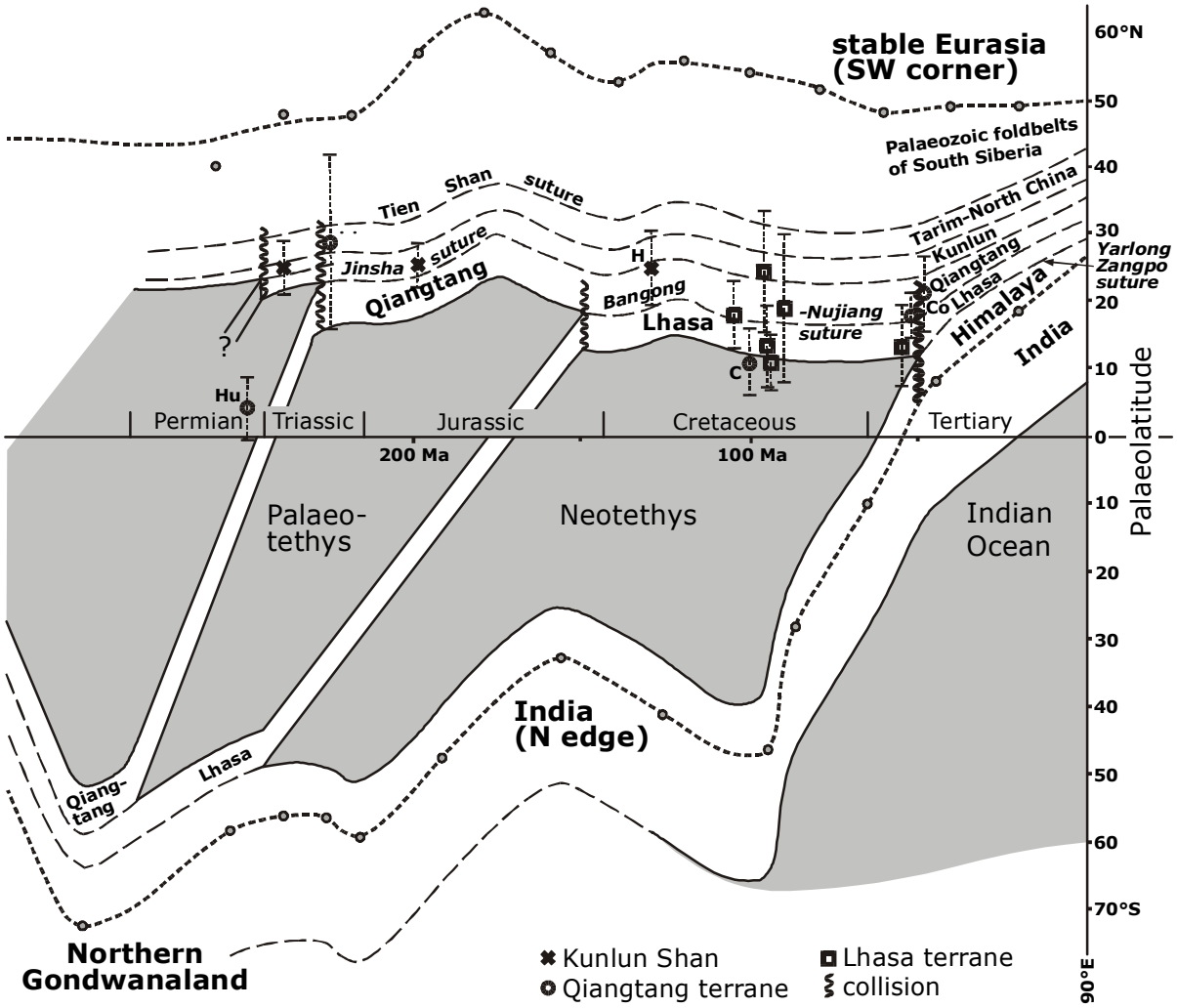

Fig. 1.1-2: *Evolution of Tibetan terrane pattern. Interpretation of changes of latitude of Tibetan terranes and India relative to stable Eurasia for a position now at 90°E (modified after Dewey et al., 1988). Additional data for comparison: C - Chen et al., 1993b (80°E), H - Halim et al., 1998 (100°E), Co - Cogné et al., 1999 (96°E), Hu - Huang et al., 1992 (98°E).*

In detail, the Qiangtang terrane – sometimes referred to as "North Tibet" – merged with eastern Laurasia, i.e. Eurasia, in Triassic-Early Jurassic times (Sengör, 1984; Chang et al., 1986). The Jinsha suture to the south of Kunlun terrane and Sonpan-Garze flysch marks the trace of the subduction zone, which brought the palaeotethys to a termination. The Kunlun-Qiangtang zone bears collision-related igneous rocks of mainly Jurassic age (Harris et al., 1988).

As a consequence of the amalgamation of Eurasia and the Qiangtang block, and the north-directed drift of the Lhasa terrane the subduction zone stepped back to the south of the Qiangtang block. The Lhasa block and Qiangtang block came into juxtaposition and were welded together through thrusting

between Late Jurassic and Early Cretaceous (Chang et al., 1986; Girardeau et al., 1985). The knowledge of igneous rocks of Jurassic to Early Cretaceous age (150-70Ma) within the Bangong-Nujiang zone contributes to the timing of the second major suturing event (Matte et al., 1996; Murphy et al. 1997). We have to take into account that the main igneous activity follows the main collision with a delay, which depends on geometrical and petrologic boundary conditions. The shortening of the northern Lhasa block during and subsequent to the Lhasa-Qiangtang collision amounts to 60% (Murphy et al., 1997). There is evidence from Cretaceous palaeomagnetic data (Chen et al., 1993a; Lin and Watts, 1988; Westphal et al., 1983; Pozzi et al., 1982) that the Tibetan terranes formed a stable margin at about 10°N at that time.

The Eurasian mosaic welded as described above was put to the test by one of the most potent plate tectonic movements ever seen in the Earth's history – the indentation of the Indian plate. The so-called "Greater India", i.e. India in its extended shape before collision, began to drift northwards from moderate southern latitudes after the break-up of Gondwana at about 90 Ma (Scotese and McKerrow, 1990). Drift rates deduced from magnetic sea floor anomalies prove this movement to have been in the range of 15-20 cm/yr – faster than any plate tectonic movement that is observed at present (Powell et al., 1988; Klootwijk et al., 1991).

The main collision was preceded by northward subduction of Tethyan oceanic crust. This is evidenced by Andean I-type magmatism building the Gangdese plutons of Early Cretaceous to Eocene ages at the southern margin of the Lhasa block (Schärer et al., 1984). At 55 to 50 Ma the main India-Tibet collision is signalled by a dramatic slowdown of India's drift-rate to 5 cm/yr (Klootwijk et al., 1991; Besse and Courtillot, 1988). The Yarlong Zangpo suture zone to the north of the Himalayan belt marks the site of the collision and the place where continental Indian crust was subducted in a dimension of some 200 to 300 km (Chemenda et al., 2000; Patriat and Achache, 1984).

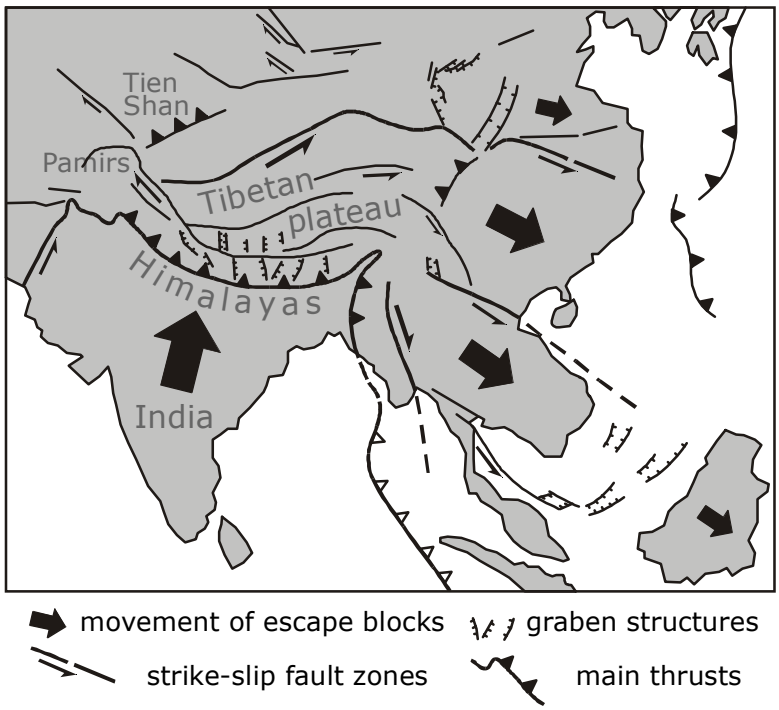

Fig. 1.1-3: *India's indentation forces eastward extrusion of escape blocks in South-East Asia alongside extensional structures (modified after Tapponnier et al., 1982).*

Until present ongoing convergence between India and Eurasia at drift-rates of 5 cm/yr is observed (DeMets et al., 1990). This leads to widespread deformation within the Tibetan plateau and Southeast Asia following the mechanism of lateral extrusion as a response on the shortening of the orogenic mass (Tapponnier et al., 1982; Tapponnier et al., 1986; Peltzer and Tapponnier, 1988) (Fig. 1.1-3).

Very common features developed during lateral extrusion are large strike-slip zone trending parallel to the extrusion direction (e.g. Altyn Tagh fault and Kunlun fault), and normal faults accompanying graben (e.g. Thakkola graben) and half-graben structures

perpendicular to the extrusion direction (Tapponnier et al., 1981; Armijo et al., 1986; Armijo et al., 1989) (Fig. 1.1-4).

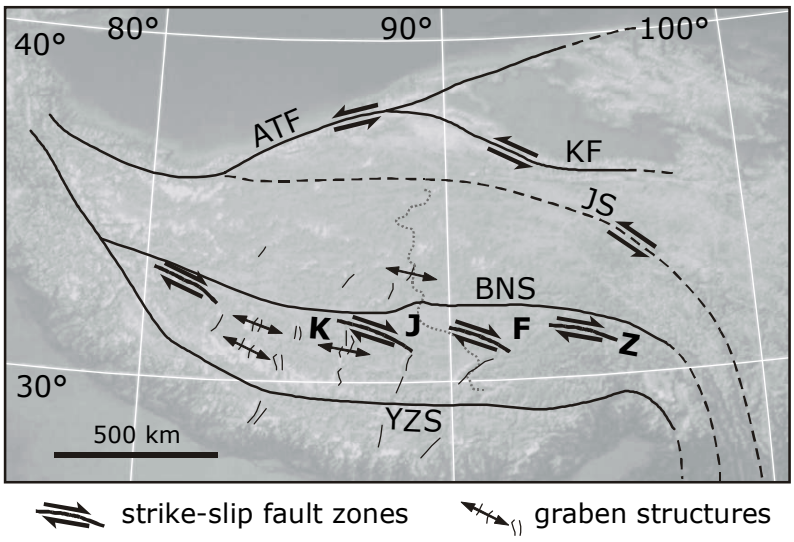

Fig. 1.1-4: *Active tectonic structures in Central Tibet (simplified after Tapponnier et al., 1981; Armijo et al., 1986; Armijo et al., 1989). KJFZ - Karakoram-Jinsha fault zone, ATF - Altyn Tagh fault, KF - Kunlun fault, JS - Jinsha suture, BNS - Bangong-Nujiang suture, YZS - Yarlong Zangpo suture, dashed line - expedition route.*

1.1.2 Previous work in the target area

Since the expeditions of Hedin in the late 19th century, which - taking into account our experience from more than one hundred years after - must have been heroic, the northwestern portions of the Qiangtang have not been entered for scientific purposes. The nearest approach to our target area in central Tibet was accomplished when the first structural and tectonic studies began with a reconnaissance structural study (Coward et al., 1988) in the course of the Royal Society - Academia Sinica 1985 Qinghai-Xizang Geotraverse expedition mainly in the vicinity of the Lhasa-Golmud road (Fig. 1.1-5). As a part of this venture Lin and Watts carried out the first palaeomagnetic investigation on central portions of the inner Tibetan plateau (Lin and Watts, 1988). In recent years some groups, mainly led by French scientists did palaeomagnetic work in eastern and western border areas of the plateau (Chen et al., 1993b; Halim et al., 1998; Cogné et al., 1999; Huang et al., 1992). With two expeditions in the framework of INDEPTH 3/GeoDepth in 1998 and 1999 a remarkable step forward towards unsealing the hidden geological secrets of the inner Tibetan plateau was achieved but there is definitely enough blank space left on the map to be filled-in by future generations of earth scientists.

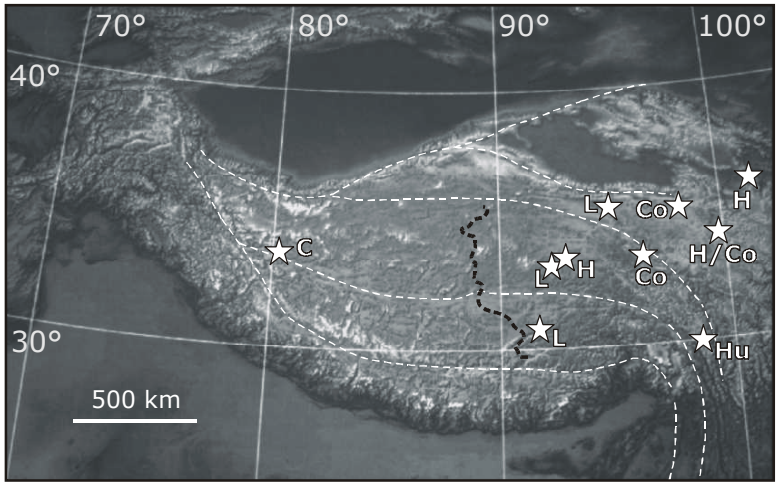

Fig. 1.1-5: *Locator map showing main working areas of previous palaeomagnetic investigations. C - Chen et al. (1993b), Co - Cogné et al. (1999), H - Halim et al. (1998), Hu - Huang et al. (1992), L - Lin and Watts (1988), dashed black line - expedition route of INDEPTH 3/GeoDepth.*

1.1 Project INDEPTH 3/GeoDepth

Project INDEPTH (**In**ternational **De**ep **P**rofiling of **T**ibet and the **H**imalayas) was inaugurated in 1992 by Chinese and U.S. scientists. Seismic data collected during the first phase imaged for the first time the Main Himalayan Thrusts, and the Moho beneath the double-thickness crust of southernmost Tibet (Zhao et al. 1993). Based on the success of INDEPTH 1, Chinese, U.S., German, and Canadian scientists extended the INDEPTH survey northward into southern Tibet during the summers of 1994 and 1995. Among other things, INDEPTH 2 investigations have provided the basis for constructing a restorable geological cross-section, suggested the possibility that the middle crust of the Tibetan plateau is partially molten, and that a cold Indian mantle lid underthrusts the southern margin of the Tibetan plateau (Nelson et al., 1996; Makovsky and Klemperer, 1996).

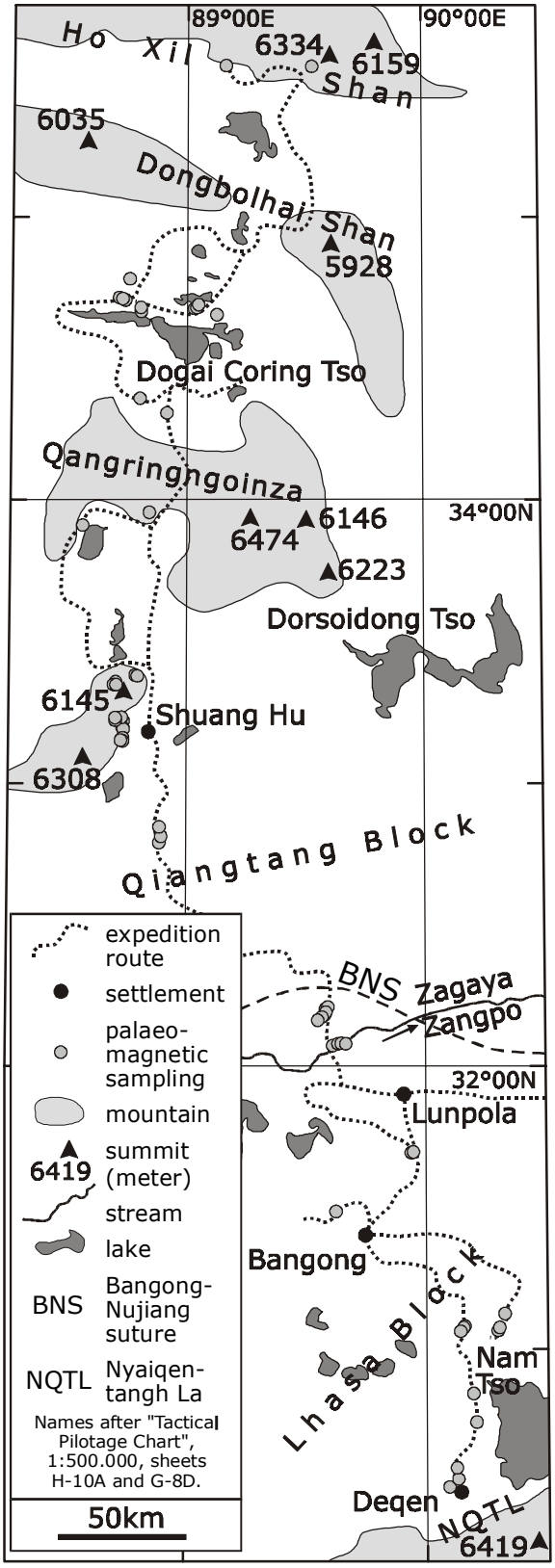

Fig. 1.2-1: *Sketch map indicating the expedition route of INDEPTH 3/GeoDepth.*

In May 1998 the Sino-U.S.-German-Canadian agreement for INDEPTH 3/GeoDepth was finalized in Beijing, China. The INDEPTH 3/GeoDepth program consisted of passive-source seismic program, active-source seismic program, magnetotelluric program, and surface geology program. The latter included mapping and structural analyses (University of Würzburg), palaeomagnetic analysis (University of Tübingen), fission track geochronology (University of Würzburg), geomorphology and neotectonics (University of Potsdam) and U-Pb accessory mineral TIMS (Thermal Ionisation Mass Spectrometry) geochronology (Syracuse University), Ar/Ar geochronology and other petrologic studies (University of California, Santa Barbara).

It was agreed that the INDEPTH program would be focussed on the region of the central Tibetan plateau lying between approximately 30° and 36° N latitude and 87° and 92° E longitude.

The geological team of INDEPTH 3/GeoDepth was active in the field in 1998 from June 27th to August 11th and in 1999 from May 1st to June 30th. Due to complicated travelling logistics, including time consuming preparations and acclimatisation in Lhasa, Tibet, base camp Lunpola was reached on July 4th 1998 and on May 8th 1999 respectively (Fig. 1.2-1).

In a first attempt the expedition pushed forward to the north under the extreme difficult surface conditions of summer 1998 (induced by unexpected heavy rainfall central China suffered from a catastrophic flood event at the same time) and reached the region to the south of Dogai Coring Tso (Lake Dogai Coring). Further progress to the north was prevented by the impassibility of fords but also by the unwillingness of drivers to make it into unknown area. Therefore, in the following the geological investigations had to proceed southward.

In the early summer of 1999 (May) the surface conditions were more sustainable and permitted the field geology team to circle around the far western bank of Dogai Coring Tso and work onwards to the north. The approach ended short of petrol supply after marching some last few kilometres on May 28th 1999 at point N35°32'/E89°09'. On the way back to the south further surveying and sampling was accomplished. During the terminating two weeks of the 1999 expedition, fieldwork was carried out near the Bangong-Nujiang suture and within the northern portion of the Lhasa block.

1.3 Methods applied

1.3.1 Sampling, field measurements

Palaeomagnetic sampling was always lead by the intention to follow precognition what suitable lithologies could be and by the idea to implement a system of reasonable testing in cases with fewer information – both, of course, limited by availability of time and outcrops.

The working areas for 1998 were chosen on the basis of palaeomagnetic and geological information from earlier research (only available to the east of our working area, see 1.1.1) and after ad hoc prognoses on the suitability for palaeomagnetic purposes of met formations in the outcrop. Of course, it has to be stated that this modus operandi is limited by the difficulty to judge with doubtlessness by means of field investigations (using eye, lens, and hammer) which formation and characteristic would yield stable remanences and would bring utilisable results. Furthermore logistic viewpoints and organisational problems respectively played an important role when implementing sampling. For example, during the initial scouting trip the attention was turned to extend the visited stretch to the northernmost accessible position as fast as possible while questionable localities for sampling were just marked to be sampled on the way back, if time allows.

The original planning for 1999 was to continue to sample within those formations, which seemed to be most promising after the 1998 sampling was evaluated. But since the 1999 expedition reached much further north into unknown territory not touched in 1998, there were again new formations to be sampled for which no precise precognition was available.

The spatial distribution of sampling sites is based on the course the expedition took and is therefore both a result of geological considerations and technological-logistical connections. Consequently, on the one hand a complete coverage of the investigated north-south section through sampling was achieved but on the other hand in some portions of the stretch the frequency of sampling is so low that drilled sites from these regions do only contribute with the character of a spot test to this study.

Sampling was done with a motor-driven portable rock drilling machine on the base of a standard chain saw. Non-palaeomagnetic scientific western staff and Tibetan drivers supported drilling.

At 73 sites (1998: 39, 1999: 34) we obtained a total of 742 orientated core samples (minimum 10 cores per site), predominantly clastic sediments of Tertiary and Cretaceous age, with Jurassic(?) carbonates and younger volcanics subordinate. The distribution of samples from one site in one sedimentary member was chosen fare enough to span secular variation.

The orientation of cores was measured by using a normal (magnetic) compass only because the intensity of magnetisation of sampled rocks was in such a low range that a deviation of the measured north direction could be excluded.

Detailed structural measurements, mainly bedding and fault plane recordings, accompanied the palaeomagnetic fieldwork wherever possible, but were limited due to being short of time or manpower.

1.3.2 Laboratory work

All sample examination and analysis of measurement results described below was carried out at the palaeomagnetic laboratory of the geophysics department at the Institut für Geologie und Paläontologie der Universität Tübingen.

In a first step the core samples of 2.5 centimetres in diameter and between 3 and approximately 12 centimetres long were cut in order to obtain standard length specimens of 2.2 centimetres.

At the beginning of the measurements the Anisotropy of Magnetic Susceptibility (AMS) was determined on a Kappa-bridge (KLY 2, Agico) by changing systematically through 15 positions. AMS data were calculated and projected by using the programs ANEXPORT, EFILE, and ASTA.

One sample per site was subjected to Isothermal Remanent Magnetisation (IRM) acquisition and demagnetisation of saturation IRM (SIRM) successively. For this purpose samples were exposed stepwise to a DC field up to 2.5 Tesla in a pulse magnetiser (Magnetic Measurements MMPM9, impulse time 5 to 10 ms). The induced remanence was measured after each step with a spinner magnetometer (Molspin Minispin, noise level 0.2 mA/m for 10 cm^3 samples). Stepwise demagnetisation of SIRM was performed thermally up to 700° C with a shielded furnace (Magnetic Measurements MMTD60) and the remaining remanence was monitored with a spinner magnetometer (Geofyzika Brno JR5, noise level 0.005 mA/m for 10 cm^3 samples).

Thermo-magnetic runs of susceptibility (κ-T) were conducted on the Kappabridge (low field measurements at 100 μT on KLY 2 with CS-3 thermal device, Agico) in order to detect magnetic minerals by means of their characteristic Curie temperature.

One pilot sample per site was selected for narrow-step Alternating Field (AF) and Thermal (TH) demagnetisation respectively to judge the appropriate method for further demagnetisation. AF demagnetisation was done with an automatically working degausser (2G Enterprise 2G600) while TH demagnetisation was accomplished by using a shielded furnace (MMTD60). The remaining remanence directions were measured after each step by using a cryogenic magnetometer ((2G Enterprise SQUID 755 R, noise level <0.01 mA/m for 10 cm^3 samples). At each step of TH demagnetisation magnetic susceptibility was controlled to detect possible mineral alterations during heating.

Following the evaluation of the measurements of pilot samples the suitable method of demagnetisation was decided and carried out on the complete set of samples.

All palaeomagnetic data evaluation was done with the program PALMAG by Maier and Bachtadse (1995).

A significant number of sites was characterised by a consistent content of hematite as remanence carrier in all core samples of the respective site. Since a set of specimens of one site is arranged along the long axis of the furnace during heating, this consistent content of hematite turned out to be a very effective tool to calibrate the furnace and to detect a supposed temperature gradient. The long axis temperature gradient of the furnace around heating temperatures of 650° C was found in the range of

50 K which is by far high enough to give reasons for careful monitoring of sample positions for later correction of displayed (false) temperatures (Fig. 1.3-1). Alternatively, dummies could be placed in the outermost sample positions on the holder – minimum 4 on each side – to avoid misleading results from the area of inhomogeneous heating.

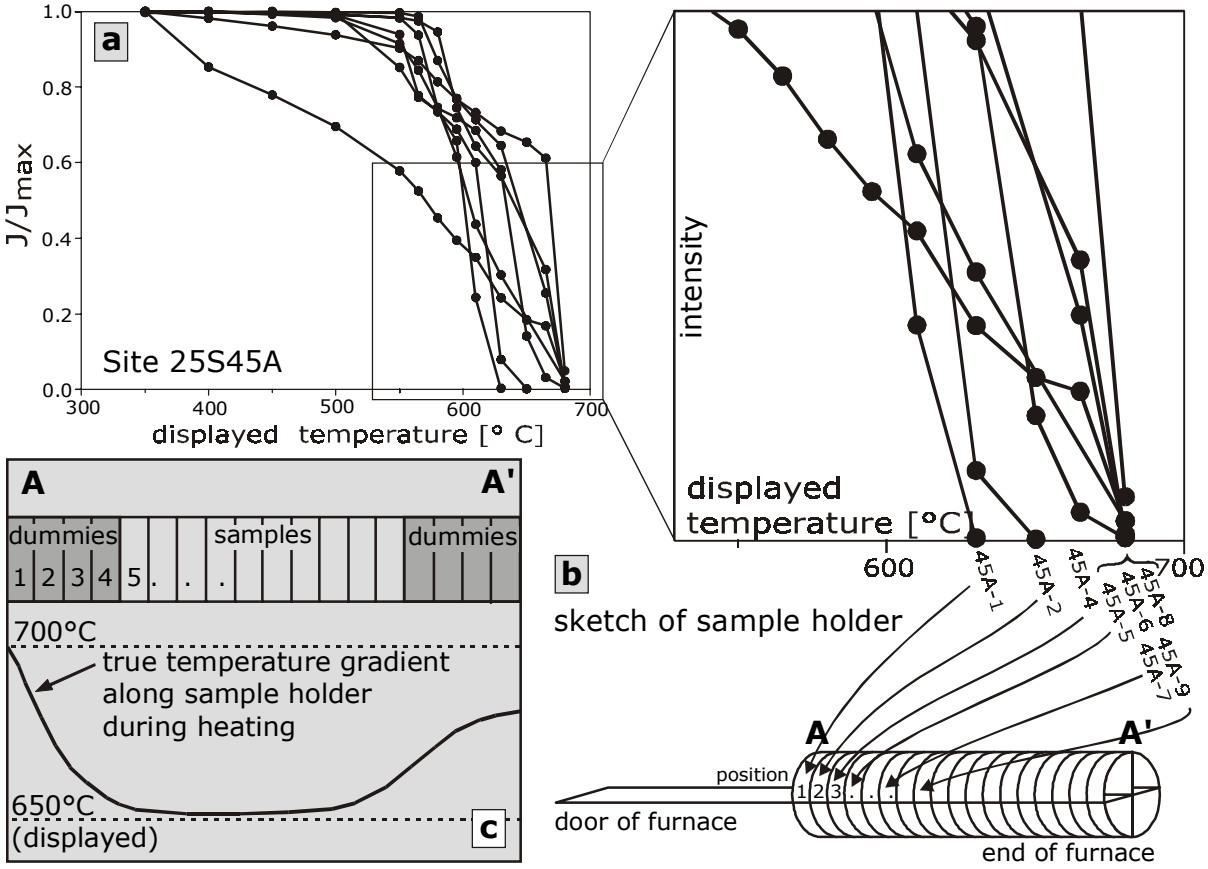

Fig. 1.3-1: *Temperature gradient of furnace MMD60 during TH demagnetisation. Homogeneous magnetic mineralogy within site 25S45A allows calibration procedure. a - thermal demagnetisation of 8 specimens, b - position of specimens during heating, c - temperature gradient as derived from experiments.*

1.3.3 Structural evaluation

Structural field measurements were subjected to stress inversion treatment by using the program library of Ratschbacher et al. (1994).

Other structural elements such as bedding planes and fold axes were evaluated with the program SPHERISTAT.

2 Cenozoic deformation in the Dogai Coring Tso range (northern Central Tibet): Consistent counterclockwise rotations deduced from palaeomagnetic and structural investigations

2.1 Geography and geological setting

2.1.1 Geography

For the first time investigations were carried out in the mountain range along the northern shore of the Dogai Coring Tso (DGC) after the area was reached at long last by crossing the inflow at the western end of the lake (s. Fig. 2.1-1 for exact localities). The belt is characterised by a moderate relief with elevations from lake level at 4750 m to 5297 m in the inner belt. No vegetation except grass and lichens occurs at this altitude. The study area does not serve as headwaters for rivers which go out of the region – all waters are collected in the lakes of the area, especially in the large Dogai Coring Tso. Despite the fact that after some four weeks of expedition INDEPTH3/GeoDepth participants had their first meeting with other human beings there (two shy Tibetan travellers who hardly approached our group when the cars came to a stop), the region is unpopulated.

2.1.2 Geological setting

Red bed sequences of probable Cenozoic deposition age are common features on the Tibetan plateau and most prominent occurrences are found in a belt to the south of the Kunlun terrane (e.g. Fenghoushan). Characteristically, these sequences are folded and thrusted and therefore represent key areas to a better understanding of the plateau evolution, especially to constrain the timing and distribution of deformation caused by the India-Asia collision, and to determine the mechanisms responsible for the crustal shortening.

The clastic sedimentary sequence of the DGC is subdivided in a basal green unit, composed of greyish green shales and fine grained sandstones, and conformably overlaying red beds which consists of reddish medium to coarse grained sandstones and conglomerates.

Some field shots (Fig. 2.2-1, see chapter 2.2.2 for detailed explanations) can hardly draw an adequate picture but give at least some impressive idea of the geology in an area crowded with outcrops, and bar of vegetation.

Microscopic investigations on thin sections reveal the multi-component character of the sediments with grains of quartz, calcite, mica, feldspar, and gneiss being most common (Fig. 2.1-2). There were only few detrital iron oxides found but an opaque sub-microscopic substance is practically everywhere in the calcareous matrix of the red beds while it is missed in the green unit.

Fieldwork revealed indications for depocentre migration and earthquake-induced sediment liquefaction, showing that syn-depositional deformation happened in the belt.

Although fossils are rare and poorly preserved, a continental deposition facies is indicated by rhizolithe intercalations and channel sediments. Minimal thickness estimations of both units add up to 2.5 km in the eastern part and reach 2.8 km in the West. The sediments of the DGC belt are tight to open folded, imbricated and thrusted southward over Jurassic limestone. A lithologic map of the area was compiled from field and remote sensing data (Fig. 2.1-3).

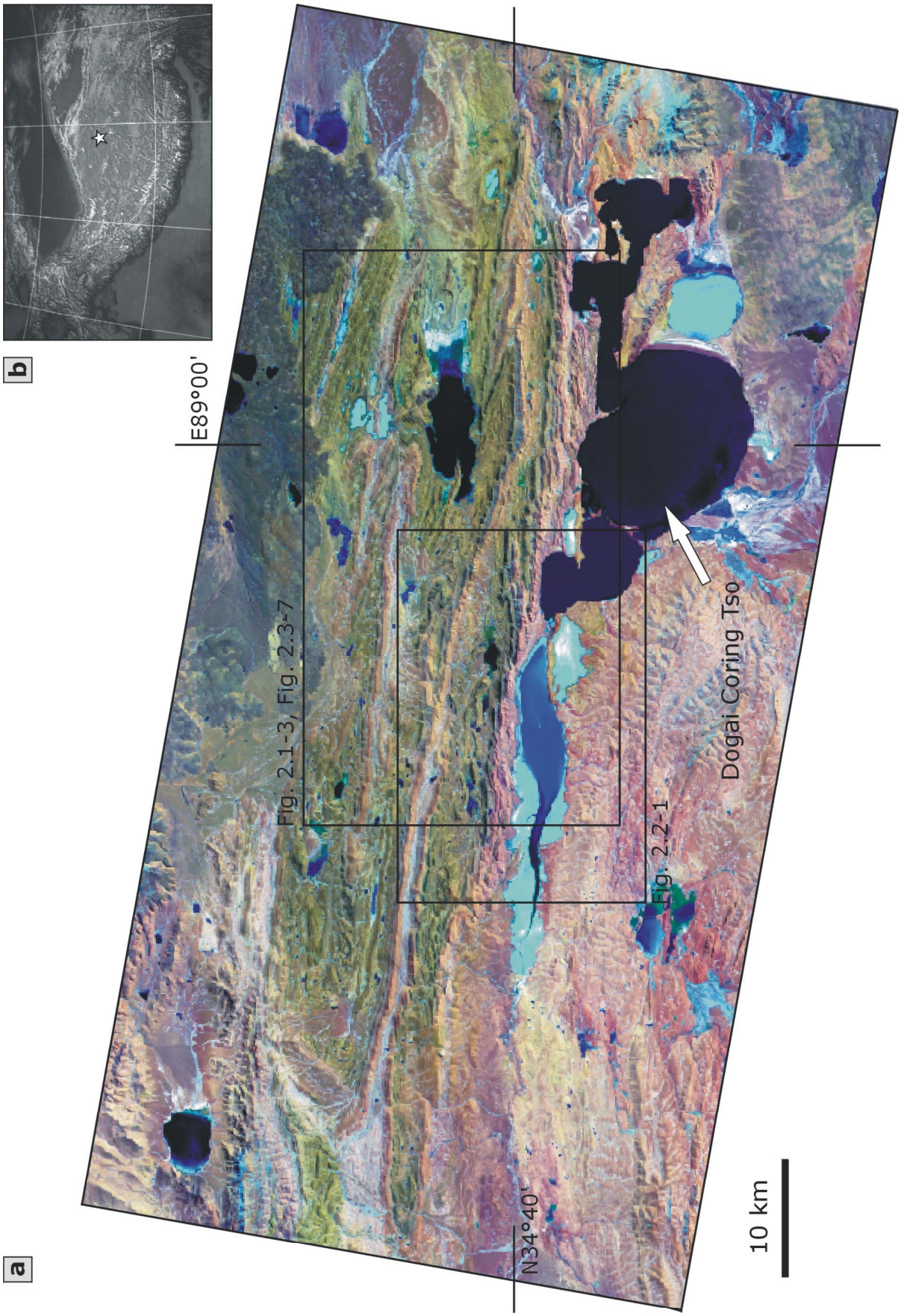

Fig. 2.1-1: *Dogai Coring (DGC) fold-and-thrust belt. a - thematic mapper (TM) of the area, due to processing techniques red and green clastic sediments in reality appear reversed as green and red colours in the TM image; b - star shows location of DGC fold-and-thrust belt in northern central Tibet.*

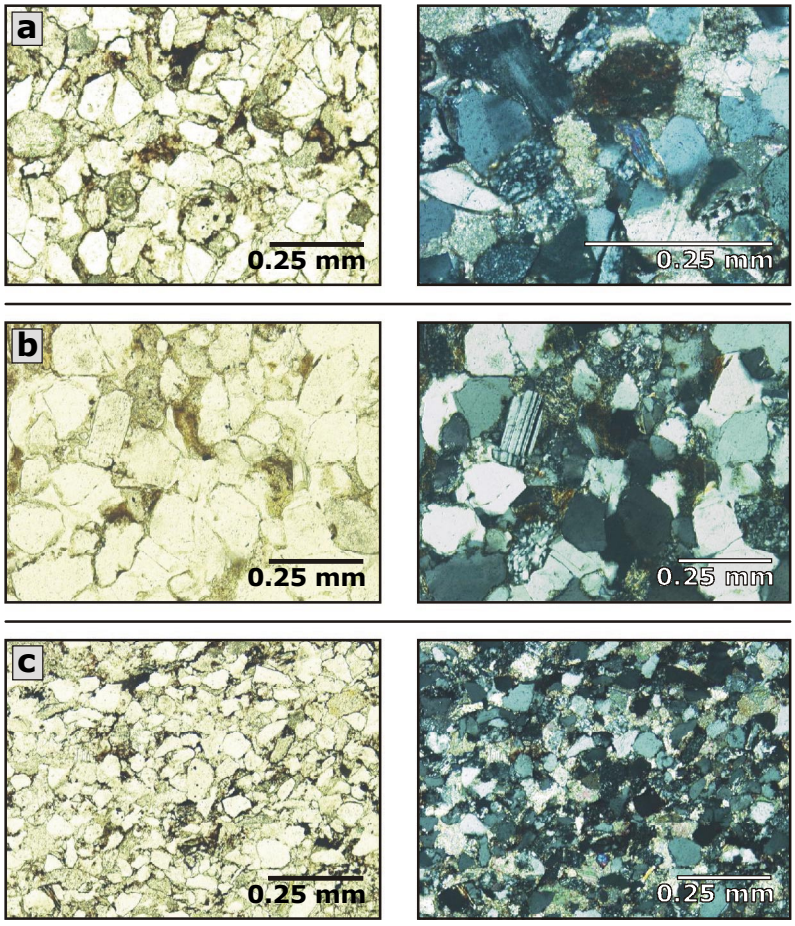

Fig. 2.1-2: *Thin sections of characteristic samples from the DGC. Left - parallel nicols, right - crossed nicols. a - sample 4K-1, b - sample 9K-1, c - sample 17M-1.*

Single grain age dating on detrital zircons (120 grains from two samples, SHRIMP-method) revealed youngest ages from 204 ± 15 Ma to 140 ± 5 Ma. The zircon ages attest that deposition in DGC cannot be older than early Jurassic to early Cretaceous. It is shown that neither Jurassic nor Cretaceous strata are reported from northern Qiangtang (Daßinnies, 2001). But the DGC clastic sediments are closely related to the major red beds of the Fenghoushan Niubao Group (Daßinnies, 2001): "Sediments of the DGC and the Fenghoushan area are characterized by a clastic sequence which is composed of a basal interbedding of mud-, silt- and sandstones that is overlain by coarser grained sandstone. Intercalations of gypsum and limestone are

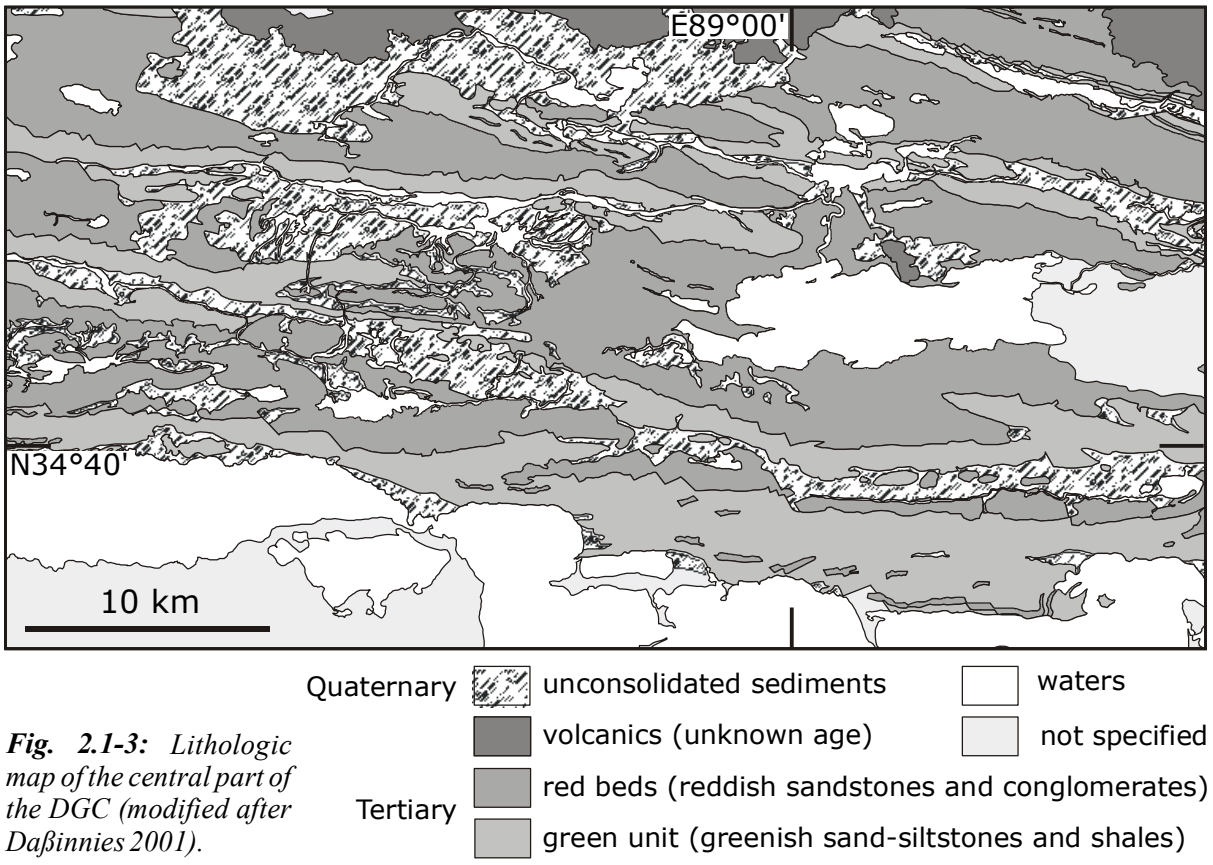

Fig. 2.1-3: *Lithologic map of the central part of the DGC (modified after Daßinnies 2001).*

common in both. Furthermore red staining and occurrence of palaeosoil indicators account for a continental sedimentation environment in the Dogai Coring and thus correspond to a sedimentary facies known from Erdagou, Fenghuoshan area." Additional evidence for the correlation of the DGC belt and the Fenghuoshan arises from a comparison of thickness variations which is consistent. Another similarity with some other red bed occurrences in northern Qiangtang is observed in the fact that volcanic rocks cap the DGC sequence.

Summarising the arguments above one have to statue that the clastic series of the Dogai Coring area, both red beds and green unit probably correspond to the Fenghuoshan Niubao Group and are likely of Tertiary age.

2.2 Structure of the Dogai Coring Tso fold-and-thrust belt

2.2.1 Special techniques of remote sensing

For remotely sensed structural interpretation, sharpness enhancement and directional filters were employed to aid resolution of linear structures. This led to preferential displaying of structural features at high angles to bedding. The principle limitation encountered using these techniques is the geometric ordering of pixel jogs causing a potential bedding mimic effect. For the most part, however, the continuation (or truncation) of the surface traces of mapped layers and structures between the areas constrained by our field traverses have been successfully interpolated.

2.2.2 Structural results

The applied remote sensing techniques allowed distinguishing between two different tectonic events, the main tectonic deformation ("palaeotectonic" after Daßinnies, 2001) and a younger neotectonic one.

The neotectonic event is represented by a conjugated set of NNE-SSW and NNW-SSE trending faults. All rocks of the DGC belt are affected by this deformation. Because the neotectonic event has minor effects on the large-scale structural pattern it is not described in detail.

The main tectonic deformation is responsible for the most obvious features of the structural geometry showing up in the TM image – surely one of the most impressive scenes one could be faced with (Fig. 2.1-1).

The effects of the main deformation phase are confined to mainly Tertiary and partly Jurassic rocks. Three strong structural elements were specified in the Tertiary to characterise the palaeotectonic event: dextral and sinistral strike-slip faults, large folds, and thrusts.

A compilation of photographs is showing these features like they are seen in the field (Fig.2.2-1). Fieldshot 1 represents the view on the southern fronts of the discrete blocks directly from south over lake Dogai Coring into the western DGC range. The bounding faults have a pure strike-slip character – the stepwise normal faulting in the photograph is just an apparent effect induced by the perspective of the image. Fieldshots 2 and 3 show characteristic approximately E-W directed views in the inner range. E-W trending, north-dipping series can be easily identified by the incorporated harder sandstones. The E-W trending ridges are cut by wrench faults of different scales and offsets. The most dominating strike-slip fault of the working area is seen from two opposed view directions in the fieldshots 4 and 5. The view to NNW (fieldshot 4) shows a syncline closure, represented by the hill in the middle, which is offset from the E-W trending fold body about 1200 meter by dextral faulting. The view to SE (fieldshot 5) goes to lake Dogai Coring and is showing strong E-W trending ridges to the

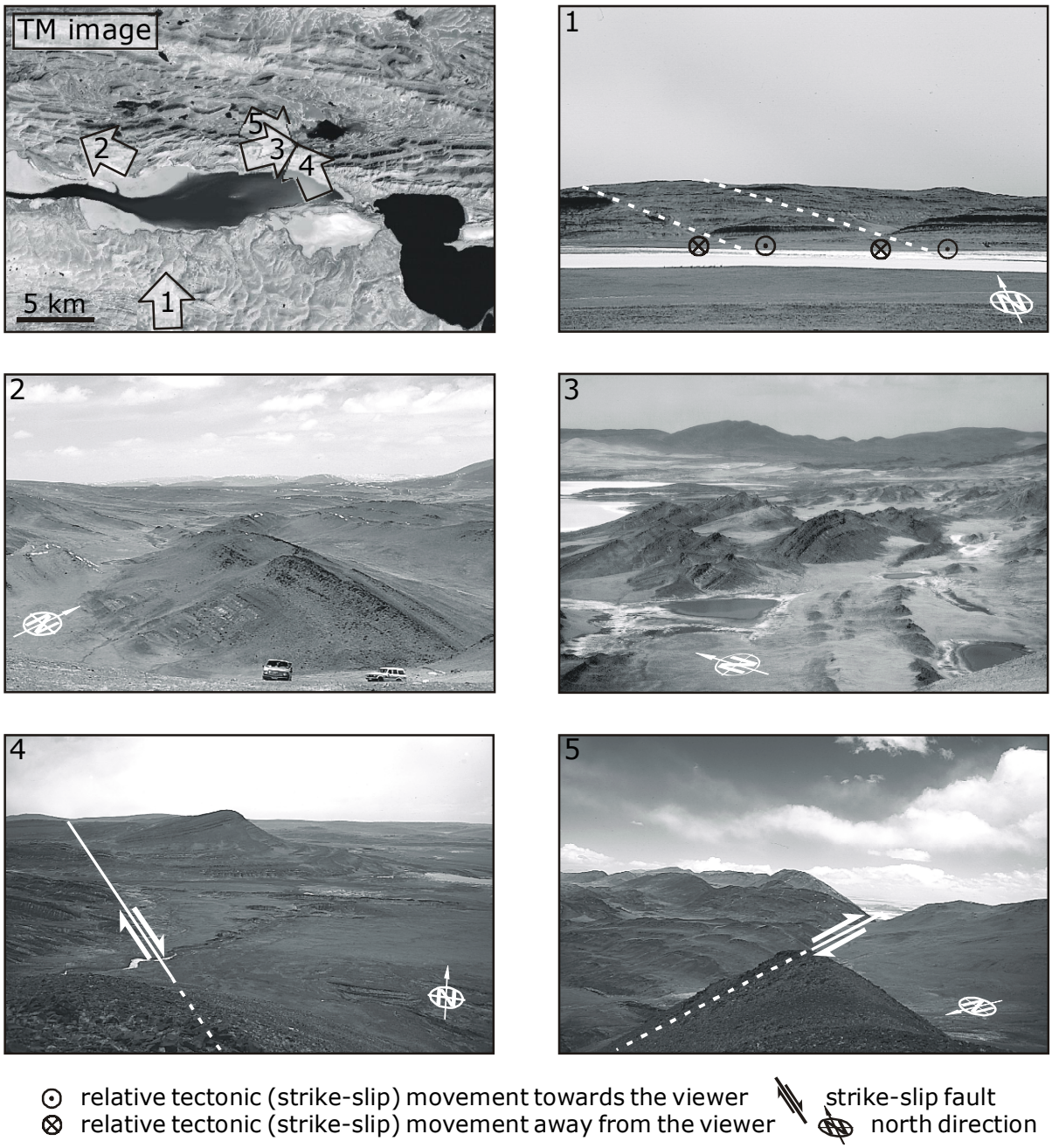

Fig. 2.2-1: *Fieldshots with structural interpretation in the DGC fold-and-thrust belt. TM image shows view direction of photographs.*

east of the dextral strike-slip fault and a morphologically smoother area directly opposed to it in the west.

Strike-slip faults are reflected by lineations and offsetting ridges in the TM image (s. Figs. 2.1-1 and 2.2-2). The faults are equally spaced and form discrete blocks. The set of NW-SE trending (330°) dextral strike-slip faults is ubiquitous in the DGC whereas sinistral strike-slip faulting is less prominent and limited to the northeastern portion of the working area. Both types show offset values from 100 up to 1200 m and do not affect volcanic rocks. Because the strike-slip faults cut through the folds, their initiation must be syn- to post-folding.

Large folds were identified by tracing bedding and morphologic ridges. The fold closures are showing up very clear in the image and give additional evidence. The trend of fold axes is straight E-W, just slightly bent near to faults where the folds are offset.

The main thrusts of the area could be interpreted from combining several indications, such as bounding element for strike-slip faults, separation of the repetition of the same lithology, bordering element of anti- and synclines, and additionally by identifying geomorphologically weaker zones. The thrusts are trending mainly E-W, sub-parallel to the Kunlun belt, and show a sinistral oblique tectonic inventory.

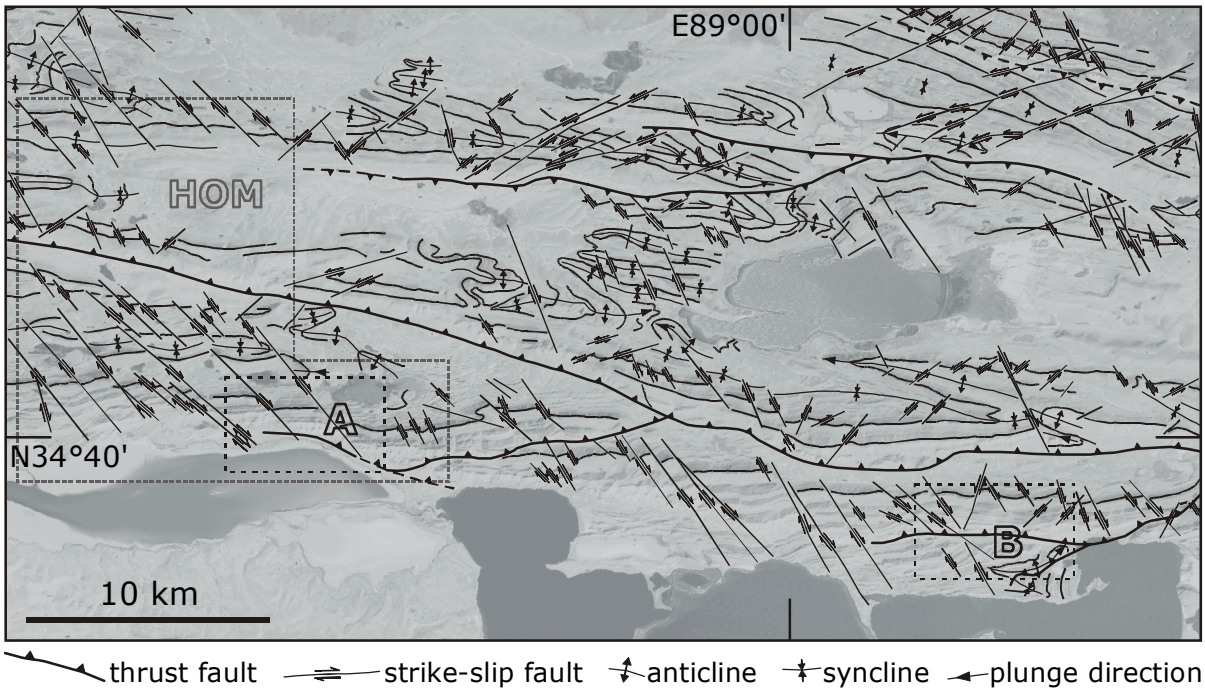

Fig. 2.2-2: *Palaeotectonic structural pattern of the DGC fold-and-thrust belt as derived from remote sensing and field investigations. Greyscale background image shows landscape contours on base of the TM. A, B - regions of detailed structural measurements (see Fig. 2.2-3). HOM - area of homogeneous structural pattern.*

From fault plane striae data a NNE-SSW to NE-SW trending principal stress axis σ_1 responsible for the investigated sinistral oblique faulting and sinistral oblique slip on the bedding planes was calculated (Fig. 2.2-3). Interestingly the directions of folding and dextral faulting need to be explained as a result of N-S orientated σ_1 or – and this seems to be evidenced by the palaeomagnetic data – as a result of NE-SW directed compression plus (subsequent) counterclockwise block rotation.

The features described above lead to the inference that the DGC represents a sinistral transpressive system with a combination of thrusting and wrenching. Discrete blocks rotated counterclockwise around vertical axes between thrusts, leaving their marks in the form of triangular gaps and dextral strike-slip faults which served as slip planes allowing a block rotation in domino style. The dextral strike-slip faults must be formed syn- to post-folding and pre- to syn-kinematic with respect to thrusting because they always offset the folds and never cut across thrusts, respectively. There are two possibilities concerning the origin of the dextral strike-slip faults: Conjugated dextral and sinistral components were of similar importance during an initial stage, but when deformation proceeded the dextral faults became dominating or – for the sake of completeness but in fact ruled out by the palaeomagnetic findings below – dextral faults formed directly related to a sinistral strike-slip component as antithetic Riedel shears (Daßinnies, 2001).

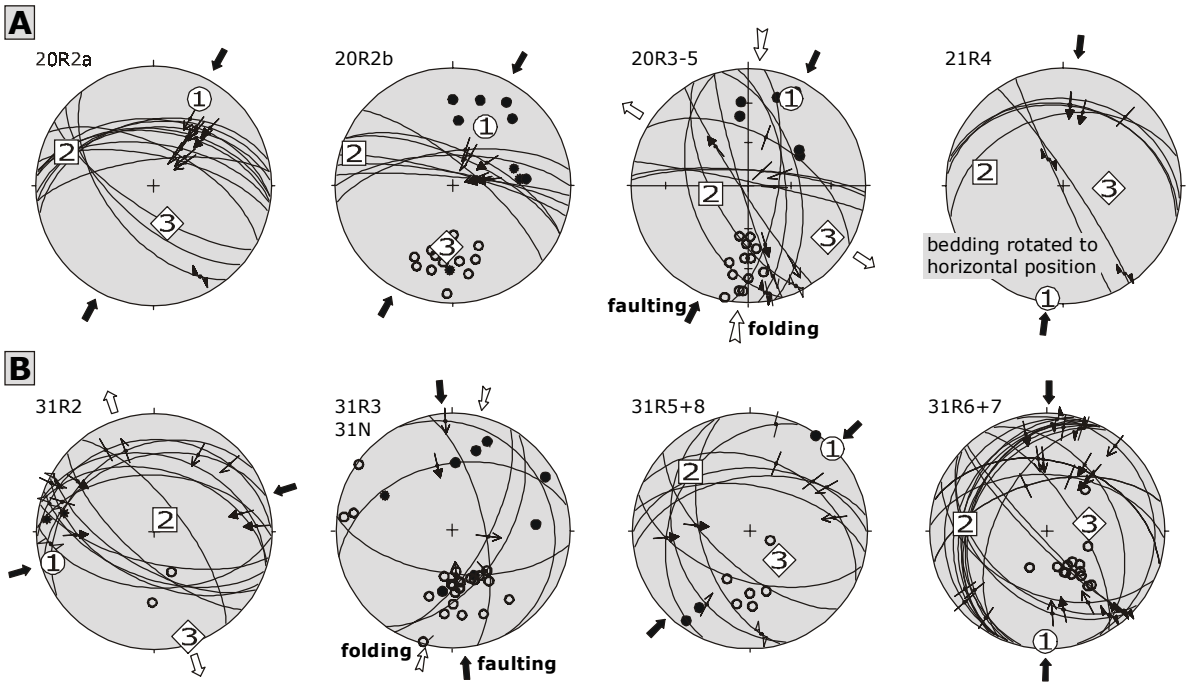

Lower hemisphere stereoplots, great circles show fault planes, arrows show hanging wall displacement direction. 1 2 3 4 degree of confidence; ① ② ③ calculated principal stress axes σ_1 (pairwise closed arrows), σ_2, σ_3 (pairwise open arrows); ∘ bedding poles, • fault planes, • tension gashes.

Fig. 2.2-3: *Example of fault plane striae data. A, B - results from regions of detailed structural measurements (see Fig. 2.2-2). For complete data presentation see Daßinnies (2001).*

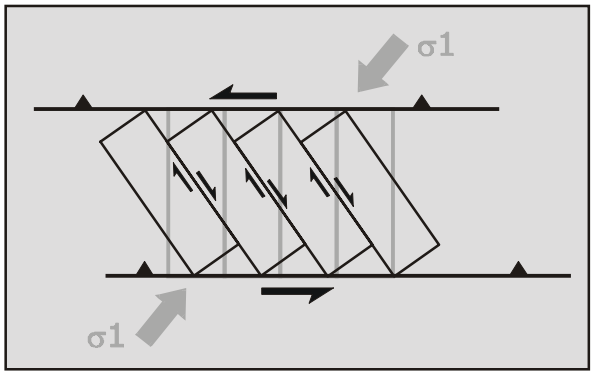

Fig. 2.2-4: *Two dimensional model of counter-clockwise, domino-style rotated blocks within a sinistral transpressional belt.* σ_1 *- consistent main principal stress axis.*

All structural analyses are consistent with a model that explains the DGC as a sinistral transpressional fold-and-thrust belt in which fault-bound blocks rotated counterclockwise in domino-style above a common decollèment in response to NE-SW compression, delimited by sinistral oblique thrusts trending subparallel to the Kun Lun belt (Fig. 2.2-4). This two-dimensional model is in accordance with that one given by McKenzie & Jackson (1986) for distributed extensional deformation.

The estimation of crustal shortening in N-S direction is complicated since the restoration of sections is compromised by insufficient image resolution and too widely scattered field data. Although the results are ambiguous in particulate estimations of N-S shortening enforced by folding are assumed to range from 25 to 58 %.

Some detailed considerations on the specific geometry of the domino block model reveal the contribution of block rotation around vertical axes on crustal shortening in N-S direction. In the area of homogeneous block pattern (HOM, Fig. 2.2-2) initially N-S-trending wrench faults are consistent with the model above and therefore assumed. A counterclockwise rotation of 35° detected from the trend of dextral faulting can account for about 20 % of N-S shortening. On the base of a known structural geometry (see geometrical sketches, Fig. 2.2-5) calculations can be derived:

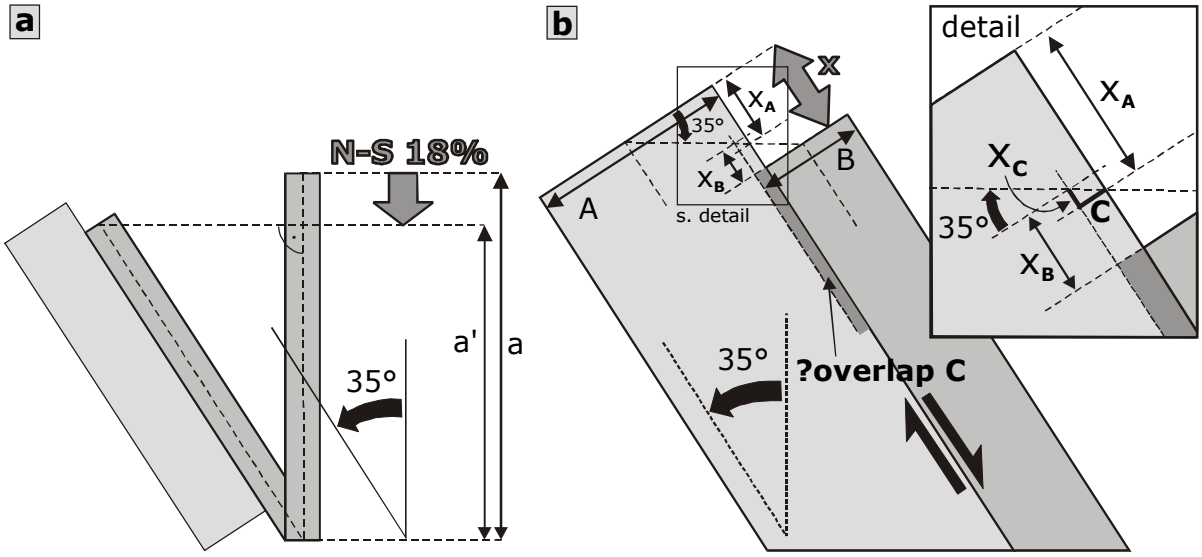

Fig. 2.2-5: *Geometrical features of counterclockwise rotated domino blocks. a - contribution of block rotation to shortening, b - displacement along right-lateral strike-slip faults*

Shortening in N-S direction is

$$a'/a = \cos 35° = 0.82 \quad \text{(i.e. 18 \% of shortening).} \qquad [2.1]$$

For areas where the displacement X along strike-slip faults is not obvious from the TM image it can be calculated from the width of discrete blocks as

$$X = X_A+X_B = [(A+B)/2] \tan 35°. \qquad [2.2]$$

Equation 2.2 is correct for pure strike-slip without any thrust component. If oblique thrusting cannot be ruled out from the TM image a potential overlap C (Fig. 2.2-5b, detail) has to be taken into account and the displacement is then

$$X = X_A+X_B-X_C = [(A+B)/2-C] \tan 35°. \qquad [2.3]$$

A given structural geometry in case of known displacement X can only fulfil equation 2.2 or 2.3 at one time and therefore a comparator check between the two possibilities provides a mathematical tool to characterise the investigated structures and to judge whether a thrust component is involved at the block-bounding faults.

Equation 2.2 and 2.3 were tested for several characteristic dextral strike-slip faults trending 330° in the TM image of the working area and all were found to fulfil equation 2.2 with sufficient accuracy. This is consistent with the substantial geological argument that they trend perfectly straight while dipping strike-slip faults would meander in the image.

Of course, the geometrical considerations above lead to the question, how can one be sure that the initial block-bounding faults were trending N-S? This question will be investigated by the help of the palaeomagnetic results.

2.3 Palaeomagnetic results from the Dogai Coring Tso fold-and-thrust belt

At 13 sites a total number of 130 orientated core specimens was sampled within the red and green clastic sediments (sand-/siltstones) of the DGC. The palaeomagnetic samples were treated as described in chapter 1.3.2. A compilation of magnetic results is shown in Table 2.3-1.

Sitename *)	Geographic coordinates		Lithology	N/n	RC	In situ directions				Bedding	Bedding corrected directions				Directions at 82% of unfolding			
	Latitude (N)	Longitude (E)				Decl	Incl	k	α_{95}		Decl	Incl	k	α_{95}	Decl	Incl	k	α_{95}
20S4K	34°42.471'	88°43.644'	red beds	10/10	H	324.7	-46.4	349.1	2.6	343/66 ot	314.3	63.2	349.1	2.6	325.4	44.2	349.1	2.6
20S5L	34°42.480'	88°43.731'	red beds	10/10	H	334.4	-23.3	44.7	7.3	351/88 ot	315.2	63.3	44.7	7.3	327.5	48.8	44.7	7.3
20S6M	34°42.625'	88°43.520'	red beds	10/9	H	344.9	-28.4	22.6	11.1	179/78	340.5	47.4	22.6	11.1	344.0	33.9	22.6	11.1
20S7N	34°42.764'	88°43.091'	red beds	10/10	H	330.5	-30.3	63.2	6.1	169/86	323.0	51.4	63.2	6.1	229.0	37.1	63.2	6.1
20S8O	34°42.884'	88°42.580'	red beds	10/10	H	326.0	-29.9	442.6	2.3	169/86	317.6	49.6	442.6	2.3	324.3	35.9	442.6	2.3
21S9K	34°40.180'	88°47.991'	green unit	10/9	M	354.2	61.7	7.0	20.9	350/45	352.1	16.8	7.0	20.9	352.2	24.9	7.0	20.9
21S10L	34°40.267'	88°47.960'	green unit	10/10	M	355.1	47.9	4.5	25.8	356/36	355.4	11.9	4.5	25.8	355.3	18.4	4.5	25.8
21S11M	34°40.610'	88°47.924'	red beds	10/10	H	57.2	86.3	51.8	6.8	328/60	332.2	29.9	51.8	6.8	332.8	40.6	51.8	6.8
22S12K	34°47.080'	88°44.906'	red beds	10/10	H	340.5	64.8	102.6	4.7	350/26	344.8	39.0	102.6	4.7	344.4	43.6	102.6	4.7
31S15K	34°39.136'	89°07.224'	red beds	10/10	H	162.8	69.0	10.8	15.4	02/65	11.5	44.5	10.8	15.4	14.1	56.0	10.8	15.4
31S16L	34°41.338'	89°02.655'	red beds	10/10	H	10.5	78.3	57.2	6.4	354/38	358.2	39.9	77.8	5.5	358.7	46.9	74.5	5.6
31S17M	34°40.780'	89°02.086'	red beds	10/10	H	348.7	27.5	36.0	8.2	205/38	322.9	53.5	36.0	8.2	330.3	49.9	36.0	8.2
31S18N	34°40.661'	89°01.728'	red beds	10/10	H	233.5	87.8	161.3	3.8	357/37	353.8	54.2	161.3	3.8	353.2	60.8	161.3	3.8

RC is remanence carrier; H: hematite, M: magnetite; N is the number of measured specimens per site, n is the number of specimens included in statistics; Decl: Declination, Incl: Inclination; k: precision parameter, α_{95}: 95% confidence limit; ot: overturned bedding.
*) The detailed sitenames (e.g. 20S4K, they include date and initial of researcher) are referred to as abbreviated forms (e.g. 4K) in text and figures.

Results of the AMS yield well-grouping principle directions of single specimen in 10 sites (Fig. 2.3-1). With k3 orientated about vertically the distribution reflects a sedimentary fabric in general. The pronounced grouping in the example of site 10L could be explained as result of hydrodynamic forces with k1 orientated parallel to the main floating direction or,

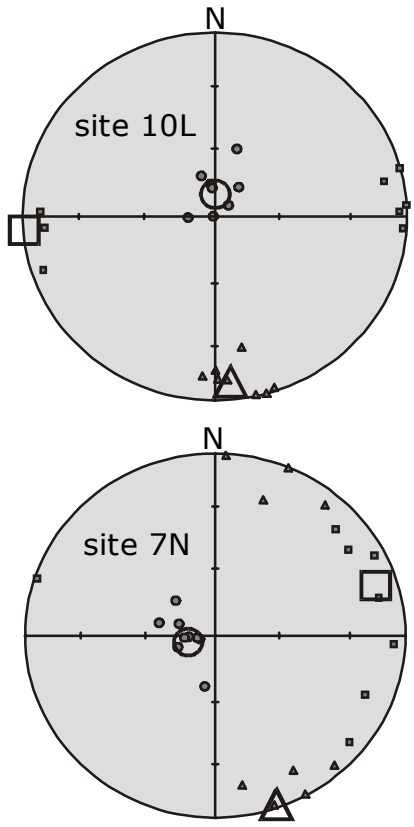

Fig. 2.3-1: *Lower hemisphere equal area stereoplots of AMS (anisotropy of magnetic susceptibility) of representative examples. All data bedding corrected.*

Table 2.3-1: *Palaeomagnetic results of sites from the Dogai Coring Tso fold-and-thrust belt*

alternatively, tectonic overprint with k1 orientated perpendicular to σ_1. The sub-vertical orientation of k3 in the example of site 7N is most likely result of sedimentation on an inclined plain or result of some tilting before remagnetisation (at ~ 20% of folding; s. Fig. 2.3-6b). The more scattered directions of k1 and k2 in example 7N may show the effect of a changing and less-pronounced main floating direction. Although the grouping in sites from the green unit is slightly better defined than in sites from the red beds there is no big difference between the two members.

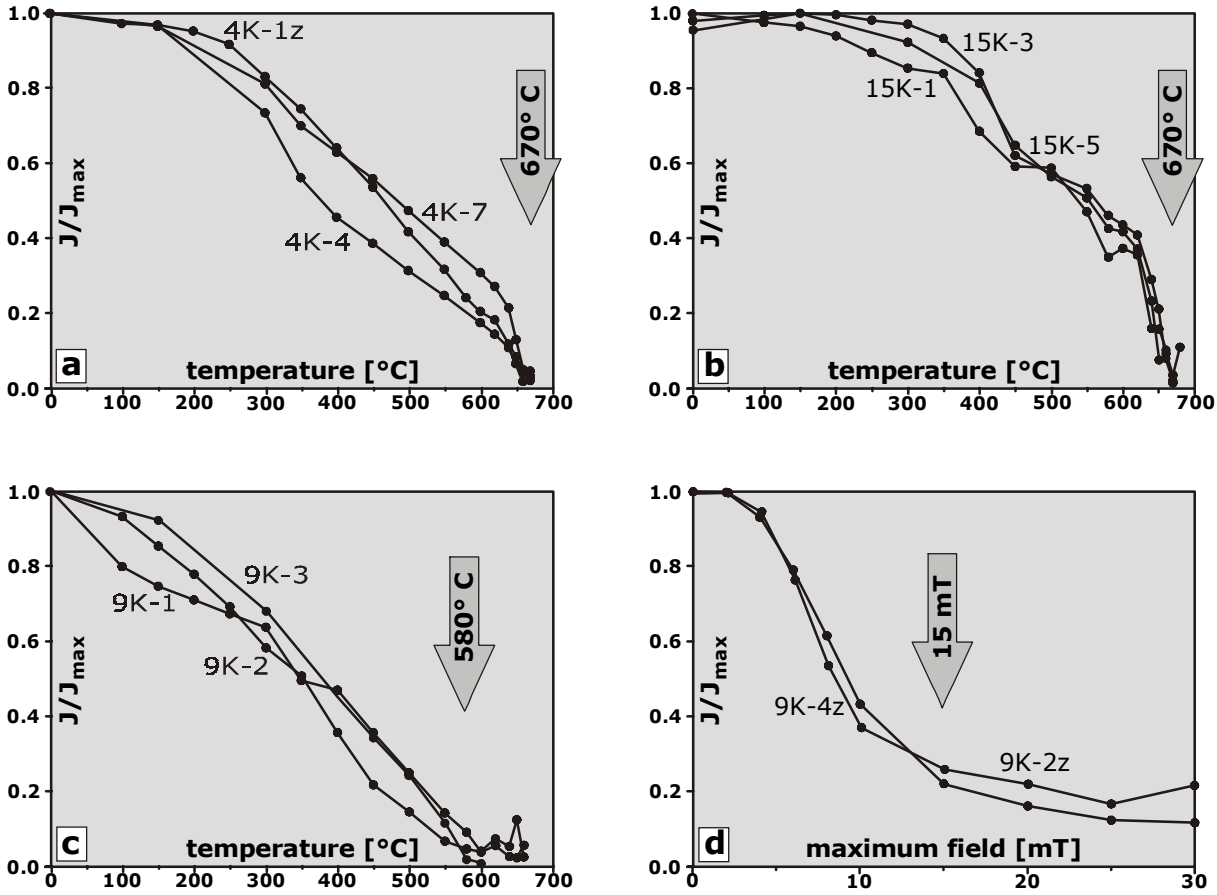

Fig. 2.3-2: *Representative demagnetisation behaviour of sites from the DGC. a, b - TH demagnetisation of sites 4K and 15K, unblocking of hematite at 670° C; c, d - TH and AF demagnetisation of site 9K, unblocking of magnetite at 580° C and demagnetisation between ~5 and 15 mT.*

Other rock magnetic properties are different in the green unit and the reddish sediments. In all sand- and siltstones from the red beds (11 sites) a stable characteristic remanent magnetisation (ChRM) is carried by hematite and can be separated after removal of a viscous component at ~200° C (Fig. 2.3-2a/b). This identification is clearly evidenced by the unblocking of the natural remanent magnetisation (NRM) at ~670° C during TH demagnetisation whereas no significant demagnetisation effect was achieved by AF demagnetisation up to 1.4 T due to the high coercive force of hematite (up to ~5 T). For most of the hematite-bearing samples the orthogonal vectorplot (Zijderveld) exhibits a very stable component with the demagnetisation path pointing directly to the origin (Fig. 2.3-3a). Some samples from mechanically weaker, altered rocks, with mostly lower NRM intensity, show a more scattering path, but can be still interpreted (Fig. 2.3-3b). Further evidence for hematite as remanence carrier is provided by IRM (isothermal remanent magnetisation) experiments (Fig. 2.3-4a, b): No complete saturation of IRM is reached at maximum fields of 2.5 T and IRM was unblocking at ~670° C during TH demagnetisation. In contrast the samples from the green unit (2 sites) contain a stable ChRM carried by magnetite (Fig. 2.3-2c/d). It is separated through both, TH and AF demagnetisation with

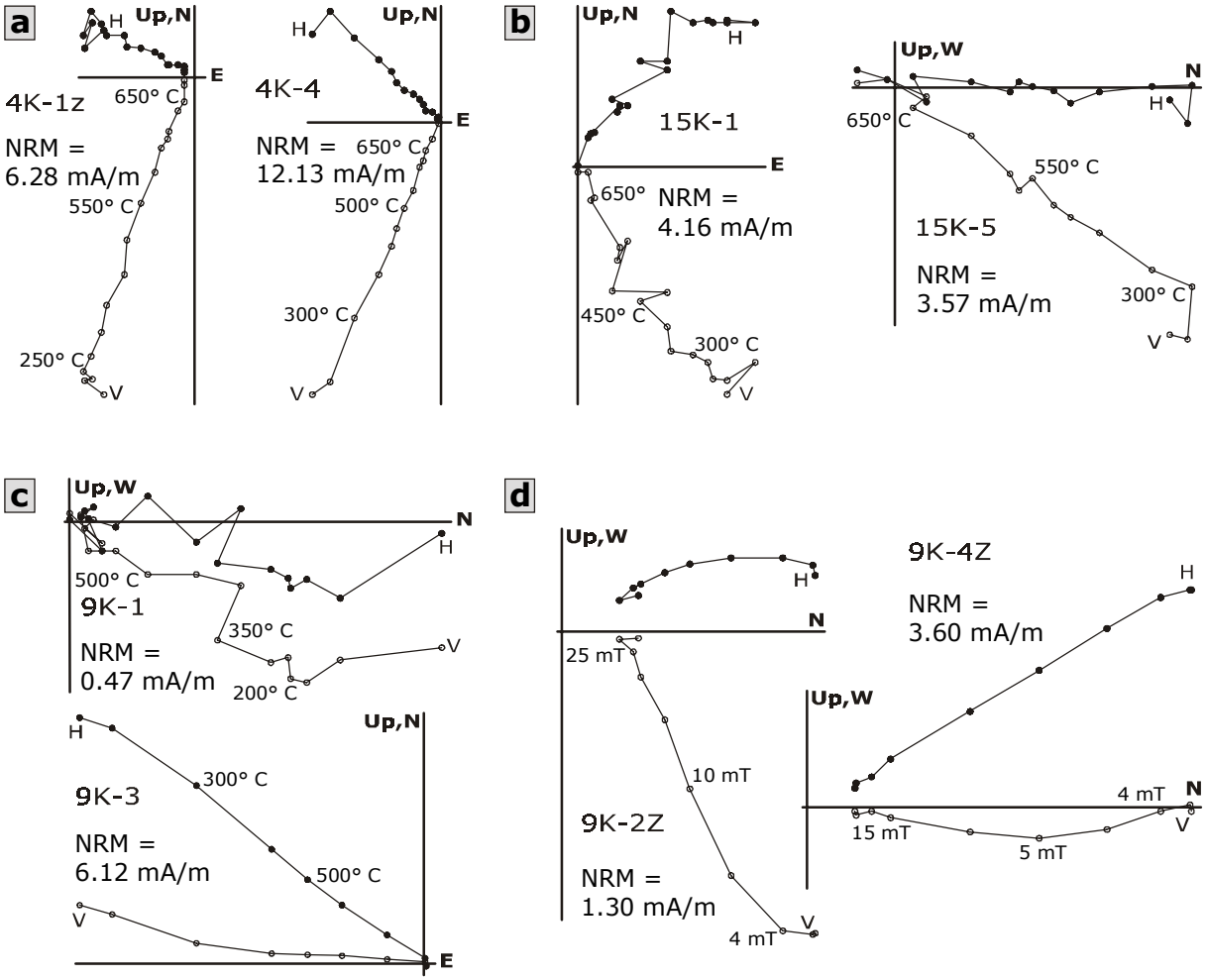

Fig. 2.3-3: *Orthogonal vector plots (Zijderveld plots) of demagnetisation behaviour of sites from the DGC. H, V - horizontal, vertical projection. a, b - TH demagnetisation of sites 4K and 15K, unblocking of hematite at 670° C; c, d - TH and AF demagnetisation of site 9K, unblocking of magnetite at 580° C and demagnetisation between ~5 and 15 mT. All data bedding corrected.*

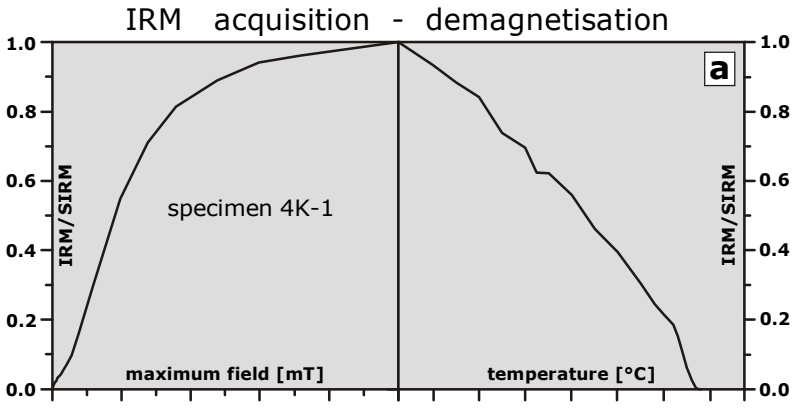

Fig. 2.3-4: *Representative curves for IRM (isothermal remanent magnetisation) acquisition and TH demagnetisation of sites from the DGC. a, b - site 4K and 15K, hematite is dominating magnetic phase; c - site 9K, magnetite is dominating magnetic phase. SIRM - saturation IRM.*

unblocking of the NRM at 580° C and demagnetisation at ~15 mT respectively. Except some specimens, the magnetite-component shows a stable behaviour during demagnetisation (Fig. 2.3-3c/d).

IRM acquisition and demagnetisation also identify magnetite as the main ferro(i)magnetic mineral (Fig. 2.3-4c): About 90 % of the SIRM (saturation IRM) intensity is reached at 200 mT and the acquired SIRM is demagnetised below 600° C.

For all sites from the red beds the single specimen remanence directions group very well within sites and reach k-values between 11 and 443 (Fig. 2.3-5a/b). Despite the clear rock magnetic behaviour the magnetite-bearing sites (9K and 10L) from the green unit show poor grouping of single specimen directions within sites (Fig. 2.3-5c/d). Irrespective of the mode of demagnetisation only k-values from 4 to 7 are achieved which is insufficient for further use of these results.

Large thrusts are dividing between more homogeneous portions of the structural pattern which is developed differently over the working area. Therefore fold tests after McElhinny (1963) and McFadden (1990) were first applied on all sites with k-values larger than 10 and in a second step on only 7 sites from the HOM area. The result of both fold tests after McElhinny is significantly positive at 99%-level and indicates a pre-folding acquisition of the ChRM. A closer look on the bedding-corrected site mean directions from the HOM area reveals a characteristic variation of inclinations (Fig. 2.3-6a) which can

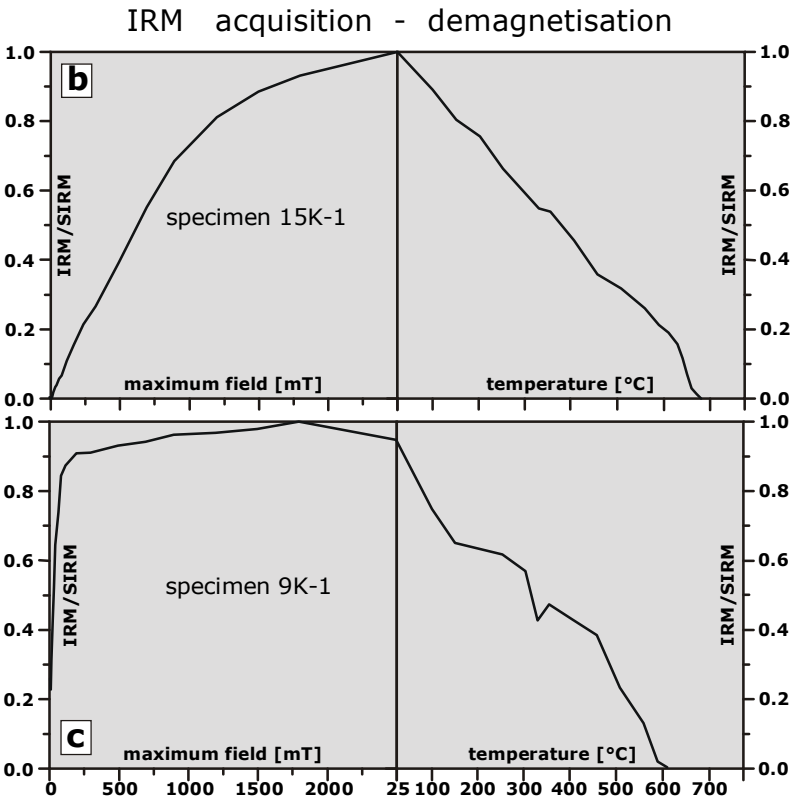

Fig. 2.3-4: *continued*

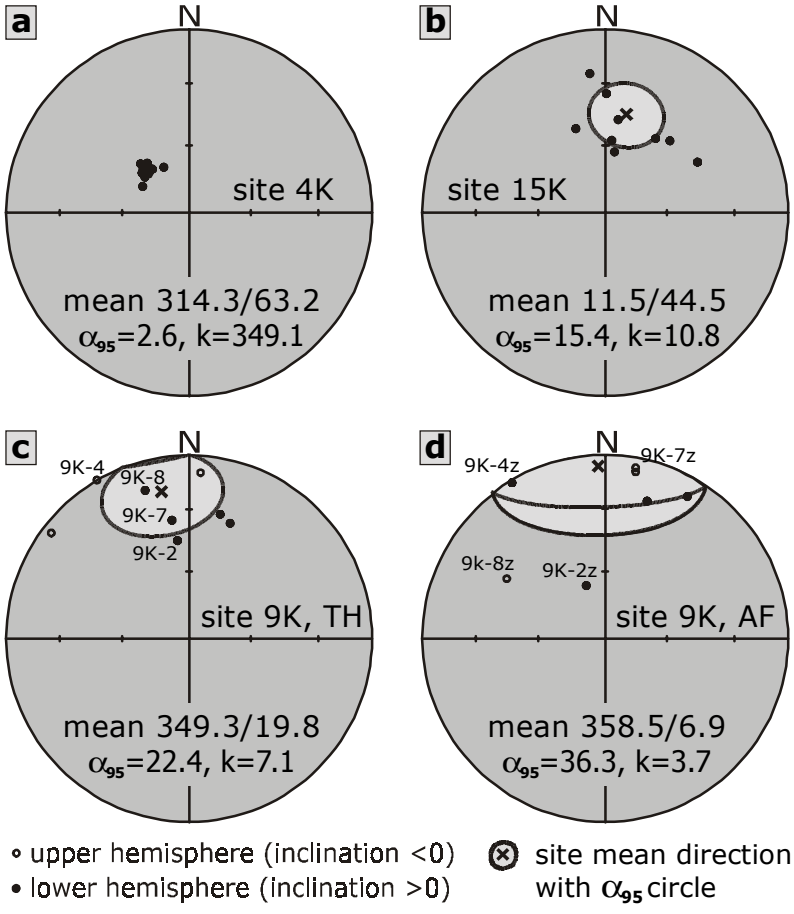

Fig. 2.3-5: *Equal area stereoplots of representative distributions of single specimen remanence directions within sites. a, b - hematite component of sites 4K and 15K isolated by TH demagnetisation; c, d - magnetite component of site 9K isolated by TH and AF demagnetisation, respectively; twin samples are marked with "z". All data bedding corrected.*

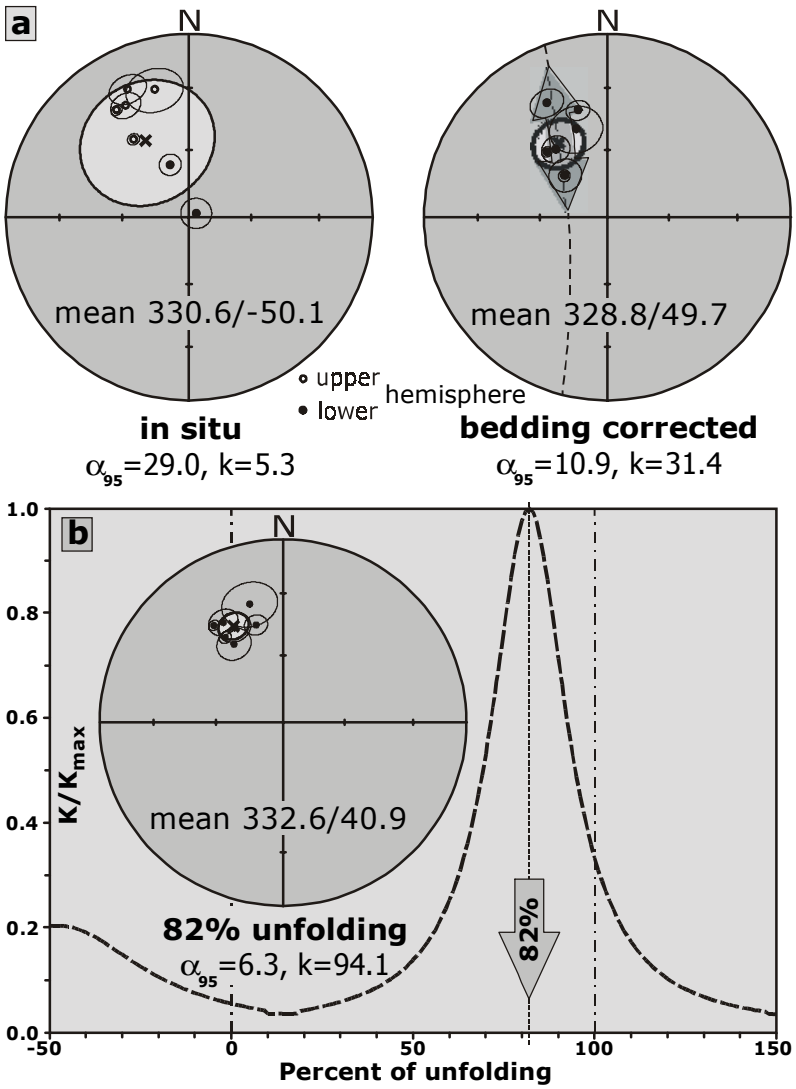

Fig. 2.3-6: *Fold test and stepwise unfolding applied on 7 sites from the HOM area. a - comparison of in situ and bedding corrected directions. Fold test (after McElhinny) is significantly positive at the 99%-level. ChRM directions after bedding correction show distribution of inclinations along a small-circle; b - stepwise unfolding (after McFadden). Best grouping of directions at 82% of unfolding.*

be interpreted as a small-circle distribution. This may indicate syn-folding remanence acquisition during the early stage of folding. The result of the fold test after Mc Fadden with calculation of stepwise unfolding for the HOM area is particularly suitable to support this assumption (Fig. 2.3-6b): The best grouping of directions is received at 82% of unfolding. Of course, the result of fold tests is limited to statements about remanence acquisition under a certain tilt of the sampled beds. A far-reaching spatiotemporal statement is not possible because it is not evidenced whether this remanence acquisition happened during a continuous tectonic process of folding or during one discrete phase of slight tilting disjoined from the main folding.

For further work it is necessary to clarify whether the stable remanences are of primary origin or the result of remagnetisation. One indication for remagnetisation is the occurrence of only normal polarity. This is unlikely in case of a primary detrital remanence because reversals of the geomagnetic field are common in the Tertiary and therefore different polarities should be recorded. If remagnetisation is true, the tectonic interpretation is limited to processes of block rotations because no safe information about latitudinal movement is preserved.

It is not clear if all sites were affected by remagnetisation but there seems to be no mattering influence of the remagnetisation process on the interpretation of the deformation history because sites with obvious remagnetisation show the same rotation as sites which remain suspicious. Additionally, remanence directions are small-circle distributed with strong effects on inclinations while declinations do not show much deviation from the overall mean. This has to be explained in part by the orientation of tectonic features – E-W-trending fold axis in a system of NE-SW compression which affects inclinations preferably – but gives also some evidence for the time of remagnetisation. Therefore the process of remagnetisation can be proposed in an early stage of the tectonic development – probably before any shortening. Even though “best grouping at 82% of unfolding” does only represent an average result over many sites it might be reasonable to assume a best-case-scenario in which the

"palaeomagnetic clock" was reset at an ideal stage of the geological history so that the ChRM directions now represent exactly the characteristic steps of the deformation history of the DGC.

Problems with this interpretation may occur if a rapid process of remagnetisation is assumed and the measured remanence directions therefore would represent the secular variation. In the case of a rapid remagnetisation over the entire working area all sites should be influenced in the same way. But a comparison between the palaeomagnetic directions in the HOM area and the sampled area further east shows that the site mean directions are consistent with the structural pattern in general and the detection of counterclockwise rotation of the ChRM is limited to the HOM area. Therefore it can be excluded that during a rapid process of remagnetisation a systematic deviation of the palaeomagnetic directions was induced by the secular variation. Additionally, the very good grouping of site mean directions at 82% of unfolding (Fig. 2.3-6b) verifies that all recognised palaeomagnetic directions are rather of tectonic origin than induced by remagnetisation processes.

The detected palaeomagnetic directions have to be further discussed under the aspect of Eurasia's clockwise rotation in Tertiary times (Tab. 2.3-2). The overall mean declination of 332.6° (Fig. 2.3-6) is just representing 28° counterclockwise rotation whereas 35° of counterclockwise rotation are determined from the dextral wrench faults in the structural pattern (Fig. 2.2-2). Under the presumption that these wrench faults initially were trending NS there are two possible scenarios to explain the discrepancy: (1) As part of Eurasia the target area rotated clockwise about 7° since the time of remagnetisation and before the wrench faults opened. (2) Remagnetisation happened after 7° of counterclockwise block rotation was accomplished. The second scenario is not in agreement with the structural findings, because folding predates the development of wrench faults and remagnetisation happens at ~20% of folding (see Fig. 2.3-6). The first scenario could be true but with the available data, both reference poles and from this study, it is difficult to judge. Because remagnetisation is younger than 40 Ma the clockwise rotation of Eurasia is smaller than 10° (Tab. 2.3-2) and thus too small to affect the result of block rotation significantly since this is almost the range of the statistical spread of declination data. Furthermore one has to ask whether the Eurasian reference poles could be used noncritical for the Tertiary of the tectonically "turbulent" Tibetan terranes. At least, the discussion about potential clockwise rotation of the target area shows that the detected 28° of counterclockwise rotation has to be taken as minimum estimation.

Table 2.3-2: *Expected remanence directions at the position of the Dogai Coring Tso fold-and-thrust belt (N34°40'; E89°00') during the Tertiary calculated from the Eurasian reference poles (Besse and Courtillot, 1991).*

Age (Ma)	Lat (N)	Long (E)	Decl	Incl
10	84.1°	149.1°	6.4°	56.8°
20	82.3°	147.6°	8.4°	57.7°
30	81.0°	132.8°	8.2°	60.0°
40	80.2°	145.4°	10.6°	58.9°
50	77.9°	149.0°	13.7°	59.2°
60	78.5°	178.7°	13.9°	53.4°
70	77.2°	192.4°	14.5°	50.0°

Ma: million years; Lat, Long: pole latitude and longitude; Decl, Incl: expected declination and inclination.

The arguments above lead to the conclusion that the palaeomagnetic results clearly support the tectonic interpretation (Fig. 2.3-7) because (a) the declinations prove a minimum of 28° counter-clockwise block rotation in the HOM area, (b) palaeomagnetic declinations scatter where the structural pattern is less pronounced (sites 16L - 18N), and (c) the k1-axes of AMS ellipsoids follow fold axes in general.

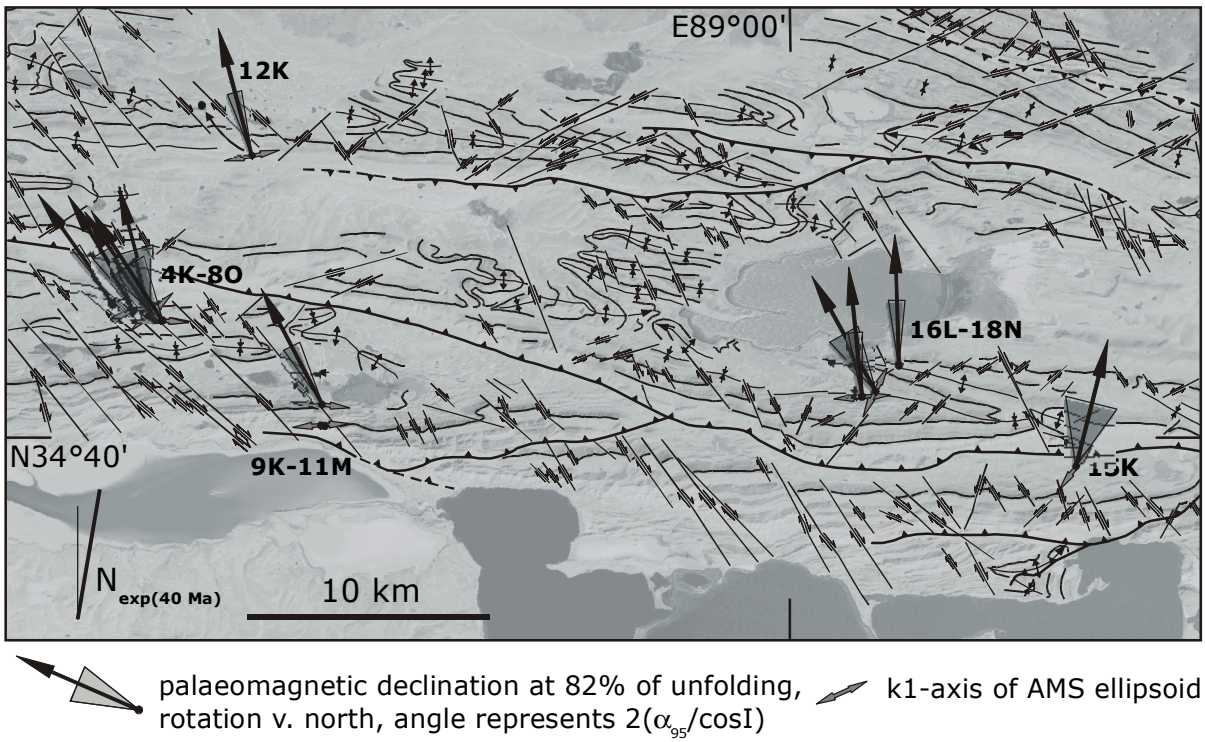

Fig. 2.3-7: *Palaeomagnetic results from the central part of the Dogai Coring Tso fold-and-thrust belt. $N_{exp(40\ Ma)}$ - expected North direction at N34°40'/E89°00' after the Eurasian reference pole for 40 Ma (Besse and Courtillot, 1991; s. Tab. 2.3-2).*

2.4 Summary of geological events

From the findings described above the following summary of geological events in the HOM area of the central DGC fold-and-thrust belt can be proposed (Fig. 2.3-8):

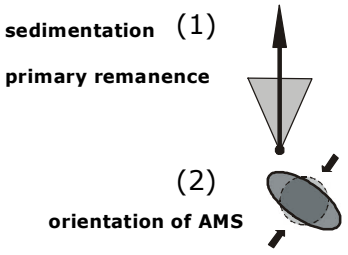

Fig. 2.3-8: *Summary of geological events in the HOM area (see chapter 2.4 for detailed explanations).*

(1) Naturally the chronological sequence started with sedimentation, diagenesis, and syn-depositional deformation of the probable Tertiary clastic series. At the same time a primary remanence was acquired.

(2) At the very beginning of layer parallel shortening, maybe in a phase before any folding, the orientation of the long axis of the AMS-ellipsoid perpendicular to the main principal stress axis is assumed.

(3) The first large-scale response on NE-SW directed shortening was than represented by folding. It cannot be excluded that also thrusting is involved. At ~20% of folding remagnetisation occurred. The magnetic directions (ChRM and AMS) were tilted during all the main folding.

(4) Folding stagnated and consequently dextral wrench faulting caused the break-up of discrete blocks.

(5) Right-lateral movement along the new-build strike-slip faults initiated counterclockwise rotation of domino-style blocks. The magnetic directions were rotated counterclockwise.

(6) Oblique thrusting became dominant and counterclockwise rotation ended. The main thrust partly over run the discrete blocks at their northern edges.

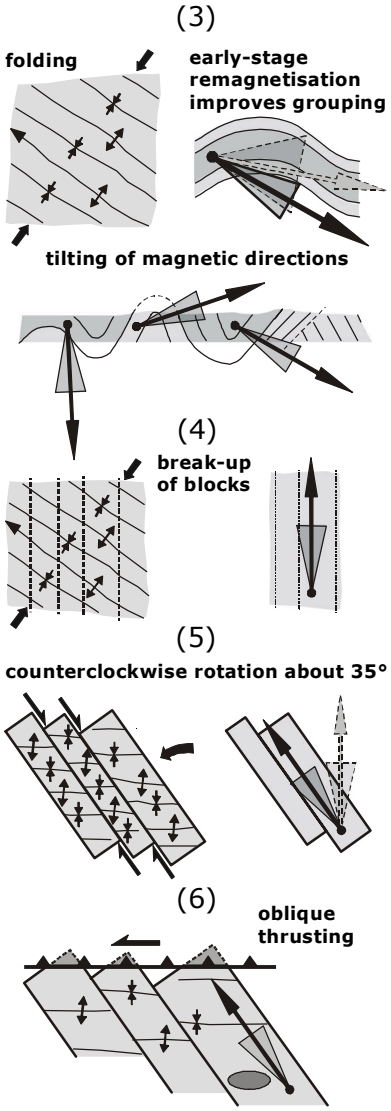

Fig. 2.4-1: *continued*

2.5 Outlook

Some open questions have to remain still under debate, especially those which ask for the absolute age of the sediments, the rate of sedimentation, and the absolute age of tectonics. Because of this uncertainty it is not clear which time span is represented in the samples which complicates the interpretation.

Another question concerns structural measurements on rotated blocks and if the orientation of the derived palaeo-stress field is correct because fault patterns are expected to vary with time and fault-slip data therefore can be rather complex and variable in space (Gapais et al., 2000).

Additionally, the relationship between the rotations detected palaeomagnetically and finite strain in deforming zones is not necessarily simple (McKenzie and Jackson, 1983).

But apart from some open questions remaining our structural and palaeomagnetic findings in the DGC show a mechanism which support that the model of northeastward growth of the Tibetan plateau - proposed for post ~10 Ma by Meyer et al. (1998) – might be also applied for the deformation during the Tertiary.

3 Evidence for left-lateral reactivation of the Bangong-Nujiang suture: A detailed palaeomagnetic and structural study on the Zagaya section, Central Tibet

3.1 Geography and geological setting

3.1.1 Geography

The investigated section accompanies an important logistic corridor right to the north of the only drivable bridge over Zagaya river ("Za'gya" after the Chinese "Official minority region topographic name translation dictionary"). The route was frequently used by different teams of the INDEPTH3/GeoDepth expeditions in 1998 and 1999 coming from nearby Lunpola base camp and heading to the settlement of Shuang Hu and to northern Tibet (s. Figs. 1.2-1 and 3.1-1 for exact localities).

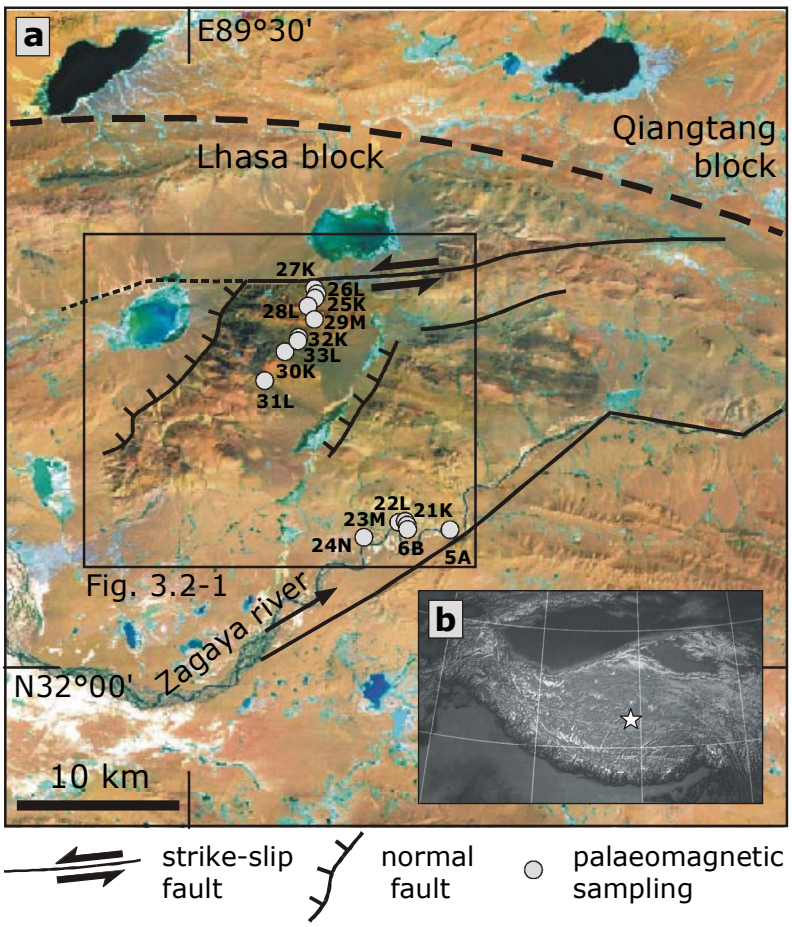

Fig. 3.1-1: *Zagaya section. a - TM image of the working area with mean structural features and site names, b - star shows location of Zagaya section in central Tibet.*

The average altitude in the main valley is about 4600 m and the highest peak of the area reach near to 5160 m. The relief is relatively moderate but also characterised by some steep cliffs, mainly build by more resistant conglomerates.

3.1.2 Geological setting

Geologically speaking the working area is situated on the northernmost Lhasa block within the Upper Jurassic to Lower Cretaceous Bangong-Nujiang suture zone (BNS) representing the site of the collision between Qiangtang and Lhasa terranes. The BNS represents an EW-trending terrane boundary identified as undulating zone through ophiolitic rock material distributed along strike.

Until present the complex structural history of the Bangong-Nujiang suture is not completely understood. The geological interpretation is complicated by several findings which seems to be contradictory: The surface distribution of ophiolitic rocks gives reason to assume north-directed subduction of oceanic crust in the course of the Lhasa-Qiangtang collision. But on the other hand the subduction-related

Bangong granite emplaced to the south of the suture implies a south-dipping subduction zone. Additionally, recent investigations by the seismic group of INDEPTH3/GeoDepth also point towards a steep south-directed subduction of Qiangtang below Lhasa terrane (Zhao et al., 2001).

Although the outcropping lithology does not change significantly between the two sides of the BNS there is evidence for Cenozoic reactivation of the suture zone. Kidd et al. (1988) report sinistral offset from a locality next to Amdo and also Xu et al. (1999) and Allègre et al. (1984) support the idea of left-lateral reactivation of the BNS. Yin et al. (1999) describe ENE-trending fault striations in the Shuang Hu area to north of the suture zone which fit well in the image. To the south of the Zagaya section the dominating active tectonic structure is represented by the right-lateral en-echelon Karakoram-Jiali fault zone (Fig. 1.1-3).

3.2 Geological mapping and structural analysis

3.2.1 New geological map of the Zagaya section

To determine and quantify crustal deformation within the Zagaya section geological mapping with structural field measurements and TM image interpretation was carried out together with a detailed palaeomagnetic study. The geological map and profile were compiled by M. Edwards on the basis of field data from several members of the field geology team (Figs. 3.2-1 and 3.2-2).

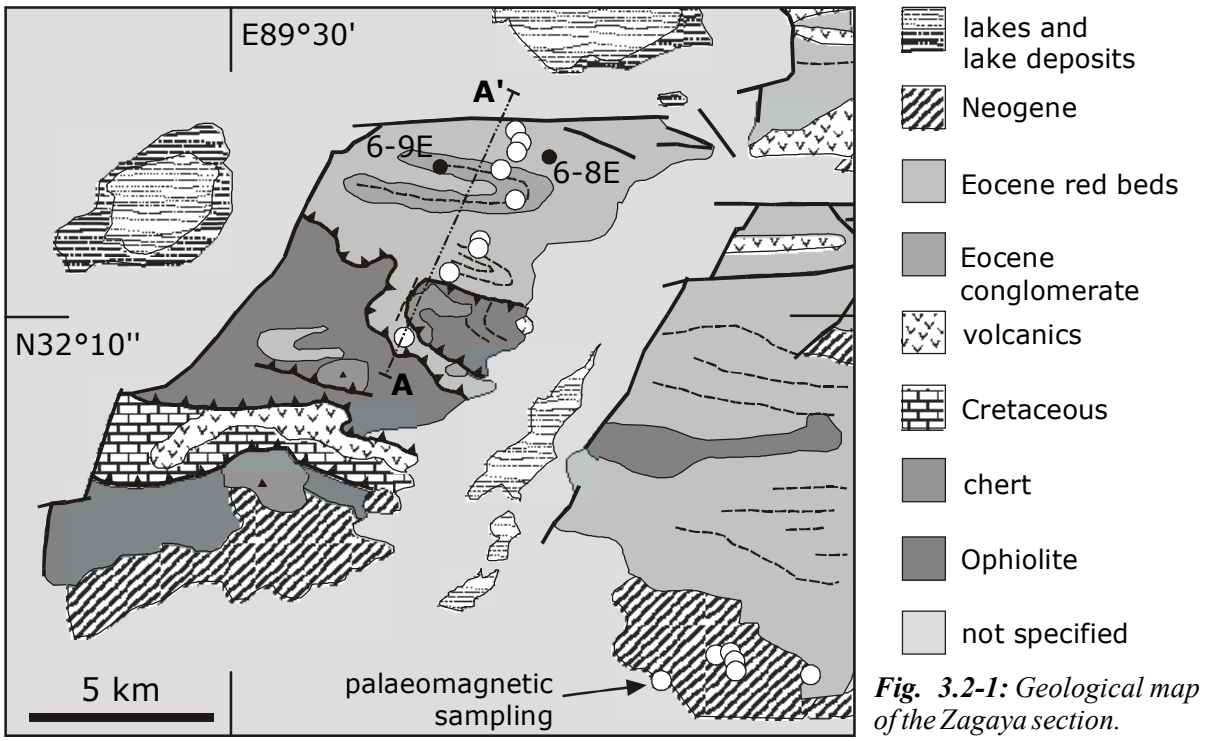

Fig. 3.2-1: *Geological map of the Zagaya section.*

The sequence is dominated by reddish sandstones interbedded with coarse conglomerates, obviously from a relatively nearby area of provenance. The sandstone is calcite-cemented, cross-bedded, and basally deposited. This unit also includes typically dark red to black silt and mudstones. The conglomerates are grain-supported with pebbles between 0.5 and 5 cm in diameter, mainly felsic/porphyric volcanics, vein quartz, and limestone clasts. Large thickness variations in grits and conglomerates due to channel deposition accompanied by distribution switches were observed.

Furthermore the area comprises an ophiolite and Eocene tectonic imbricate (ophiolitic melange) consisting mainly of rocks from the red bed unit and volcanic portions. In detail there are dark

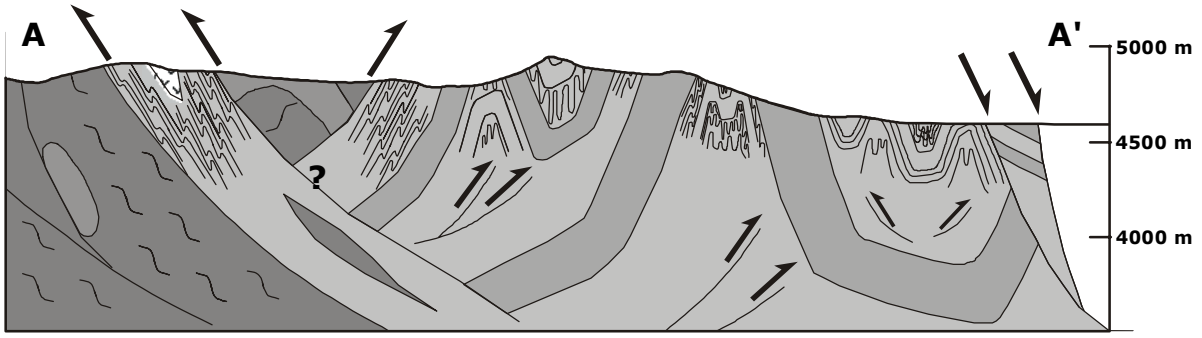

Fig. 3.2-2: *Geological profile A - A', symbols and colours as in Fig. 3.1-2.*

sandstones and gritstones with black- to green-stained volcanic fragment cobble conglomerate and purple-stained pebble conglomerate. Extensive imbricated or intrafolded ophiolitic material including spectacularly mobile serpentinite or serpentinised ultramafic material, marble and chert breccia layers frequently provides strong member to rheology interface of serpentine layers.

Pink and red chert forms large knobs and conspicuous bodies that have acted as stiff members and have visibly ploughed through weaker parts of tectonic imbricate resulting in damage zones at frontal and lateral sheared contacts.

To the south of the working area, best exposed at the northern riverbank of Zagaya river, pale grey, beige and mauve, not very well consolidated muds, silts, and fine sands with locally volcanic derived sediments are dominating.

An earlier working hypothesis for the age of the clastic series was Cretaceous and Jurassic (Kidd et al., 1988). But there is no evidence from biostratigraphic data and their assumption of Mesozoic age of the red beds is just based on correlating TM image interpretation in areas of extensive fieldwork further east with the TM image of the Zagaya section. After visiting the Zagaya section, Kidd regards these units today as post-collision in age, most likely Eocene within the Palaeogene Niubao Formation. Main reasons for this classification are that there is no direct indication for Cretaceous age and the structural position of ophiolite-related volcanics below the red beds which is in contrast to what would be typical for the Cretaceous red beds (Blumenwitz, 2001). And what is even more important, similar red rocks from the Fenghuoshan belt are dated as Eocene (Smith and Juntao, 1988; Kidd et al., 1988).

In the partly consolidated rocks to the south which unconformably overlie the red bed unit diagenesis is more advanced than for known Quaternary rocks and Neogene is the most likely age.

The limestones and volcanics (plus locally clastics) imbricated within the Zagaya section are similar to the rocks of known Cretaceous age mapped and dated immediately to the south in the Lhasa block and therefore a Cretaceous age is assigned.

3.2.2 Structural investigations

The most obvious structures which can be recognised in the TM image are sharp and steeply west-dipping normal faults building the western boundary of two characteristic blocks. Another well-defined structure in the image is an assumed left-lateral EW-trending strike-slip fault limiting the central two blocks to the north and truncating the sampled sequence (Fig. 3.1-1).

The deformation in the northwestern Zagaya section is characterised by a polyharmonic, EW-trending governing folding (first order) with the fold axis plunging moderately around 40° to the west (Figs. 3.2-2 and 3.2-3b). Inevitably, folding predates faulting because the folded sequence is part of the blocks which are cut by far reaching normal and strike-slip faults. Some second and many third order folding is locally ptygmatic due to locally large relative thicknesses of the lower viscosity layers. At all scales, parasitic folds concentrate spectacularly in the hinge regions, frequently accompanied by

internal thrust decollèments. Overturned limbs of tight and isoclinal second order folds due to steeply inclined axial surfaces lower order ("parasitic") folding in mudstones to appear as "collapse folding". In a few cases early axial planar cleavage is distinct from a later crenulation cleavage and the correct fold asymmetry relationship is clear. Intense cleavage development in mud and shale units but not in the sands, grits or conglomerates suggests late cleavage development (after any layer parallel shortening). This is consistent with the notion that the Eocene sediments were not fully consolidated at the onset of horizontal contraction. Thrusting within the profile was recognised on a north-dipping plane with top-to-the-south directed movement of the main Eocene red bed unit onto the ophiolitic melange. Additionally, the highest peak of the area (5162 m), formed by very resistant knoll of chertite/rhyolite "floating" in ophiolitic melange, seems to represent a pop-up structure. It is possibly developed due to reworking (folding/tightening) of a klippe (originally thrust from south) and thereby opposite sense reactivation of klippe original sole thrust (indicated by opposing arrows, Fig. 3.2-2). Alternatively, the pop-up structure may have been "fed" by slices of ophiolitic rocks that are imbricated into the red bed unit where the detachment folding abates and the basal decollèment ramps up to present exposure levels (represented by question mark, Fig. 3.2-2). Further south the ophiolitic melange and the red bed unit is thrust on Cretaceous limestones and volcanics.

A useful restoration of the folded and thrusted rocks along the Zagaya Section is not possible. There are no constrained hanging wall cut-offs in the thrust sheets containing ophiolitic rocks in the southern part of the section, and moreover, a quantifiable stratigraphy is precluded by the pre-Neogene deformation state of the ophiolite obduction melange. In the northern portion of the section, the detachment folding of the Eocene rocks is only slightly more informative. About 60% shortening is represented by all (visible and interpreted on the cross-section) of the large governing fold. The likely decollèment (detachment) horizon is localised upon gypsiferous red clays which have a very low shear strength when wet. Calculating a depth to detachment is severely impeded by (1) the likelihood that these Eocene rocks were not yet fully compacted before horizontal strain and therefore have undergone significant internal deformation during shortening, (2) the incomplete nature of the governing fold (all depth to detachment calculation techniques require at least a full antiform) and thereby uncertainty in the depth of the regional datum (the horizontal line/surface above which the excess material is located), and (3) the unconstrained dip of the detachment (Edwards, pers. comm.).

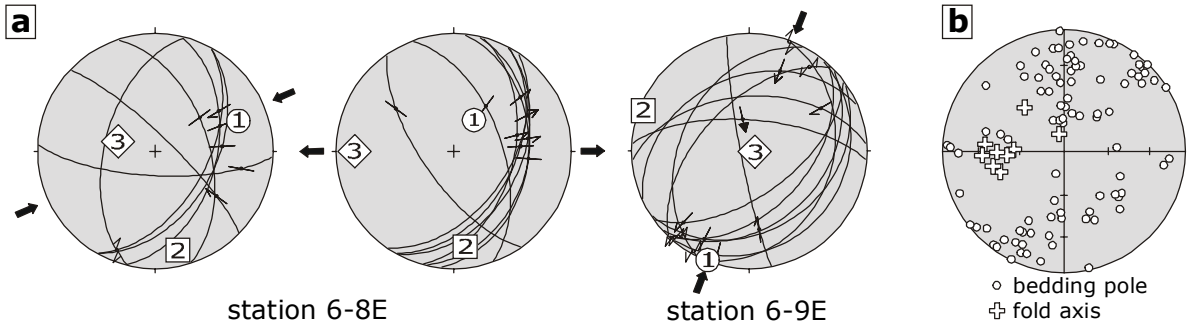

Fig. 3.2-3: *Structural data from the Zagaya section. a - fault plane striae data (symbols as in Fig. 2.2-3); b - bedding data.*

From analysed fault-slip data (sub-) horizontally ENE-WSW and NNE-SSW trending principal stress axis σ_1 were calculated (Fig. 3.2-3a). Additionally, it was possible to isolate data representing EW-trending extension with principal stress axis σ_3 trending EW and σ_1 vertical respectively.

3.3 Palaeomagnetic results from the Zagaya section

3.3.1 Rock magnetic properties

Most of the rock magnetic and remanence investigations of chapters 3.3.1 and 3.3.2 were performed in the framework of a diploma thesis by Blumenwitz (2001).

From sampling at 15 sites within the Eocene and Neogene strata of the Zagaya section a total number of 150 orientated core specimens was obtained. The palaeomagnetic samples were treated as described in chapter 1.3.2. A compilation of magnetic results is shown in Table 3.3-1.

Sitename *)	Geographic coordinates		Age	Lithology	N/n	RC	Component	Bedding	Bedding corrected directions			
	Latitude (N)	Longitude (E)							Decl	Incl	k	α_{95}
5S1A	32°04.614'	89°40.109'	Eoc.	red sandst.	10/9	H	300-650° C	105/52	56.4	42.0	24.1	10.7
5S2B	32°04.805'	89°38.404'	Neog.	brown silt-/sandst.	10/10	M	0-25 mT	106/21	23.4	32.6	44.6	7.3
7S21K	32°04.840'	89°38.246'	Neog.	green/red siltst.	10/8	M	0-120 mT	90/18	21.4	31.8	27.0	10.9
7S22L	32°04.834'	89°38.178'	Neog.	grey/gree siltst.	10/5	M	0-50 mT	94/24	22.8	28.9	37.0	15.4
7S23M	32°04.824'	89°38.102'	Neog.	green sandst.	10/-	(M)	-	(113/19)	-	-	-	-
7S24N	32°04.215'	89°36.920'	Neog.	green/red silt-/sandst.	10/-	(M)	-	(196/57)	-	-	-	-
8S25K	32°12.439'	89°35.558'	Eoc.	red sandst.	10/9	H	300-600° C	184/76	325.2	44.8	11.9	19.5
(2 Comp.)						H	640-690° C		316.0	47.6	3.2	34.3
8S26L	32°12.469'	89°35.573'	Eoc.	red sandst.	10/9	H	350-580° C	166/42	324.0	20.3	14.3	14.1
(2 Comp.)						H	650-690° C		347.8	21.7	27.1	10.1
9S27K	32°12.470'	89°35.570'	Eoc.	red sandst.	10/9	H	325-690° C	03/42	334.1	16.1	60.1	7.2
9S28L	32°12.036'	89°35.019'	Eoc.	red sandst.	10/-	(H)	-	(184/68)	-	-	-	-
9S29M	32°11.450'	89°35.205'	Eoc.	red sandst.	10/9	H	325-600° C	342/49	332.8	35.3	11.9	19.5
(2 Comp.)						H	650-690° C		347.5	29.6	28.2	9.9
10S30K	32°10.346'	89°34.163'	Eoc.	grey/red sand-/siltst.	10/9	H	350-580° C	220/85 ot	10.8	39.8	62.2	7.1
(2 Comp.)						H	630-690° C		18.8	39.3	30.7	10.1
10S31L	32°09.587'	89°33.158'	Eoc.	red/brown sandst.	10/9	H	400-620°C	104/45	18.9	28.1	14.4	13.8
(2 Comp.)						H	630-690° C		0.4	32.1	37.3	8.5
11S32K	32°10.838'	89°34.925'	Eoc.	grey/red sand-/siltst.	10/9	H	350-680° C	015/82	347.5	35.0	29.8	9.6
11S33L	32°10.751'	89°34.861'	Eoc.	grey/red sand-/siltst.	10/9	H	325-670° C	198/83	351.8	46.2	9.5	17.5

For explanations see Tab. 2.3-1.

The evaluation of the AMS revealed oblate and prolate susceptibility ellipsoids in the investigated rocks (Fig. 3.3-1). An undisturbed and undeformed sedimentary layer is characterised by oblate shape with k_{min} perpendicular to bedding. The oblate ellipsoid just represents the result of platy grains of hematite lying parallel to bedding or elongated magnetite grains with k_{max} randomly distributed in the bedding plane, or results from paramagnetic behaviour. Beginning tectonism with layer-parallel shortening (or regular-directed hydrodynamic forces during sedimentation) can be reflected in prolate shape. In the case of layer-parallel shortening the oblate ellipsoid representing bedding is changed into prolate shape with k_{max} perpendicular to the principal stress direction. The prolate ellipsoid forms when authigenic minerals grow under stress with k_{max} perpendicular to the principal stress direction. In the Zagaya area most of the samples display a corrected degree of anisotropy P' smaller than 1.03 which is – dependent on the

Table 3.3-1: *Palaeomagnetic results of sites from the Zagaya section*

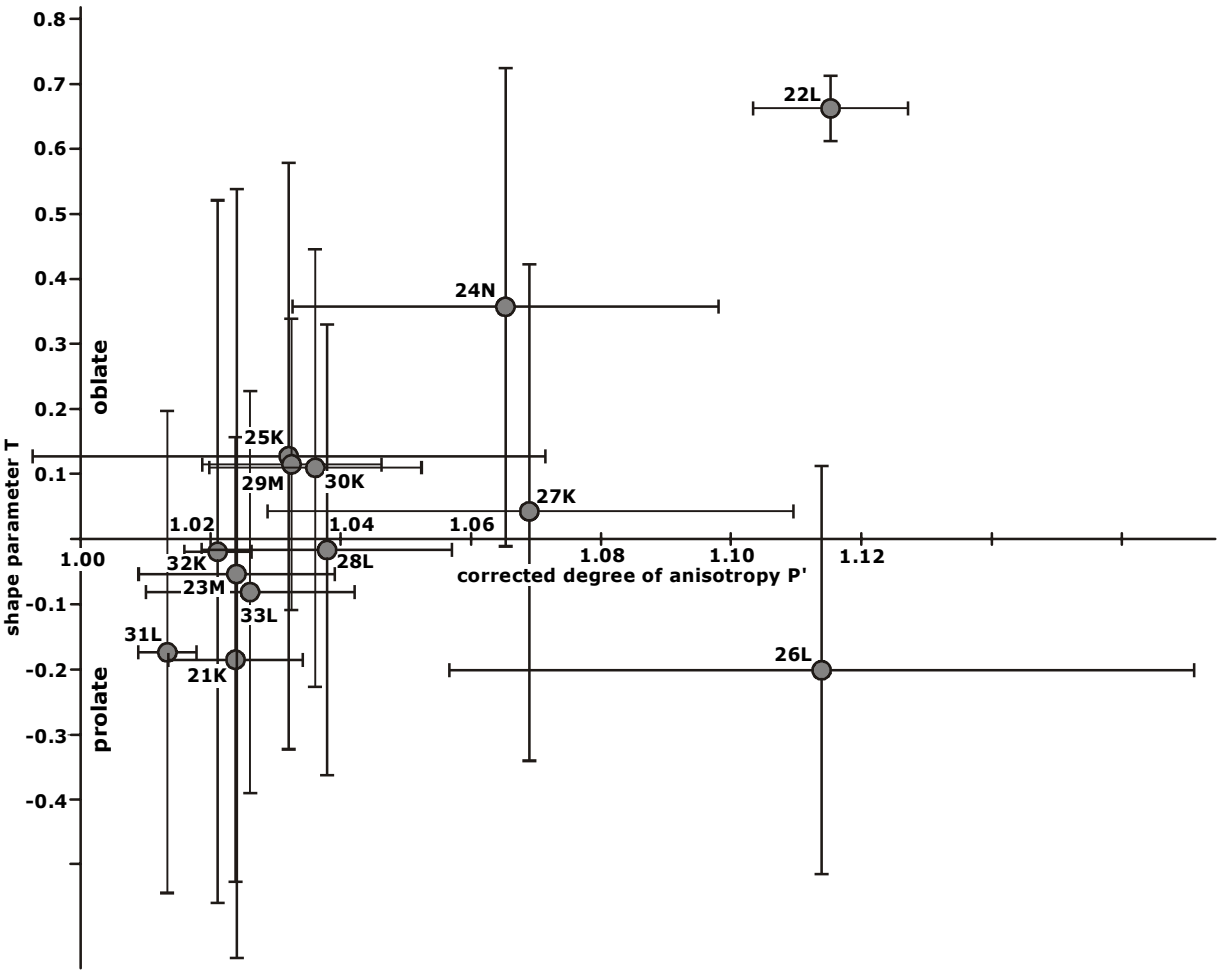

Fig. 3.3-1: *AMS investigation: Shape factor T plotted versus degree of anisotropy P' to characterise ellipsoid of AMS as prolate or oblate (after Jelínek, 1981). Arithmetic means of specimens, bars represent standard deviation.*

given mineral composition – typical for weakly deformed sediments. Additionally, the classification into sites with prolate and oblate AMS ellipsoid is in good accordance with the macroscopic geological observations: Sites 31L, 32K, 33L, and 27K are part of the tectonic imbricate and therefore more strained and mature than the other sites, which display an undisturbed sedimentary fabric. There is no unambiguous explanation for the prolate shape of the totally undeformed site 21K. But since this site is dominated by magnetite it may represent an example where elongated grains of magnetite were adjusted with their long axis in one direction by regular-directed hydrodynamic forces. Most of the samples show a good grouing of principle directions in

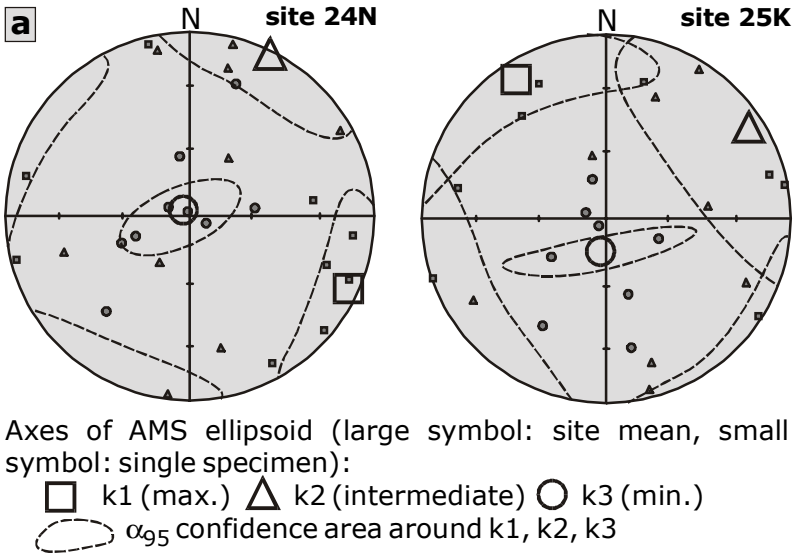

Fig. 3.3-2: *Lower hemisphere equal area stereoplots of AMS (anisotropy of magnetic susceptibility) of representative samples. a - oblate shape, b - prolate shape. All data bedding corrected.*

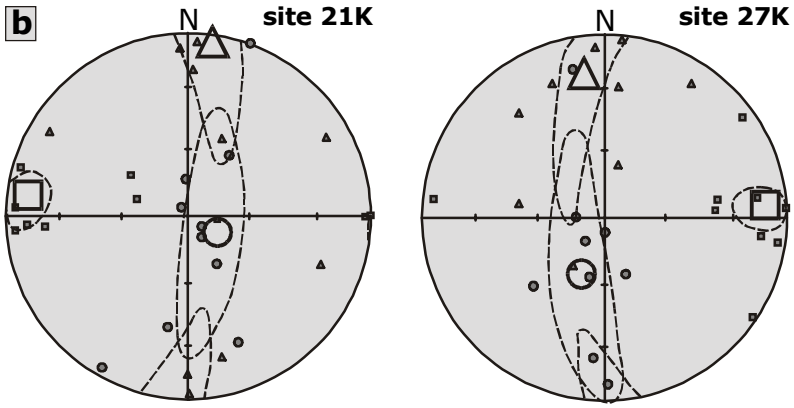

Fig. 3.3-2: *continued*

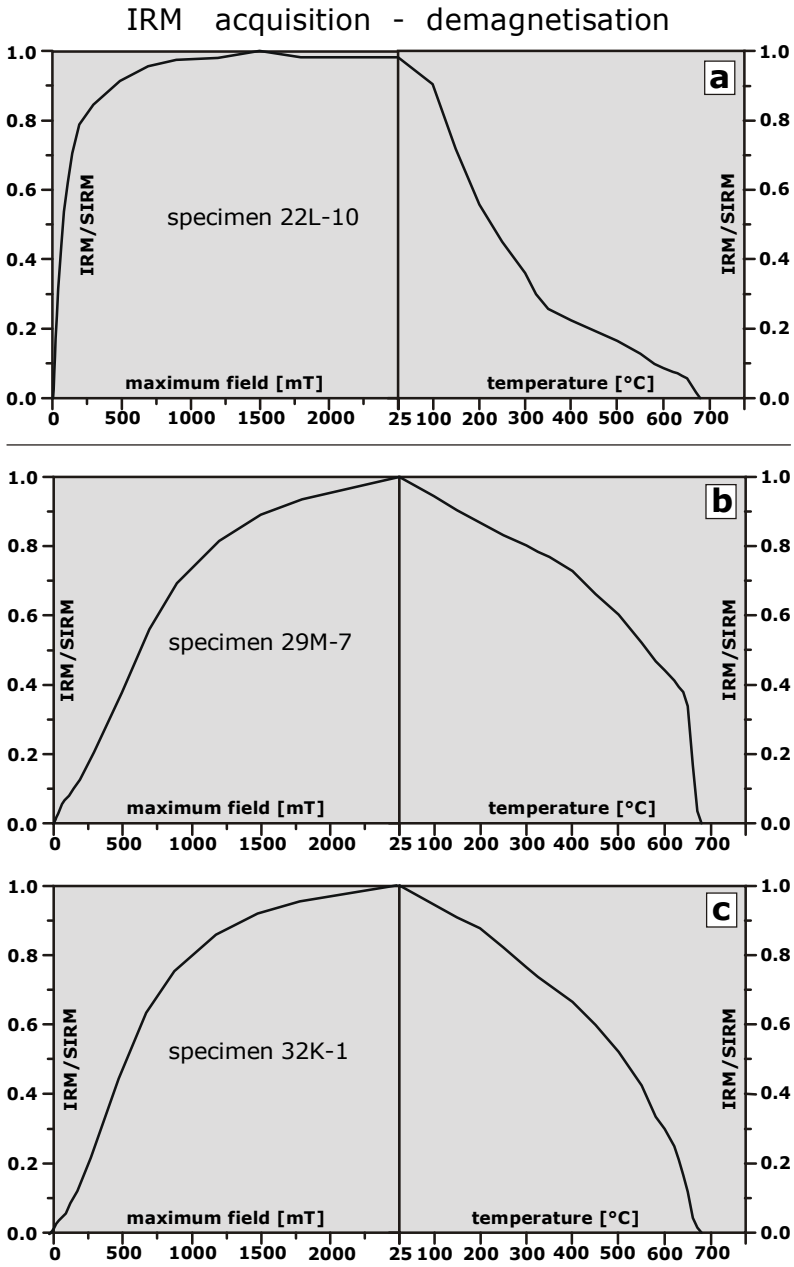

Fig. 3.3-3: *Representative curves for IRM (isothermal remanent magnetisation) acquisition and TH demagnetisation of sites from the Zagaya section. a - site 22L, contribution of magnetite to the magnetic spectra; b, c - sites 29M and 32K, hematite is dominating magnetic phase. SIRM - saturation IRM.*

the equal area stereoplots (Fig. 3.3-2) but unfortunately the database is to small to derive a systematic palaeo-stress field.

To provide first evidence for the identification of ferro(i)magnetic minerals, IRM measurements were carried out (Fig. 3.3-3). From IRM-acquisition and thermal demagnetisation curves of SIRM the investigated specimens can be divided into two groups: All Neogene sites in the SE part of the working area are dominated by magnetite as shown by relatively low saturation fields (Fig. 3.3-3a). Because 80% of saturation is reached at around 300 mT while complete saturation needs 1.5 T it is possible that there are also small amounts of a harder magnetic carrier (most likely hematite) in the mineral composition. The other group is represented by all Eocene sites which have consistent properties. Hematite is identified because no complete saturation of the IRM is reached at maximum fields of 2.5 T and because the IRM is unblocking predominantly at temperatures between 650 and 680° C (Fig. 3.3-3b/c). For 5 samples the observed run of the demagnetisation curve is more complicated (e.g. specimen 29M-7, Fig. 3.3-3b). It is inferred that the kink at ~630° C signifies an unblocking spectrum with possibly two heaite components, behaving magnetically harder and softer.

The differentiation between the two groups of samples is continued and supported by the respective Curie temperatures T_C

found during thermomagnetic investigations (Fig. 3.3-4). Crushed samples (not-extracted) from the Neogene layers exhibit heating curves with major decrease of susceptibility clearly defined at around 580° C, therefore identifying magnetite (Fig. 3.3-4a). The thermomagnetic curve of specimen 21K-6 is interpreted as showing new formation of magnetite during heating at ~500° C. Subsequently the magnetite signal is decreasing and at temperatures higher than $T_{C\ (Mag)}$ only some remaining hematite signal is seen. The new-build magnetite as interpreted from the heating curve is also evidenced by the strong rise in susceptibility during cooling.

In samples containing both, magnetite and hematite, the strong signal of magnetite (magnetically softer and spontaneous magnetisation 250 times higher than hematite) would dominate the result even with a minor contribution to the composition. The missing of any magnetite effect in the heating curves of Eocene samples (Fig. 3.3-4b) and the characteristic decrease at $T_{C\ (Hem)}$ is therefore identifying that only original hematite exists. The cooling curves of the hematite-bearing samples display a remarkable increase of susceptibility below 600° C because of the new formation of magnetite at higher temperatures. In the cooling curve of specimen 29M-3 two distinct increases at ~550 and 300° C give evidence for new formation of two magnetite components.

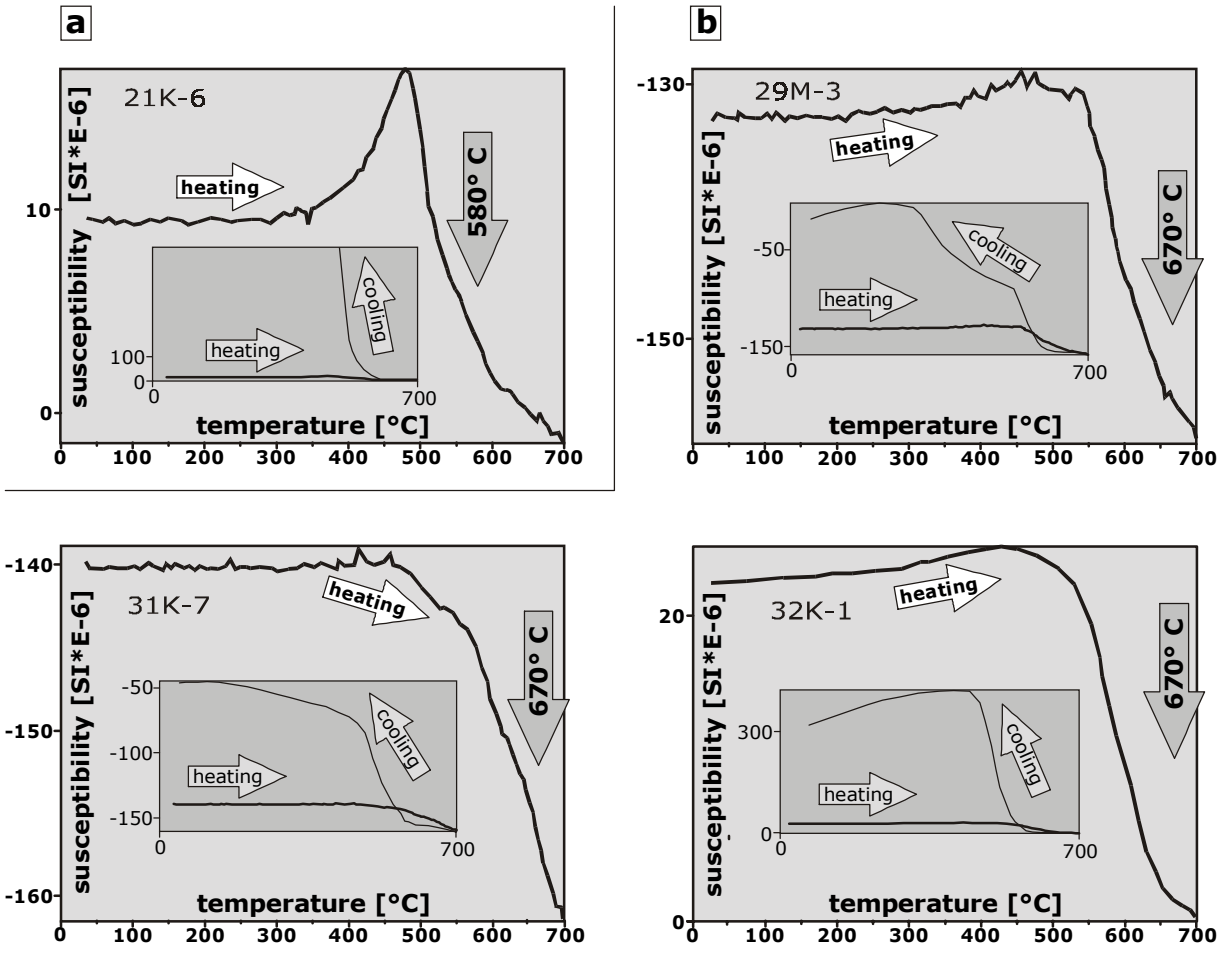

Fig. 3.3-4: *Thermomagnetic curves for representative specimens. The small inserts show both, heating and cooling; the large figures show the enlarged heating curves. a - example for sites dominated by magnetite, b - examples for sites dominated by hematite which converts into magnetite.*

In 12 of 15 sites NRM analysis revealed proper demagnetisation behaviour (Table 3.3-1).

A ChRM of sites from the SE area (Neogene) is demagnetised by AF treatment between 10 and 60 mT (Fig. 3.3-5a). It is carried by magnetite or magnetically softer hematite, or a mixture of both components which is in agreement with the IRM and κ-T investigations above. For most samples a

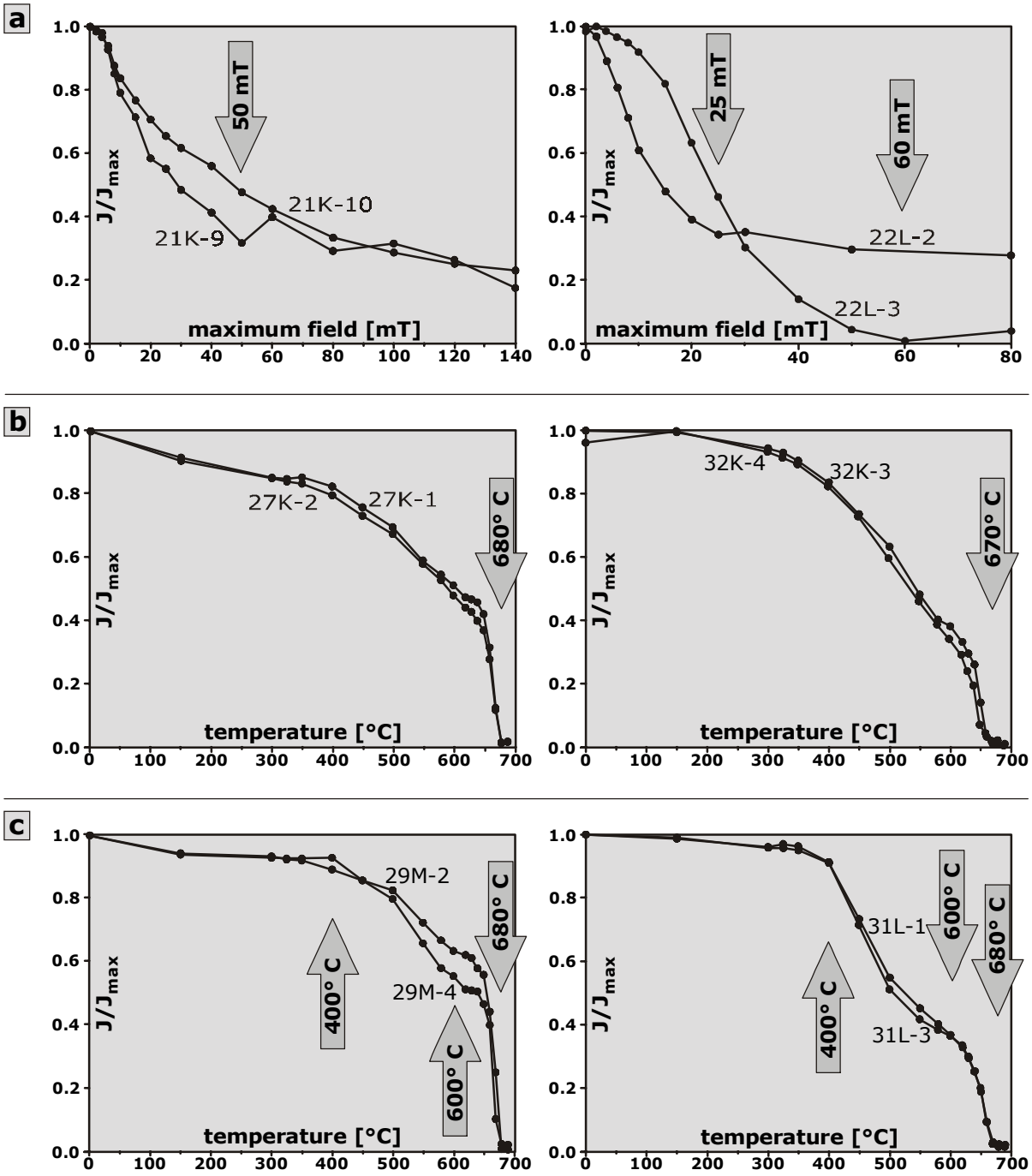

Fig. 3.3-5: *Representative demagnetisation behaviour of NRM of sites from the Zagaya section. a - AF demagnetisation of sites 21K and 22L, demagnetisation of magnetite between ~10 and 60 mT; b - TH demagnetisation of sites 27K and 32K, unblocking of one hematite component at ~680° C; c - TH demagnetisation of sites 29M and 31L, two hematite components (s. Fig. 3.3-6c) are demagnetised between 400 and 630° C, and above 650 °C.*

residual NRM component was remaining after AF demagnetisation and only in some cases (specimen 22L-3, Fig. 3.3-5a) the NRM could be removed completely. The residual magnetisation must be carried by a component with higher coercivity, which – according to IRM experiments above – should be a magnetically harder phase of hematite. The samples with a ChRM carried mainly by magnetite or magnetically softer hematite (or a mixture of both) exhibit a stable behaviour in the orthogonal vectorplot (Zijderveldplot, Fig. 3.3-6a). For all samples the demagnetisation path represents a straight line and with some exceptions (specimen 22L-2, Fig. 3.3-6a) it points directly to the origin.

The red beds of the central section (Eocene) were demagnetised thermally (Fig. 3.3-5b/c). In most sites a viscous component accounting for up to 20% of the NRM intensity and with random distributed directions was found below ~300° C. After removal of this viscous component a stable ChRM carried by hematite could be separated. In 5 sites the ChRM consists of one hematite component, which unblocks in the temperature interval between ~350 and 680° C (Fig 3.3-5b). Again, this is in good agreement with the IRM and κ-T investigations. The demagnetisation path in the Zijderveld plots is

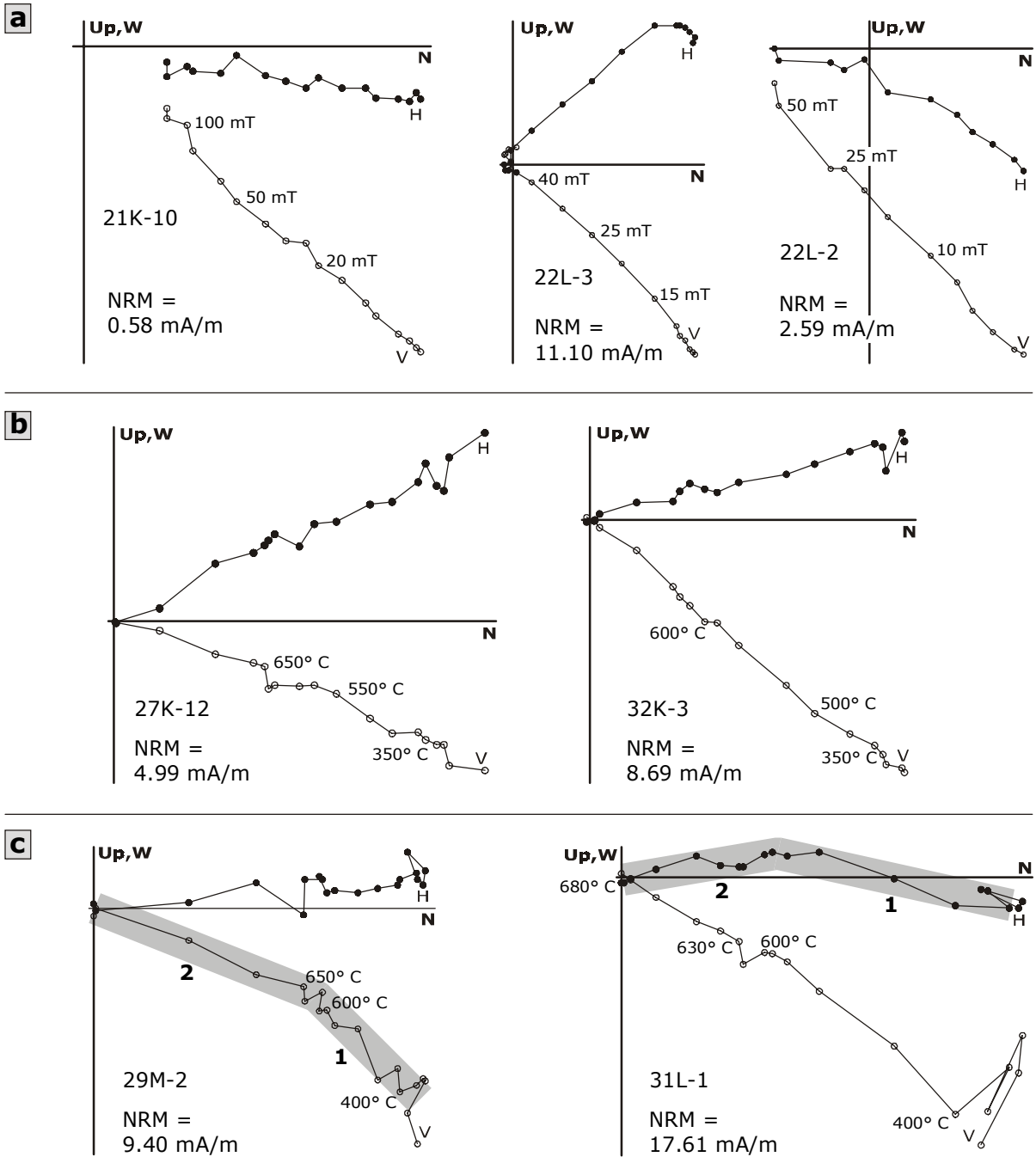

Fig. 3.3-6: *Orthogonal vector plots (Zijderveld plots) of demagnetisation behaviour of sites from the Zagaya section. H, V - horizontal, vertical projection. a - AF demagnetisation of sites 21K and 22L, magnetite is demagnetised between ~10 and 60 mT; b - TH demagnetisation of sites 27K and 32K, unblocking of one hematite component at ~680° C; c - TH demagnetisation of sites 29M and 31L, two hematite components (1, 2) are demagnetised between 400 and 630° C, and above 650 °C. All data bedding corrected.*

directed precisely towards the origin (Fig. 3.3-6b). In the case of the other 5 sites from the Eocene red beds the demagnetisation behaviour is more complicated and shows two ChRM components: A ChRM1, typically destroyed in a broad unblocking interval between ~350 and ~600° C, and a ChRM2 with unblocking between ~630 and 680° C (Fig. 3.3-5c). The demagnetisation path in the vector plot is showing a clear separation between the two straight segments of ChRM1 and ChRM2, the latter pointing directly towards the origin (Fig.3.3-6c). Because IRM and thermomagnetic investigations imply that the remanence of both components is carried only by hematite (Figs. 3.3-3b/c and 3.3-4b) ChRM1 and ChRM2 have to be explained by hematite of different grain size. Probably the ChRM1 is carried by hematite of ultra fine (pigmentary) grain size and the ChRM2 is carried by hematite of larger grain size.

3.3.2 Remanence analysis

For all samples included in statistics single specimen remanence directions with well-grouping site means and k-values between 9 and 62 are achieved (Table 3.3-1).

The geographical distribution of sites is in that way that six sites with unclear structural position are situated within a small zone on the bank of Zagaya river in the SE of the working area (Fig. 3.1-1). Two of these sites could not contribute to the palaeomagnetic results because they do not show proper magnetic behaviour. All of the remaining nine sites are strung along a straight N-S-trending section in the centre of the working area and eight of these sites yielded results which could be included in statistics (Fig. 3.1-1 and Table 3.3-1). In order to reduce the "degrees of freedom" under these circumstances further interpretation was only performed on the palaeomagnetic results of sites from the central section between the two characteristic normal faults.

Despite the fact that the higher unblocking ChRM2 is generally clustering more clearly than the lower unblocking ChRM1 for both, ChRM1 and ChRM2, remanence acquisition prior to folding is evidenced by the significant fold test (after McElhinny, 1964) at the 99%-level (fold test for ChRM1 given in Fig. 3.3-7). Taking into account that only normal polarity is observed in the bedding corrected data and that reversals of the geomagnetic field are frequently occurring in the Tertiary remanences most probably have been remagnetised during a relatively short time period.

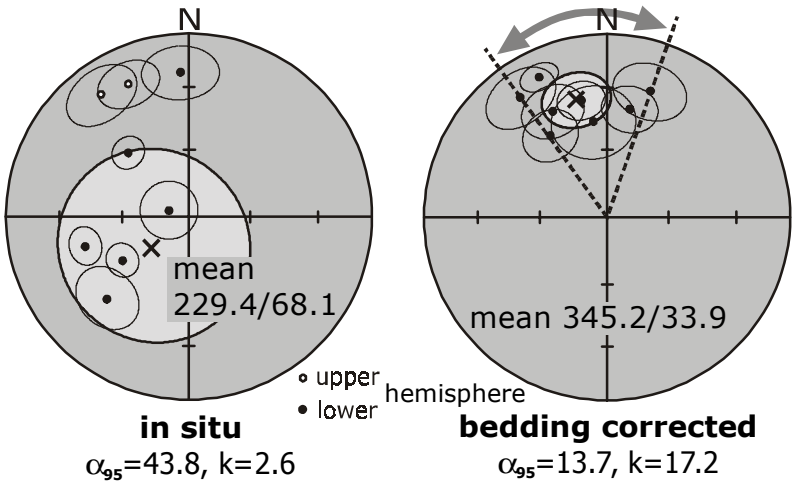

Fig. 3.3-7: *Fold test on 8 sites from the northwestern area of the Zagaya section. Fold tests (after McFadden and McElhinny) are significantly positive at the 99%-level. After bedding correction, declinations show a larger spread than inclinations. ChRM1 directions.*

It is difficult to judge whether ChRM1 or ChRM2 is older. Because remagnetisation sometimes has a "cleaning" effect on the remanence directions and thereby improves the grouping, it might be possible that the better-grouping ChRM2 is younger than the ChRM1, but both, of course, older than folding.

There seems to be some systematic difference between the mean directions of ChRM1 and ChRM2 since ChRM1 shows a larger counterclockwise rotation after bedding correction at three sites (Table 3.3-1). Nevertheless, the difference is not at the 99%-level of confidence (respective α_{95}-cones of the

two components overlap in most cases). Because of the overlapping means of ChRM1 and 2 differentiation between the two components plays no major role for the following interpretation and only the ChRM1 is discussed.

Thus, the calculation of stepwise unfolding (fold test after McFadden, 1990) was applied on ChRM1 directions of sites from the central Zagaya section. Best grouping of directions was received at 93% of unfolding (Fig. 3.3-8). This result is interpreted as a clear "pre-folding" acquisition of ChRM1 under the given geological conditions because the data set from only eight sites is small. Granted for example that some of the bedding measurements from relatively small outcrops in large-scale cross-bedded sediments are erroneous just by some degrees, which cannot be ruled out even when working to the best of one's knowledge, a misleading influence to the calculation of stepwise unfolding can be acquired easily.

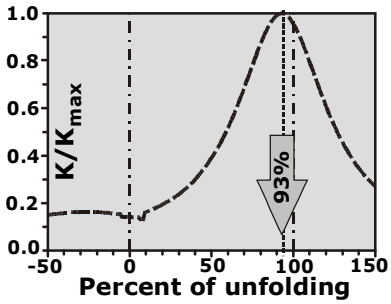

Fig. 3.3-8: *Stepwise unfolding applied on ChRM1 of 8 sites from the northwestern Zagaya section (after McFadden). Best grouping of directions at 93% of unfolding.*

3.3.3 Interpretation of remanence directions

Even though the mean directions from the central section pass the fold tests (after McElhinny, 1964; after McFadden, 1990) significantly positive at the 99%-level there is a striking effect in the set of bedding corrected data (Fig. 3.3-7): Declinations of sites from the central Zagaya section are remarkably spread. This distribution will be most crucial for the interpretation in the following chapter.

Before, a brief look on inclinations of sites from the central Zagaya section shows 10°-30° lower values (Table 3.3-1) than expected for a stable Eurasia from the APWP (apparent polar wander path) by Besse and Courtillot (1991). But referring to many results from Tertiary red beds in central Asia a 15°-30° shallower inclination ("the low inclination anomaly problem") could be considered as the expected normal case (Cogné et al., 1999; Thomas et al., 1993; Gilder et al., 1993; Gilder et al., 1996; Zhao et al., 1994). One possibility to explain the discrepancy between predicted and observed palaeolatitudes is found in nonridgid behaviour of the Eurasian plate in the Tertiary combined with intracontinental shortening of Asia under the penetration of India (Cogné et al., 1999). Although the results from the Zagaya section are scattered (calculated latitudinal difference amount to 15° within the section) they seem to support this model. The scattering could be explained as effect of primary inclination flattening of different magnitude during sedimentation and diagenesis. Alternatively, the large spreading of palaeolatitudes assembled in a relatively small area could result from long wavelength folding prior to remanence acquisition. This interpretation could not be ruled out by the fold test (Fig. 3.3-8) that indicates 7% of folding to have occurred before remanence acquisition – even tough the fold test is more likely significant for pre-folding acquisition of the remanence (see above).

In order to investigate the spatial distribution of rotations, declinations were projected into a straight N-S-line, which is perpendicular to the truncating strike-slip fault to the north (Fig. 3.3-9, see Fig. 3.1-1 for tectonic details). An interesting trend can be detected: The angle of counterclockwise rotation - with respect to declination of site 31L - increases to the north and thereby with proximity to the shear zone. The declination of site 31L was taken as a point of reference for the relative rotation because this site represents the farthest distance to the shear zone and is therefore most likely the least influenced. This is also supported by the fact that the declination direction of site 31L is approximately in accordance with the predicted post-Cretaceous declinations for stable Eurasia (Besse and Courtillot, 1991).

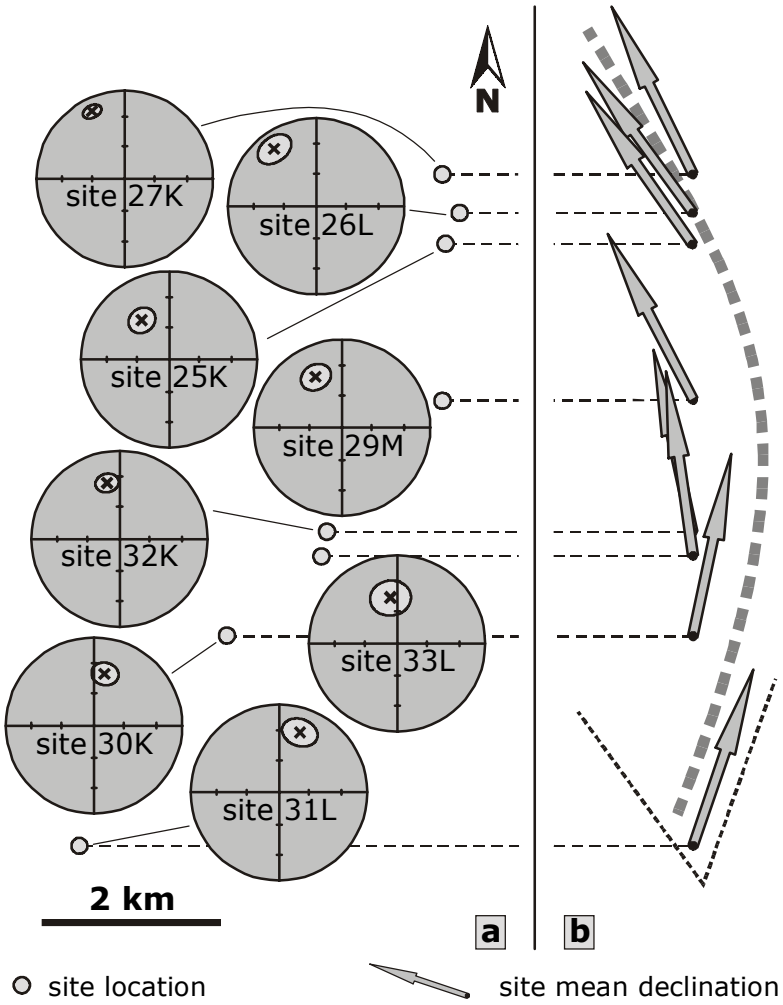

Fig. 3.3-9: *Spatial distribution of site mean directions. a - site mean directions in lower hemisphere stereoplots shown with site locations in map view, b - site mean declinations projected into N-S-line. All data bedding corrected.*

After the clear trend of increasing counterclockwise rotation towards north and with proximity to the shear zone is recognised the exact characteristics of this increase constitutes the next point to be analysed (Fig. 3.3-10). Based on this plot with amount of rotation versus distance to shear zone it can be seen that the increasing amount of rotation follows a linear trend. The maximum relative rotation happens between site 31L and site 26L and amounts to 55° while a gradient of rotation per distance of 8.1 °/km is determined graphically. The linear behaviour of the increase of rotation with proximity to the shear zone implies that the investigated sites underwent one uniform tectonic movement.

At least three discriminable geological events took place in the working area, which are (a) sedimentation and acquisition of primary remanences, (b) folding with shortening and tilting of remanences, and (c) block rotation around vertical axes with rotation of remanences. The question for the correct chronological order of these events cannot easily be solved because it defies direct palaeomagnetic control whether folding or block rotation occurred first. Two pos-

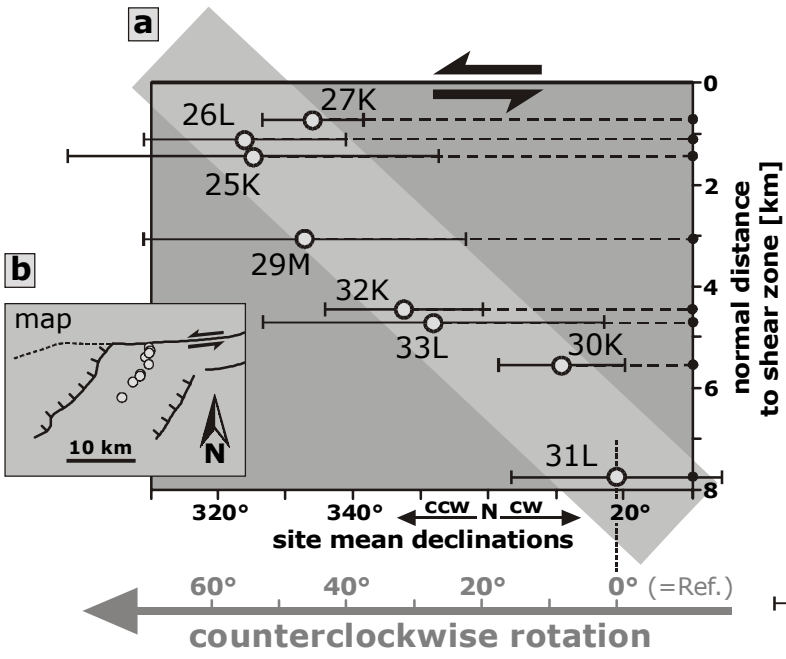

Fig. 3.3-10: *Rotation with distance to shear zone. a - amount of rotation versus normal distance to shear zone, b - tectonic sketch map. ccw - counter-clockwise, cw - clockwise.*

sible cases for the chronological order of geological events are presented in a schematic comparison (Fig. 3.3-11). One plot (Fig. 3.3-11a) is identical with the original data presentation in Fig. 3.3-10 while for the other the distribution of declinations was broadened graphically (Fig. 3.3-11b). This provides a speculative illustration for the case that folding would have postdated block rotation. It is obvious that the coordinate axis of normal distance to shear zone carries only "recent" and therefore fixed information about localities (Fig. 3.3-11). In contrast the values on the coordinate axis of site mean declinations vary greatly with different geological settings and thus could provide important information about the chronological order of palaeo-events (see two possible cases in Fig. 3.3-11). An intense and heterogeneous folding as it affected the Zagaya unit (Fig. 3.2-2) that happened after block rotation would have spread the declinations (Fig. 3.3-11b) and would have prohibited a well-defined linear trend. Under the presumption of a systematic and simple solution for the chronological order of tectonic events as the likeliest the linear trend of declinations in the original data set (Fig. 3.3-10) demonstrates that folding predates block rotation in the Zagaya section.

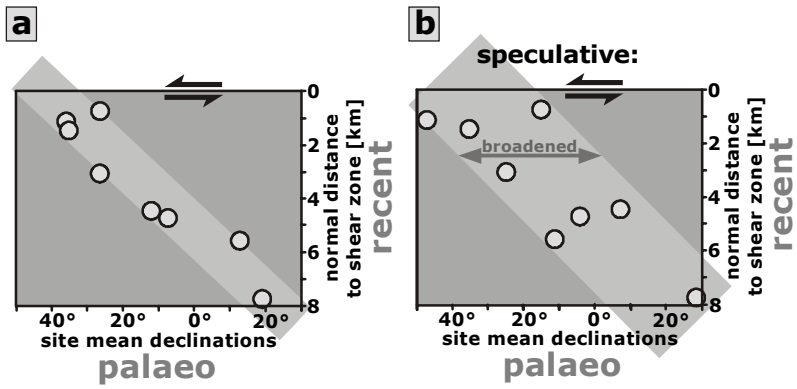

Fig. 3.3-11: *Schematic comparison of two possible cases for the chronological order of geological events. a - folding predates block rotation, simplified after Fig. 3.3-10; b - (speculative) folding postdates block rotation. Note that axis of "normal distance" could give only recent vaues while axis of "declinations" carry palaeo-information about geological processes. See Fig. 3.3-10 for symbols and site names.*

3.4 Discussion of tectonic models

3.4.1 Possible tectonic models

It will be discussed now which tectonic model could explain the declination pattern of sites from the Zagaya section most consistently. Different models (modified after Nelson and Jones, 1987) show theoretical counterclockwise declination and block rotations when deforming an initial squarish block at a left-lateral fault (Fig. 3.4-1). The models are characterised by (A) domino-style block rotation with antithetic shear, (B) continuous simple shear, and (C) small blocks with variable internal rotation. By comparison with the original declination pattern measured in the Zagaya section the different models can be evaluated. In model A only two

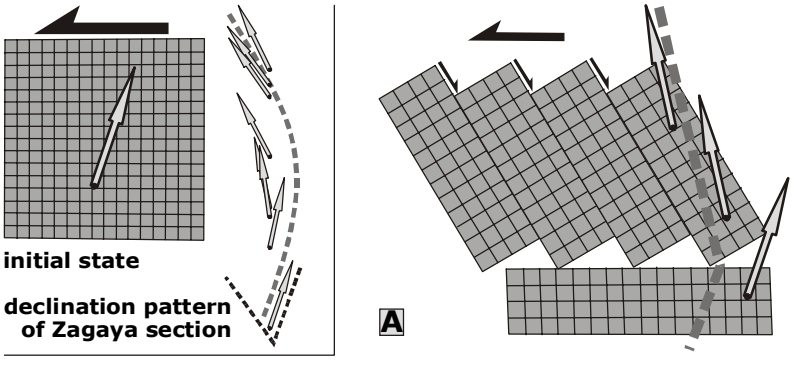

Fig. 3.4-1: *Three different tectonic models explain left-lateral simple shearing of an initial square. Comparison of resulting declination pattern with declination pattern of the Zagaya section. A - domino-style block rotation with antithetic shear, B - continuous bulk simple shear, C - small block model with variable internal rotation. Modified after Nelson and Jones (1987).*

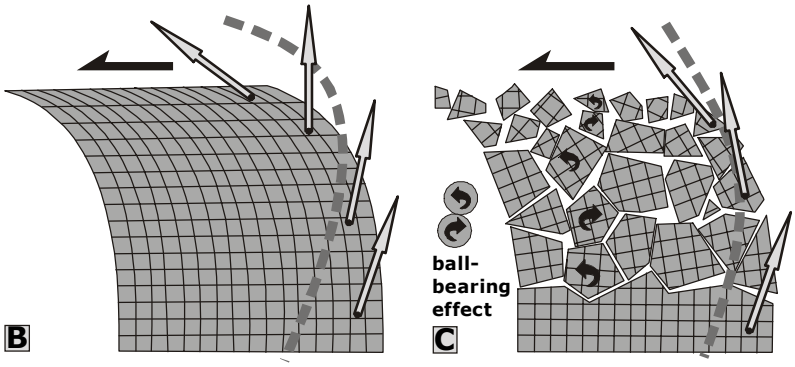

Fig. 3.4-1: *continued*

distinct declinations are realised on domino-style blocks. This resembles the given structural geometry but is not in agreement with the found declinations. In model B the northernmost declinations are approaching the fault asymptotically while the initial block is deformed homogeneously. This model does neither show the correct declinations nor represent the correct structural pattern. The declination pattern of model C is in very good accordance with the declination data of the Zagaya section. But this small block model with variable internal rotation does not correspond to the described structural pattern which was analysed in the field and from the TM image (Fig. 3.1-1). Additionally, the original model C (Nelson and Jones, 1987) does not take into account that variable internal rotation of small blocks will also result in clockwise rotation for some of the fragments because of ball-bearing effects (s. Fig. 3.4-1, C).

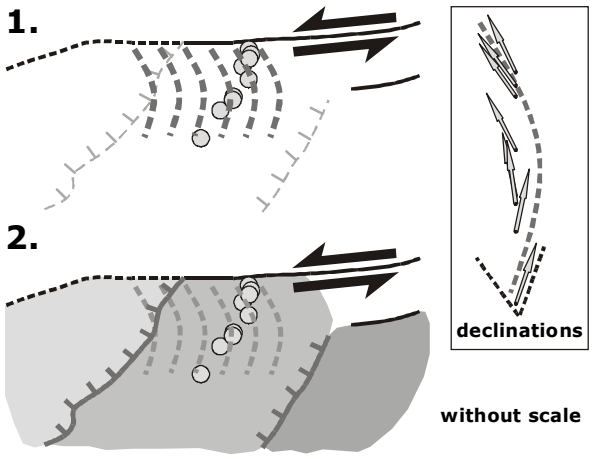

Fig. 3.4-2: *Principal sketch of two post-folding deformation phases in the Zagaya section. 1. internal deformation, 2. normal faulting, break-up of blocks. Symbols as in Fig. 3.1-1.*

Synthesising the different arguments on common models it seems to be the most possible solution to explain the post-folding deformation in the Zagaya section as two-phase: Internal small-scaled left-lateral brittle shear as seen from declinations is followed by normal faulting with the break-up of blocks as youngest stage (Fig. 3.4-2).

3.4.2 Tectonic interaction in the central northern Lhasa block

The findings presented above are summarised in brief: (1) The Zagaya section within the northernmost Lhasa block is dominated by Eocene red sediments and an ophiolitic melange. (2) The section is intensively folded, shortening estimated with about 60%, and calculated σ_1 principal stress axes trend ENE. (3) Stable characteristic remanences acquired prior to folding are mainly carried by hematite. (4) Declination directions within the central section show counterclockwise rotations increasing with proximity to the truncating left-lateral strike-slip fault in the north. (5) Folding predates block rotation because the rotation of declinations shows a linear increase. (6) Common models fail to explain both, the recognized declination pattern and the structural features. (7) Deformation seems to be two-phase with internal small-scaled brittle shear followed by normal faulting and the break-up of blocks as youngest stage.

From these detailed results a left-lateral tectonic inventory for the deformed section is concluded. Assigning this interpretation into a slightly larger image means that pre-existing structures within the Bangong-Nujiang suture zone respond with left-lateral reactivation to post-collisional deformation. Furthermore the left-lateral structure bounding the Zagaya section could be part of a conjugated fault branch to the right-lateral Karakoram-Jiali fault zone (Fig. 3.4-3). Finally, this constellation fits in the well-established large-scale pattern of eastward lateral extrusion of continental blocks due to frontal compression in the course of the India-Asia collision (Tapponnier et al., 1982).

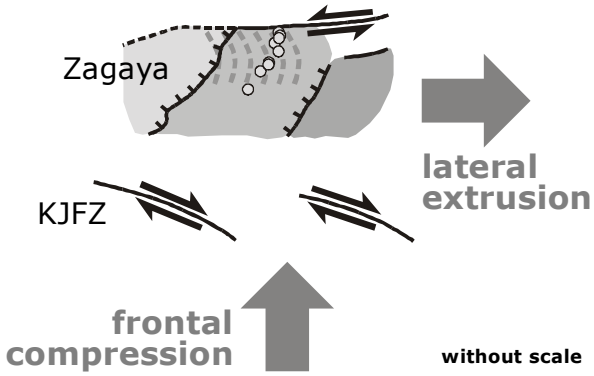

Fig. 3.4-3: *Principal sketch of tectonic interaction in the central northern Lhasa block. Symbols as in Fig. 3.1-1. KJFZ - Karakoram-Jinsha fault zone.*

4 Further palaeomagnetic and structural investigations from several areas within the scope of the INDEPTH 3/GeoDepth expeditions - implications for future work

4.1 Northern Lhasa block

4.1.1 Investigations in the Nam Tso area: Results from the Baoji section

The section was named after the village of Baoji situated N31°00', E90°10', approximately half way between Bangong and Deqen at the foot of some dominating limestone ridges.

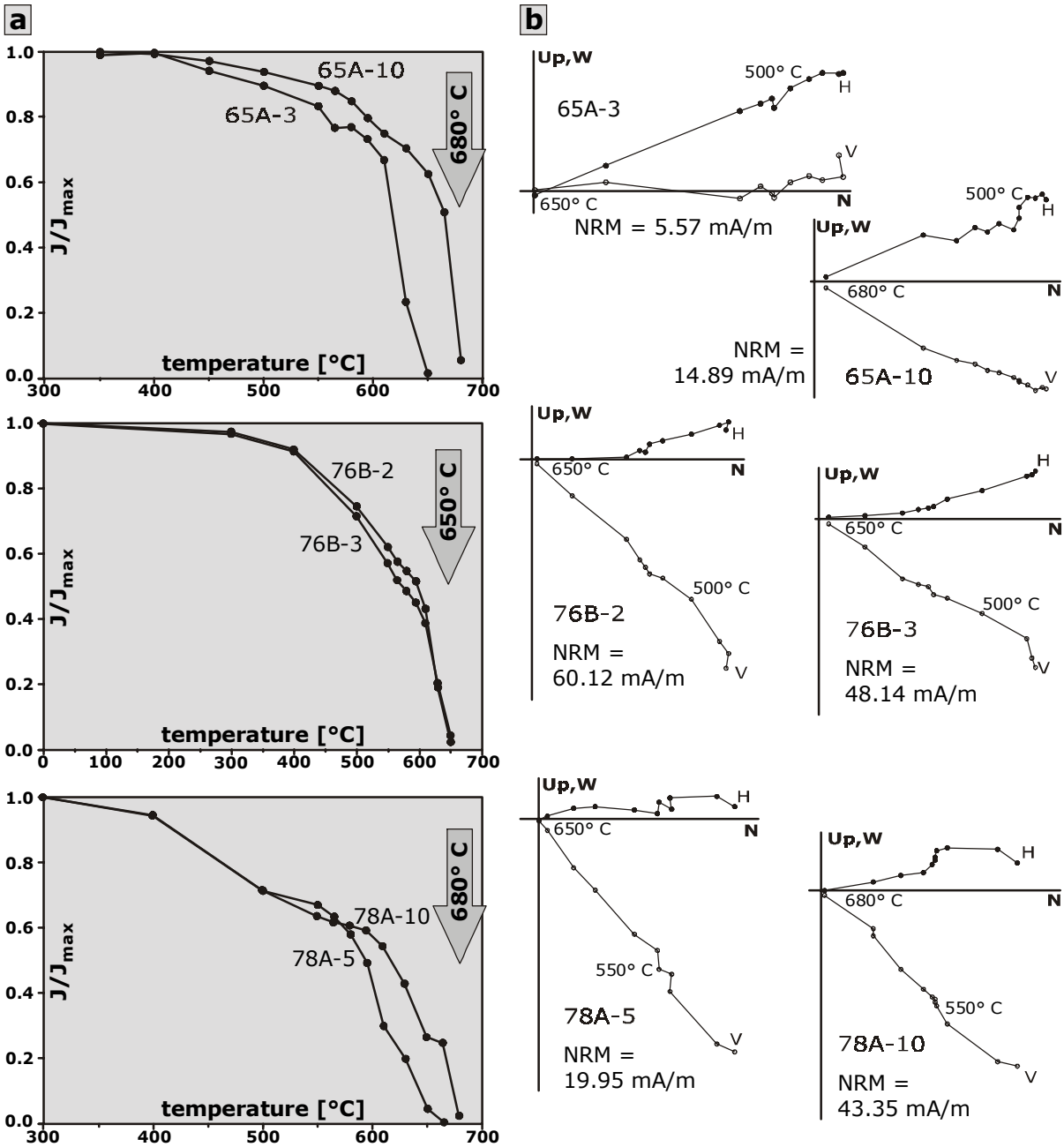

Fig. 4.1-1: *Representative examples of demagnetisation of sites from the Baoji section. a - TH demagnetisation, b - orthogonal vector plot (Zijderveld plot) of TH demagnetisation, data bedding corrected.*

To the north of Baoji the sequence consists mainly of folded sand-/siltstones (mostly redbeds) and massive limestone ridges, both of probably Cretaceous age. To the south of Baoji the investigation of the sequence is complicated by more discontinuous outcropping and "exotic" members, the latter giving reason to assume an ophiolitic origin. The southernmost part of the sequence in the vicinity of Deqen is dominated by acid to intermediate volcanics, of most likely Cretaceous age.

At 14 sites 138 orientated core samples were obtained. Most of the sites (11 of 14) show a stable magnetic behaviour with well-grouped specimen directions. However, site mean directions are dispersed.

Characteristic remanences in red beds are carried by hematite, with one component being demagnetised at 650-680° C (Fig. 4.1-1a). Orthogonal vector plots show straight demagnetisation paths (Fig. 4.1-1b). Characteristic remanences in volcanics are carried by hematite and magnetite respectively as shown by subsequent AF and TH demagnetisation (Fig. 4.1-2). But both components show identical directions.

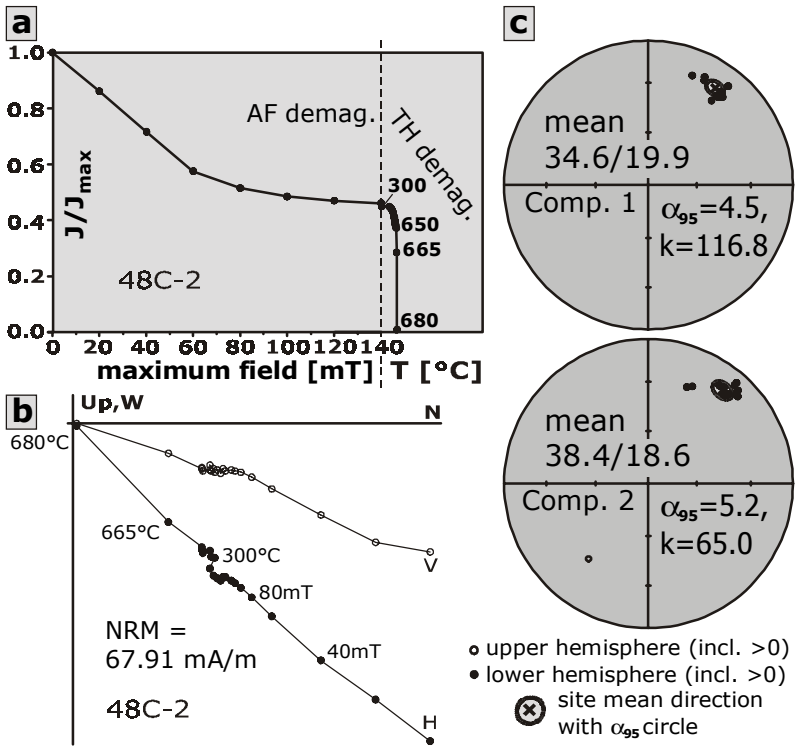

Fig. 4.1-2: *Comparison of two ChRM components of site 48C showing identical directions. a - AF and TH demagnetisation, b - orthogonal vector plot (Zijderveld plot) of demagnetisation behaviour, c - equal area stereoplots of magnetite and hematite component. All data bedding corrected.*

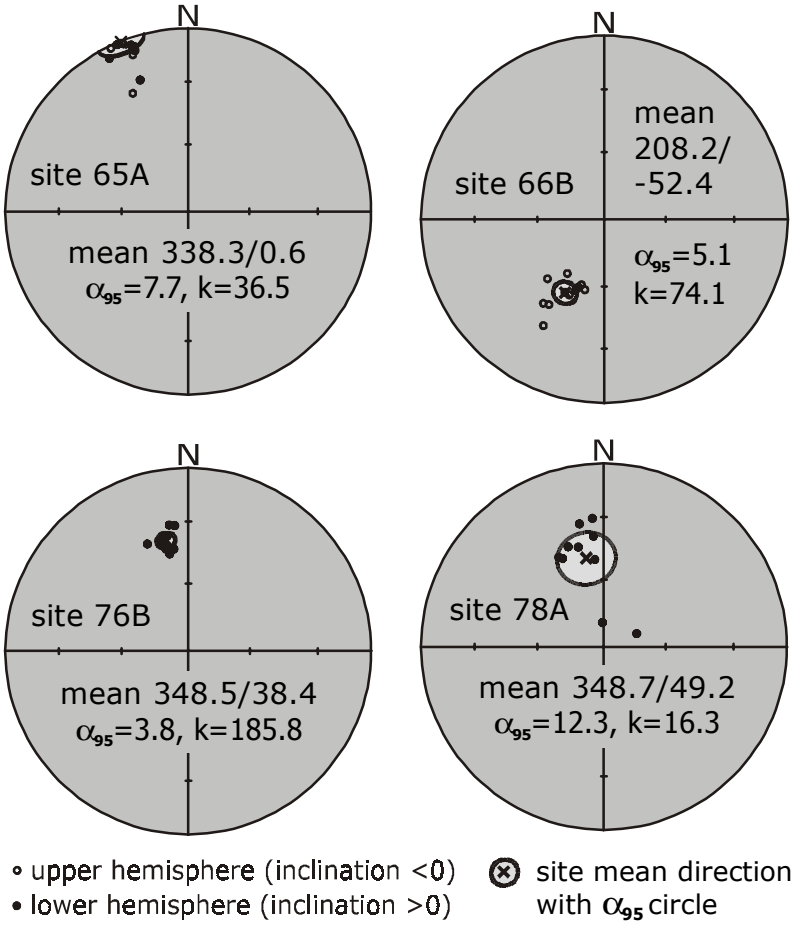

Fig. 4.1-3: *Equal area stereoplots of representative distributions of single specimen remanence directions within sites from the Baoji section (s. also site 75A, Fig. 4.1-4). All data bedding corrected.*

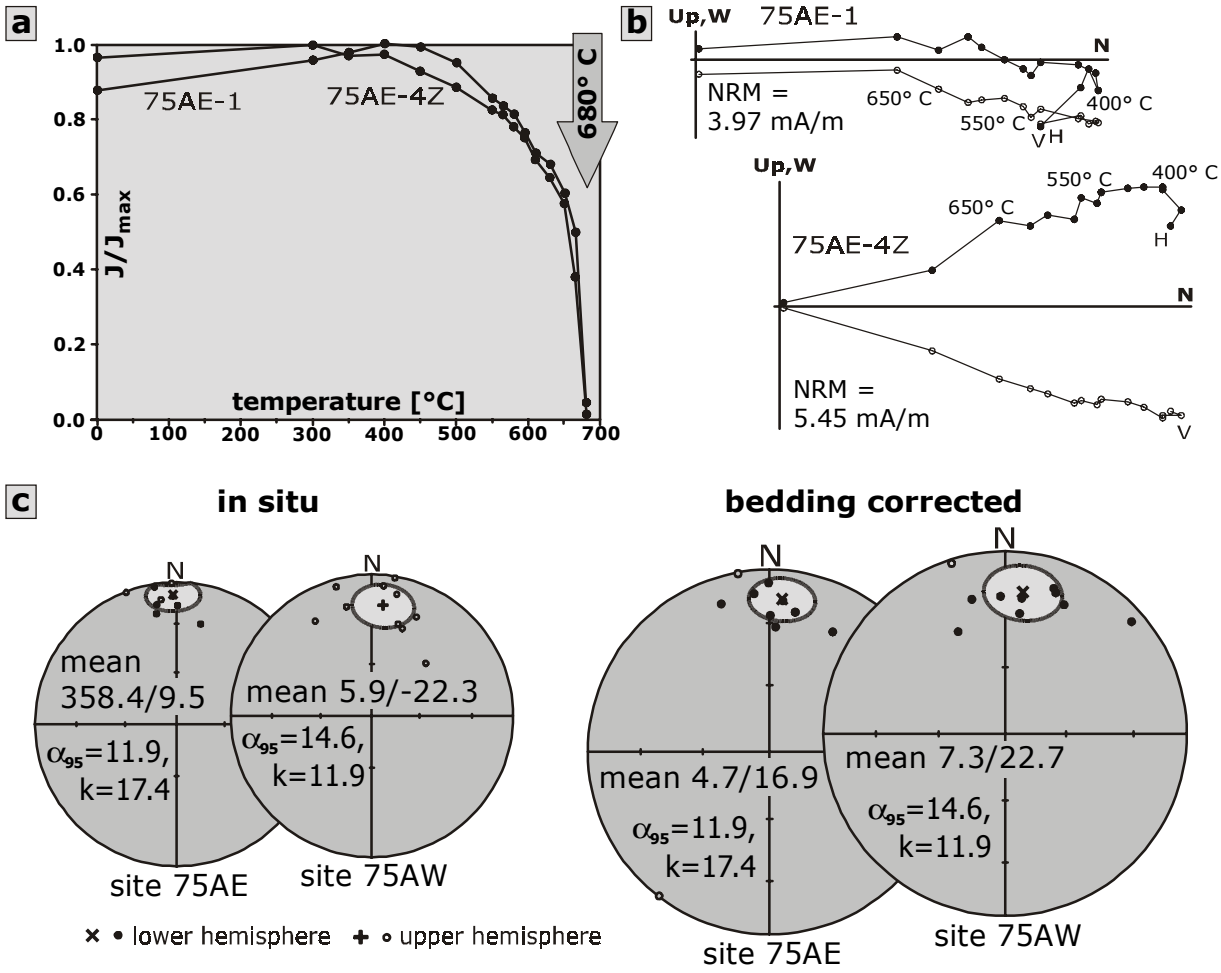

Fig. 4.1-4: *Baoji section. a - representative demagnetisation behaviour of specimens from site 75A, unblocking of hematite at 680° C; b - orthogonal vectorplots (Zijderveldplots) of demagnetisation behaviour of site75A. H, V - horizontal, vertical component, data bedding corrected; c - lower hemisphere equal area stereoplots of in situ and bedding corrected remanence directions (foldtest). 75AE - eastern limb, 75AW - western limb.*

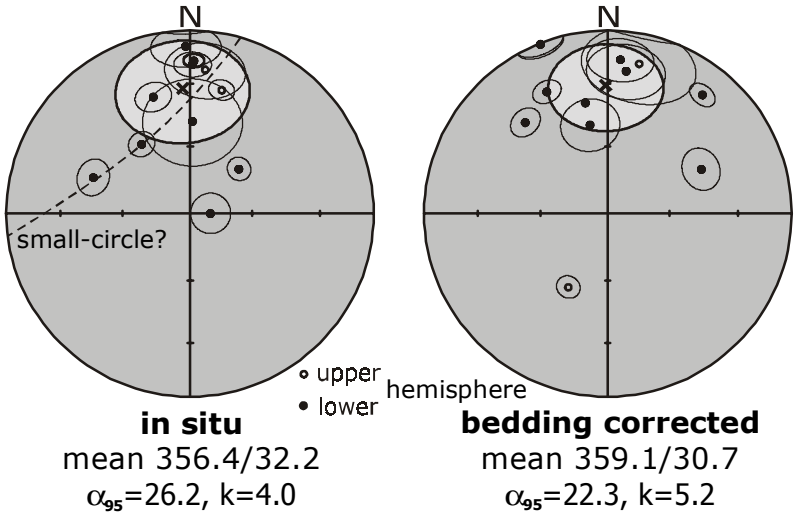

Fig. 4.1-5: *Fold test on results from the Baoji section, northern Lhasa block. No significance.*

Values for precision parameter k within sites range from 16 to 185 (Fig. 4.1-3). Concerning the separated directions it is conspicuous that results from similar rock types show nearly the same directional data (example 78A, 76B) while results from sites which are situated nearby (example 75A) but differ in rock composition and grain size show deviating results. At site 75A with samples from two limbs of one local fold it is evidenced that the remanence was acquired before folding (positive fold test) (Fig. 1.1-4). Nevertheless, the over-all fold test for the data set of the whole section is of no significance (Fig. 4.1-5).

Because a renewed geological map of the section is just in preparation the palaeomagnetic declinations are shown in a sketch on base of simple locator map (Fig. 4.2-6). It is obvious that the distribution of declinations absconds from a simple explanation. Especially the existence of both dispersed site mean directions and well-grouping single remanence directions seems to be paradox. It might be possible that there are some structural features not identified as yet which complicate the analysis. But an alternative explanation is to assume the separated remanences to be of syn-orogenic character and therefore different remagnetisation age. In this case, a fold test is not the appropriate tool to describe parts of the magnetic and geological history of the investigated area. Instead, it seems to be promising to test the idea of syn-orogenic remanence acquisition and therefore small-circle distribution (s. Fig. 4.1-5) with an extended data set and apply the method of small-circle reconstruction (Waldhör et al., 2001). However, the area in the northern Lhasa block is distinguished by easy accessibility with moderate field difficulties and predestined hence for further sampling, precise geological mapping, and structural investigations to provide a reliable base for any more advanced study.

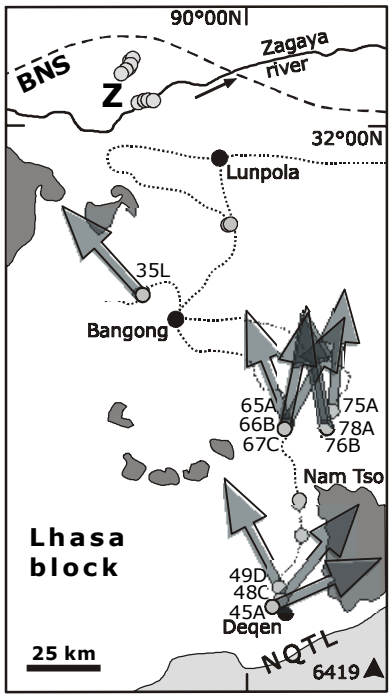

Fig. 4.1-6: *Sketch map with declinations from sites of the central Lhasa block. Data bedding corrected.*
BNS - trace of Bangong-Nujiang suture. Z - Zagaya section, see chapter 3. NQTL - Nyaiqentangh La range. Further explanations as in Fig. 1.2-1.

4.1.2 To the north of Duba basin thrust and Bangong granite: Structure of a folded section

An example for fault plane striae data analysis with the results of stress inversion treatments calculated after Ratschbacher et al. (1994) is shown in Fig. 4.1-7.

The location is situated on the Lhasa block, ca. 70 km to the south of the Bangong-Nujiang suture where deformed phyllites of probable Cretaceous age are in contact with massive limestone ridges (see sketch, Fig. 4.1-7a, c). The steep-dipping phyllites are tightly folded (fold axes mainly trending EW, Fig. 4.1-7b).

Four homogenous populations of fault plane striae data were separated from the complete data set indicated by well-grouping principal stress axes. From field constraints (different generations of fault plane striae were discriminated by using overprint and cutting criteria) the most probable chronological order is as follows:

(a) a less pronounced NE-SW compression,

(b) a very prominent thrust movement resulting from NNE-SSW compression, followed by

(c) a dextral strike-slip system under NW-SE compression, and

(d) as possible finale stage some normal faulting. Under the thrust regime (population b) bedding planes of the intensively folded member were frequently activated as fault planes (see bedding in Fig. 4.1-7b).

Even if this is just an investigation at an isolated spot it is possible that the different stress directions described above are consistent over larger areas. Data from other stations should be taken to find out about the likeliness of this assumption.

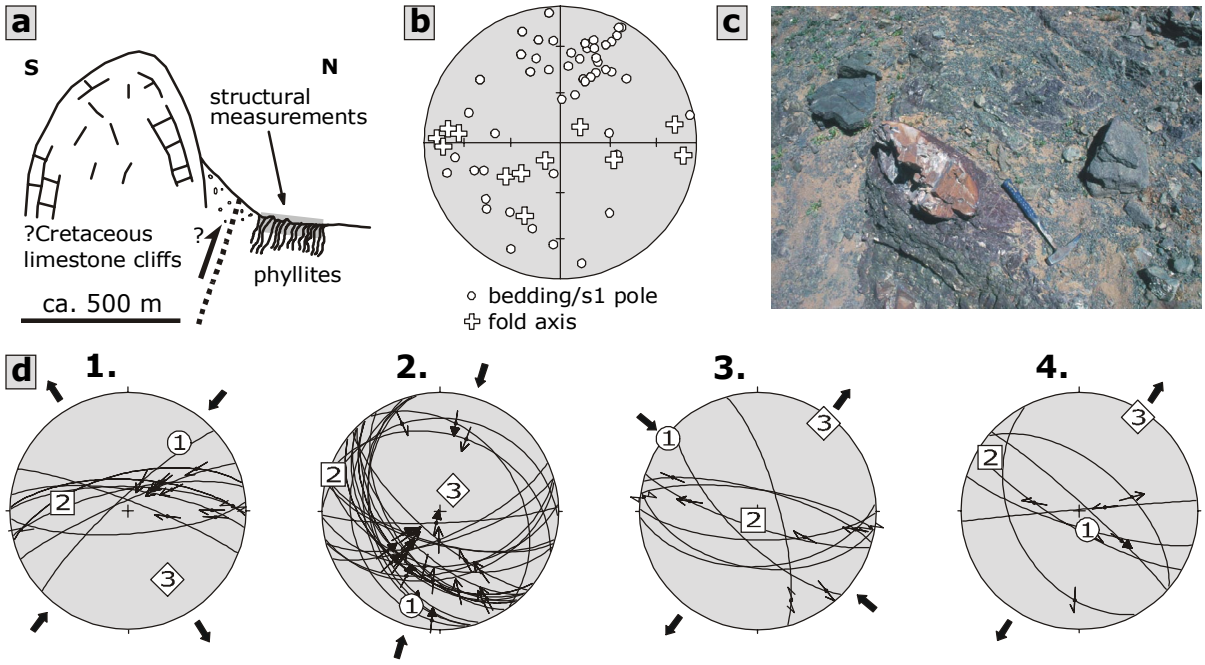

Fig. 4.1-7: *Structural analysis of section in the northernmost Lhasa block, ~70 km to the south of the Bangong-Nujiang suture at N31°45.700/E89°50.600. a - sketch of profile, b - lower hemisphere equal area stereoplot of bedding and fold data, c - field shot of deformed phyllites, d - fault plane striae data (symbols as in Fig. 2.2-3), separation of four successional populations.*

4.2 Qiangtang block

4.2.1 The Shiagar mountains (Shuang Hu dome)

Geography

The Shiagar mountains (Shuang Hu dome) lie to the west of the village of Shuang Hu (4920 m; E88°45', N33°15') which is reached after one hard off-road day from Lunpola base camp (Figs. 4.2-1, 1.2-1). It represents the last permanently inhabited settlement when approaching further north into central areas of the plateau.

The Shiagar mountains are characterised by relatively steep slopes and cliffs in the frontal parts and moderate slopes when coming to the internal areas. They rise from ~5000 m to elevations of 6300 m with 6340 m being the highest (nameless) peak.

Geology; previous work

The Shiagar mountains have been recognised as a metamorphic core complex with blueschist melange outcropping in the central part (Kapp et al., 2000). After them Blueschist was subducted towards south under the Qiangtang block during Triassic times when the Jinsha suture was active. In Upper Triassic to Lower Jurassic the metamorphic core was exhumed along low-angle normal faults (detachment faults). The Shiagar mountains range is flanked by red beds of maximum Cretaceous age.

The SSW-NNE-trending Shuang Hu graben bounds the mountains to the east. INDEPTH 3 participant Peter Blisniuk and his group studied this feature in detail (Blisniuk et al., 2001).

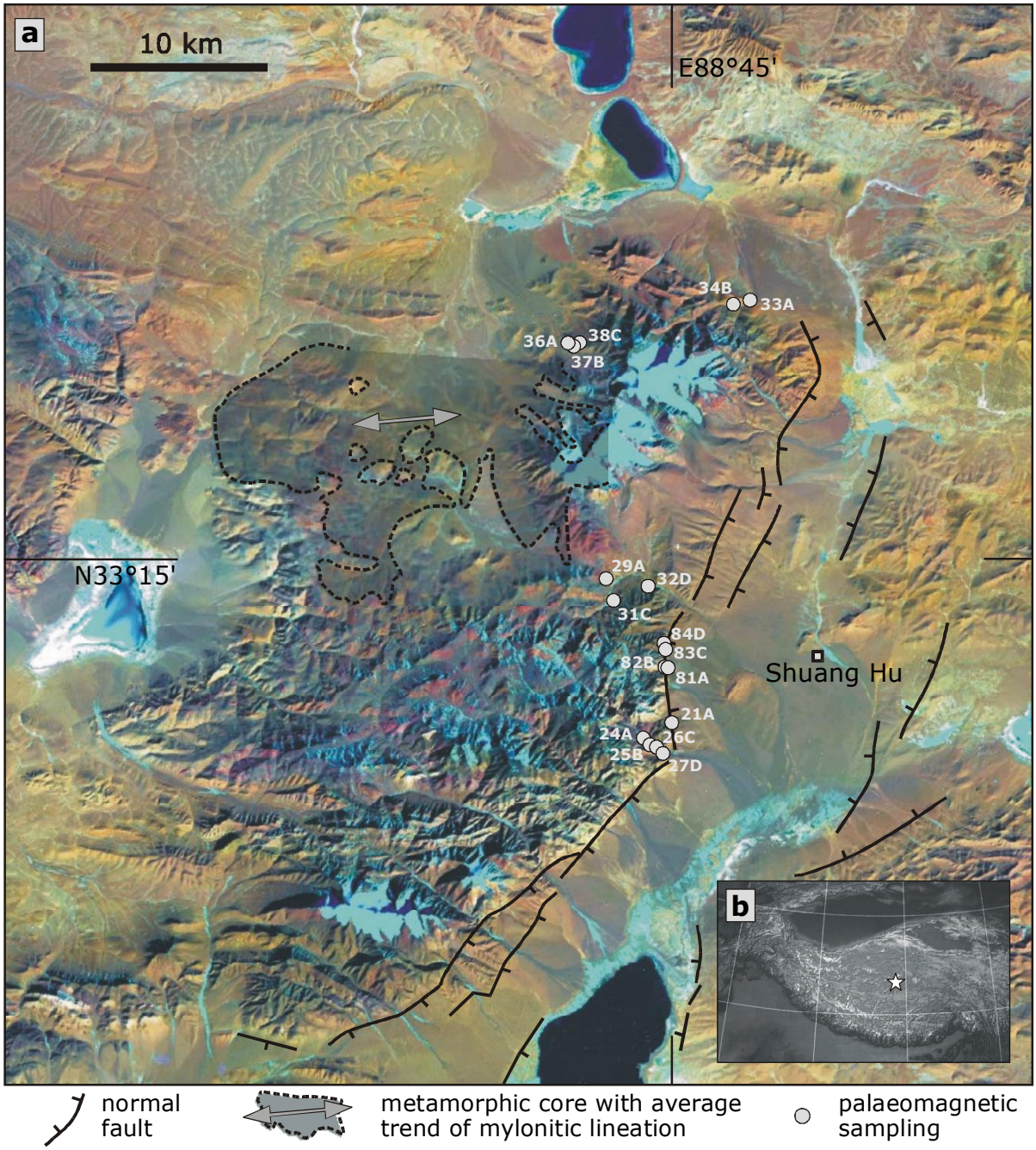

Fig. 4.2-1: *Shuang Hu area (Shiagar mountains). a - TM image with site locations; graben-bounding normal faults after Blisniuk et al. (2001); metamorphic core simplified after Kapp et al. (2000); b - star shows location of Shuang Hu area in central Tibet.*

Magnetic properties, palaeomagnetic constraints

The magnetic results in the Shuang Hu area are more dispersed than in other investigated areas. This seems to be due to strong lithological inhomogeneities, heavy weathering, and mechanical destruction (all could be somehow connected to the domal tectonics).

At 17 sites in the red beds of maximum Cretaceous age 170 orientated core samples were obtained. The results of magnetic measurements from 14 sites were utilisable for further interpretation (firstly, the quality of grouping of directions was disregarded). The remanences are dominated by a hematite component which is demagnetised at around 680° C (Fig. 4.2-2); one site (24A, Fig. 4.2-2b) shows two (anti-parallel) components which are demagnetised at 350° C and 580° C respectively. These temperatures lie in the unblocking range of magnetite but there is now further evidence because IRM acquisition characterises hematite without exception. Possibly, very fine grained hematite that

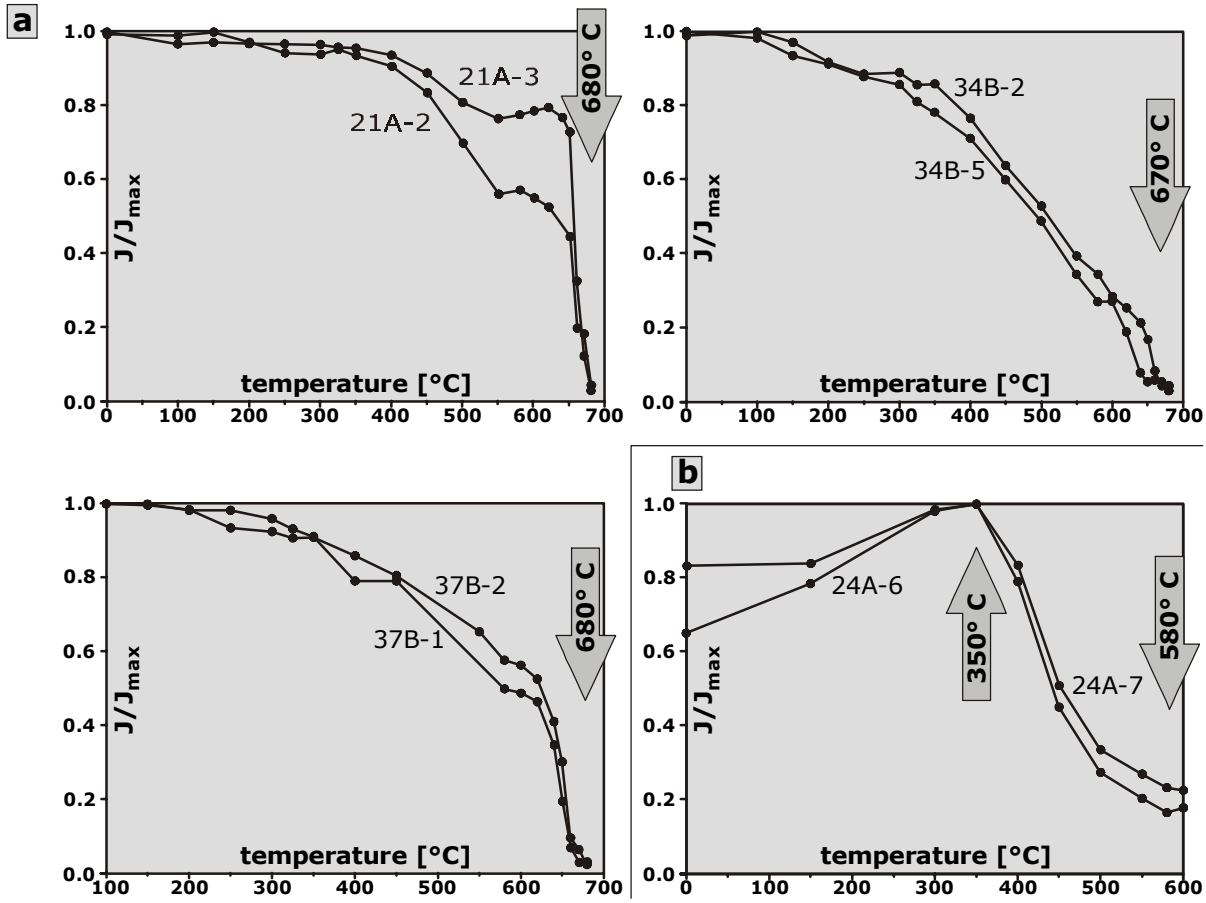

Fig. 4.2-2: *Representative demagnetisation behaviour of sites from the Shuang Hu area. a - TH demagnetisation of sites 21A, 34B, and 37B; unblocking of hematite component at ~680° C; b - TH demagnetisation of site24A, demagnetisation of two anti-parallel (s. Fig. 4.2-3b) components at 350° C and 580° C.*

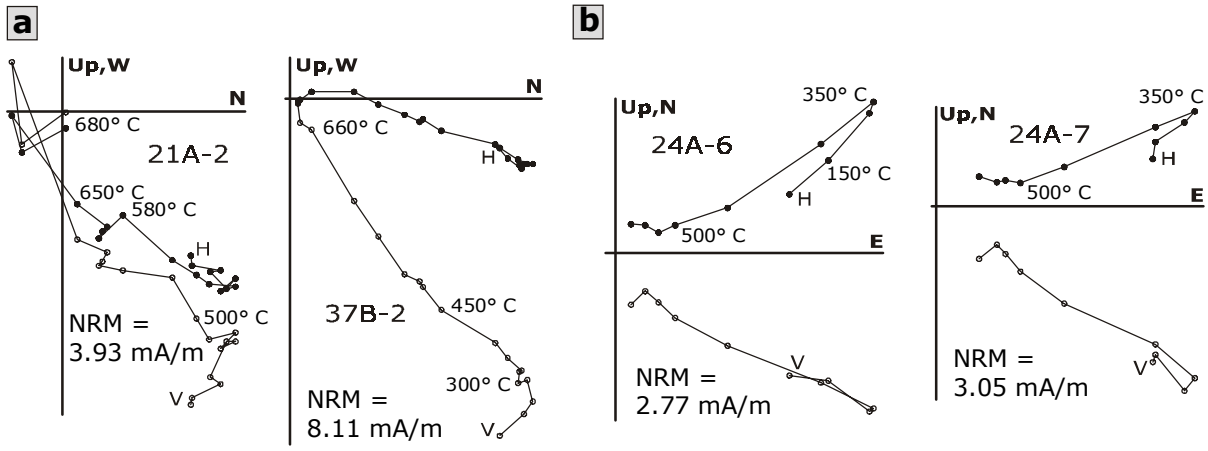

Fig. 4.2-3: *Orthogonal vector plots (Zijderveld plots) of demagnetisation behaviour of sites from the Shuang Hu area. H, V - horizontal, vertical projection. a - TH demagnetisation of sites 21A and 37B; unblocking of hematite component at ~680° C; b - TH demagnetisation of site24A, demagnetisation of two anti-parallel components at 350° C and 580° C. All data in situ.*

unblocks far below the Curie-temperature of hematite (~680° C) as shown for lake sediments (Phartiyal et al., 2003), is responsible for this behaviour. Most of the orthogonal vector plots (Zijderveld plots) show demagnetisation paths where the "straight" lines are "defined" by slightly noisy demagnetisation behaviour (Fig. 4.2-3). Since the NRM values are not significantly lower than in other areas this might have to do with the reasons for dispersed results mentioned above.

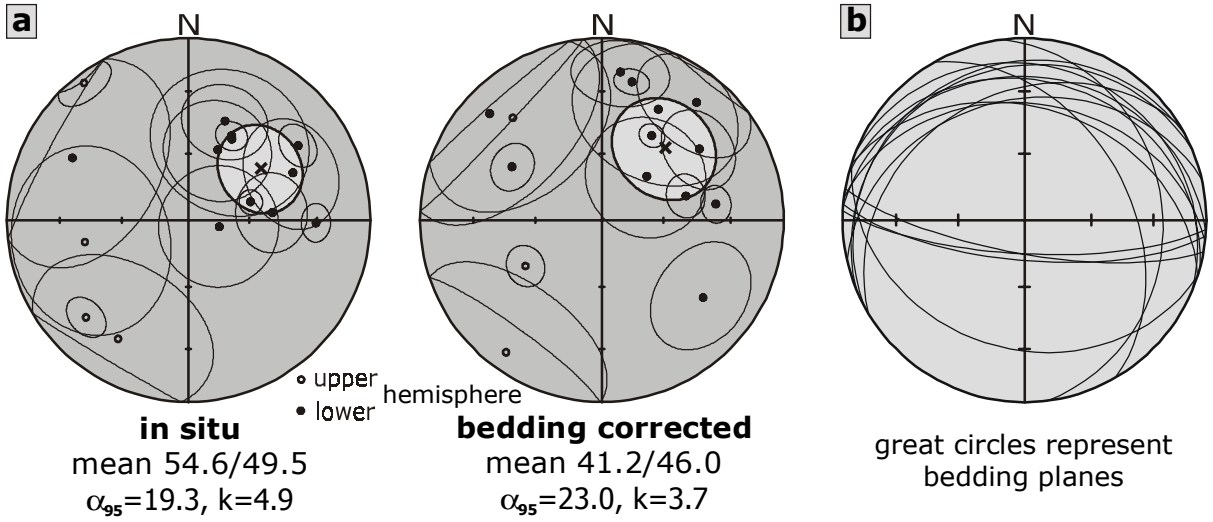

Fig. 4.2-4: *a - fold test on results from the Shuang Hu area. No significance. b - bedding of sites.*

The grouping of single specimen remanence directions within sites reaches k-values between 3 and 52 (Fig. 4.2-4a). Under the condition that results with k-values lower than 10 should not be accepted for further interpretation the investigation of most of the found directions would have ended here. But for a pilot study in a remote area it seems to be reasonable to go a littler further and get out of the given data set what is ever possible to outline the future perspectives: The fold test is without significance (4.2-4b). This could be result of bedding data that are quite flat with similar dip direction. This in combination with dispersed site mean directions means that the fold test has to remain without result necessarily because differentiated alternatives are missing. Stepwise unfolding after McFadden results in best grouping at 37% of unfolding (Fig. 4.2-5). The declinations for 37% of unfolding show a ~40° clock-wise rotation of the Shiagar mountains, at least a rotation into the NE-segment (Fig. 4.2-6).

Possible geological events

The statement "best grouping is achieved at 37% of unfolding" means that the "main" remanence acquisition took place when 63% of the final folding was reached. Because grouping is not good and mineralogical processes remain unclear it is difficult to say whether remanence acquisition happened at one – more or less – discrete moment in time or if remanence acquisition was somehow "spread" continuously over a time interval. Since the regarding rocks have never reached temperatures near to 650 °C (more likely never reached any temperature above 300 °C) a chemical remagnetisation is the process that has to be assumed. Is it possible that one ~abrupt incidence caused ~instantaneous consequences (micro fibres, fractures, presence of fluids) at a certain stage of the tectonic development? At least one cannot exclude this.

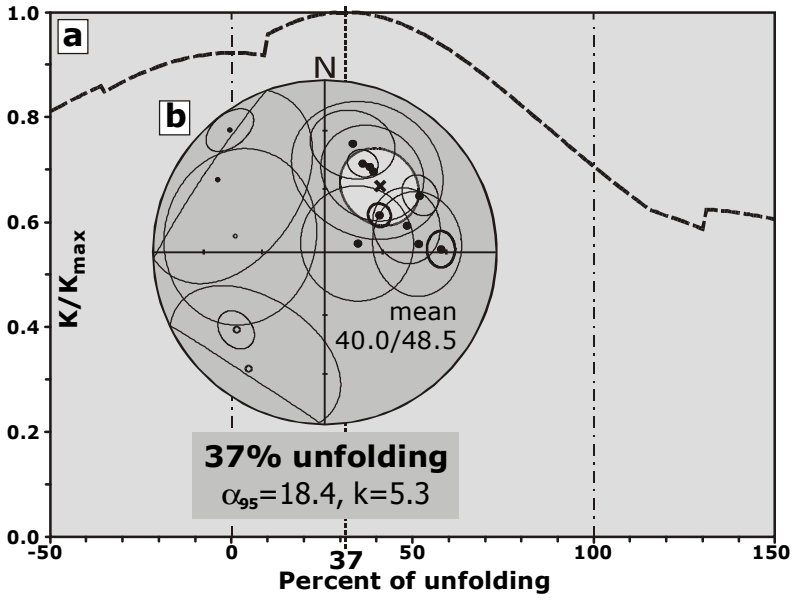

Fig. 4.2-5: *Stepwise unfolding (after McFadden) applied on 15 sites from the Shuang Hu area. a - best grouping of directions at 31% of unfolding, b - lower hemisphere stereoplot for 37% of unfolding.*

The following sequence of events is consistent with the findings above: (a) sedimentation – (b) first phase of folding (63%) with spread of primary remanences – (c) remagnetisation in the early stage of the next phase of deformation – (d) folding (37%) with spread of remagnetised directions – (e) today: exhumed blue-schist dome flanked by folded red beds with relatively dispersed palaeomagnetic remanence directions. But what caused the folding, and when did it happen? Even though these questions could hardly be solved there are at least three suspicious phases: 1. Up-doming of the metamorphic core at (or since!) 200 Ma. This would be too early to affect sediments of maximum Cretaceous age. 2. Deformation due to the Lhasa-Qiangtang collision at the Bangong-Nujiang suture (150 Ma). Deformation could have propagated through parts of the Qiangtang block and meets the undeformed (not, if up-doming goes on) Cretaceous red bed series. 3. Deformation due to the India-Eurasia collision at the Yarlong Zangpo suture (~55 Ma). Deformation could have propagated through Lhasa and Qiangtang block and meets the deformed (or undeformed) Cretaceous red bed series of the Shiagar mountains.

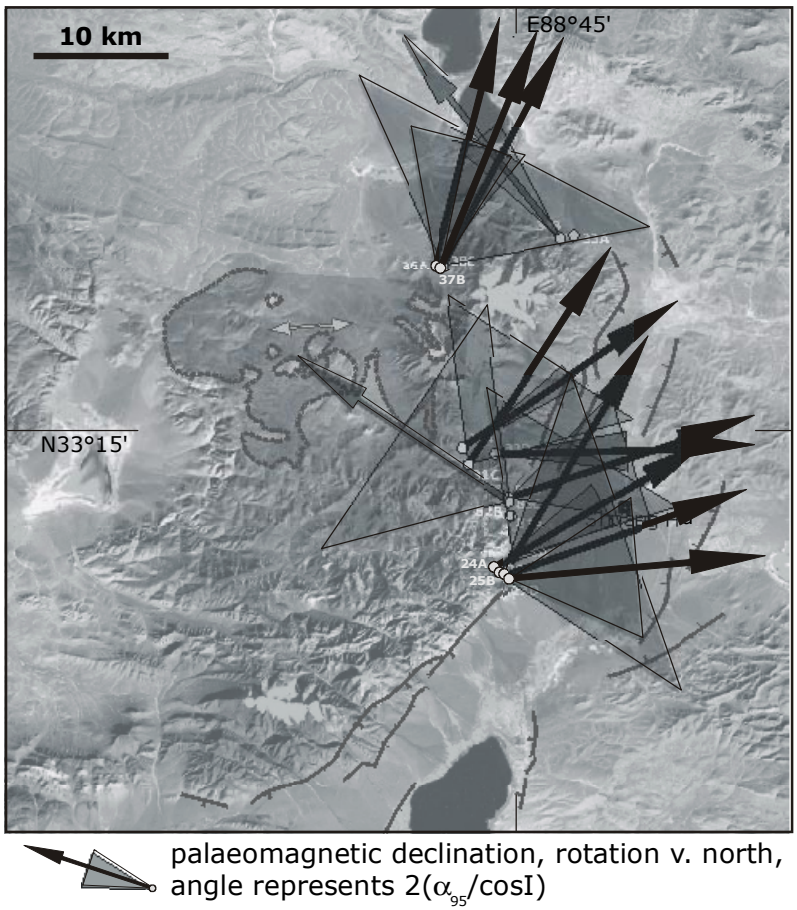

Fig. 4.2-6: *Declinations from sites of the Shuang Hu area (Shiagar mountains) corrected with 31% of unfolding for best grouping (see Fig. 4.2-5). For further explanations see Fig. 4.2-1.*

What caused the difficulties?

In the Shuang Hu data set the grouping of data is too poor after classical standards. Maybe the rectification of standards has to be accepted for studies with pilot character in remote areas. Different processes might have contributed to the ambiguous results:

The primary remanences were not grouping as well as in other investigated areas, therefore the remagnetisation did not "clean" the direction as well as in other areas.

Remagnetisation did not affect the area or single sites and core sample homogeneous.

Missing precise directions (small-scale) could be due to rock composition and/or certain weathering processes (other than in other areas).

Deformation of the metamorphic dome is active and moving during and since sedimentation; this prevents any stable direction on a large-scale.

The active faults (domal low-angle normal faults and graben-bounding steep normal faults) do induce a style of deformation/tilting which is not restored by a standard unfolding procedure.

Open questions

If real, what does the clockwise rotation tell about the regional tectonics?

Does it contribute to the image that the Shuang Hu graben is trending ~40 °; i.e. in a direction as if it would have been rotated from an initial N-S direction in the same style?

Is that reasonable, means: Was there enough time left to rotate since the graben opened?

Does the orientation of the mylonitic lineation become senseless if rotation is assumed?

Do the domal faults undergo rotation, too?

Improvement, further work and sampling

It is a dilemma of the investigations in the Shiagar mountains that the geological process that obviously left some marks in the samples can hardly be caught with adequate reliability on base of the available data set. The large scattering of single specimen directions within sites forms the most rigid obstacle for more advanced studies. It should be clarified by rock-magnetic experiments whether the magnetic minerals are capable carrying stable remanences and how remagnetisation could have affected the rocks. Future work should then focus on sampling central parts and W/SW-exposed flanks of the Shuang Hu dome. This could help to discriminate between effects induced by the up-doming - symmetrical features are assumed - and effects induced by N-S-directed shortening - with preferred directions clearly detectable.

4.2.2 Fold-and-thrust structures to the SE of Shuang Hu, Narmagh fold belt

The Narmagh fold belt is situated at ~E89°00', N32°45'to the southeast of the village of Shuang Hu (Fig. 1.2-1). The hilly range with peaks at around 5000 m lies on the right-hand side of the dirt road on the way north to Shuang Hu. This is the reason why the Narmagh fold belt attracted a great deal of attention: The characteristic folding caught our eyes already when sitting in the cars. The folding is showing up quite impressive the "road" is passing by perpendicular to the fold axes trending EW (s. structural map, Fig. 4.2-7).

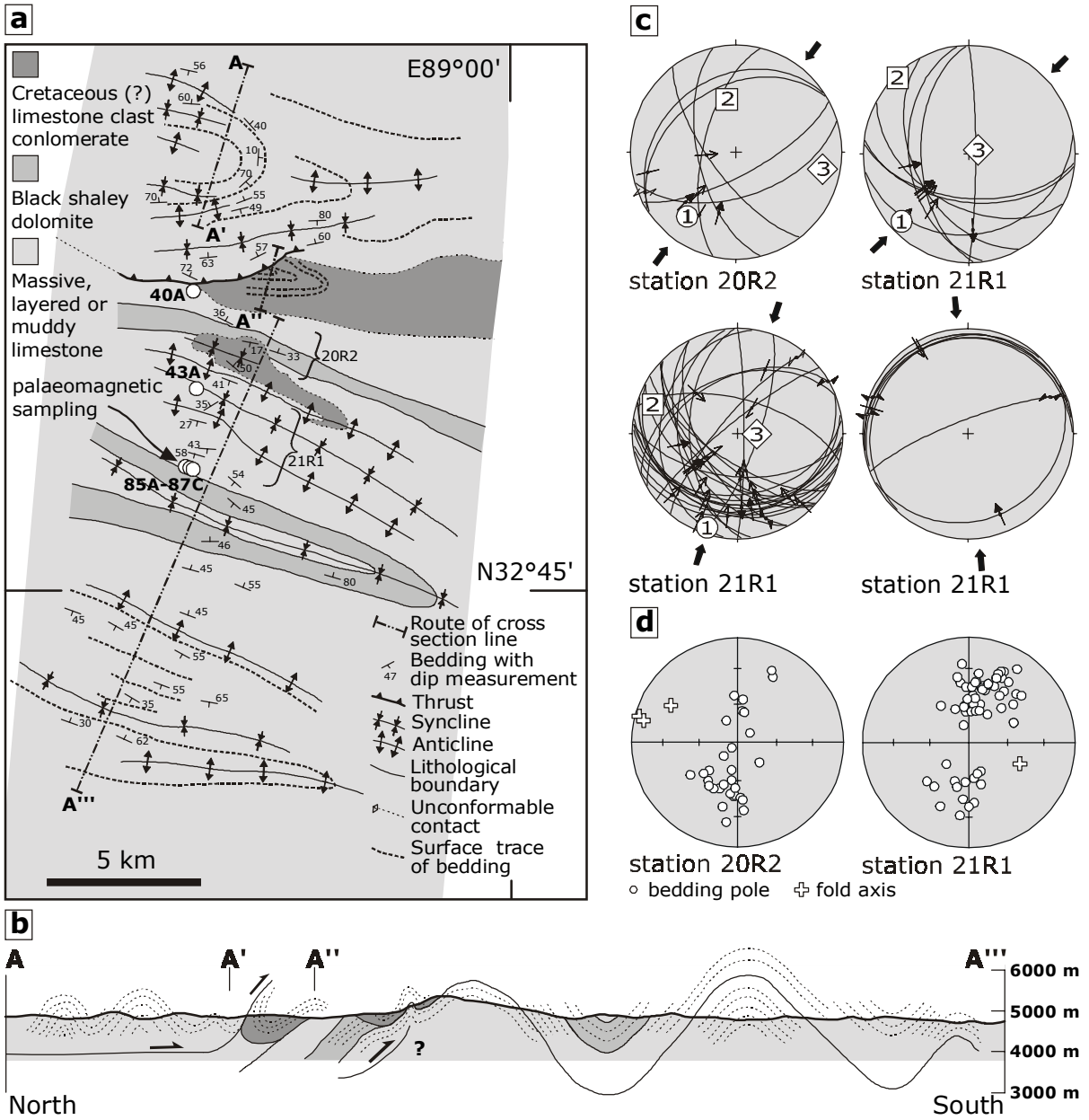

Fig. 4.2-7: *Structure of the Narmagh section. a - structural sketch map, b - geological profile, c - fault plane striae data (symbols as in Fig. 2.2-3); d - bedding data.*

Again, we stood in front of a pilot area with very little pre-information. Available maps do not show enough details to find precise information on an area of 10 by 20 kilometres. Our working hypothesis for the limestone clast conglomerate is "Cretaceous" (Fig.4.2-7a). The muddy limestones and shaley dolomites could be Jurassic than. The characteristic limestone clast conglomerate is situated in tectonic "pockets", may be following a primary sedimentary structure.

Tectonically, we see a ruling open folding, with axes trending ~120°, and a ~north-dipping thrust - movement top to the south – in the northernmost part of the profile (Fig. 4.2-7b, d). The principal stress directions calculated from the fault plane striae data trend approximately NNE-SSW and are in good agreement with the large-scale features therefore.

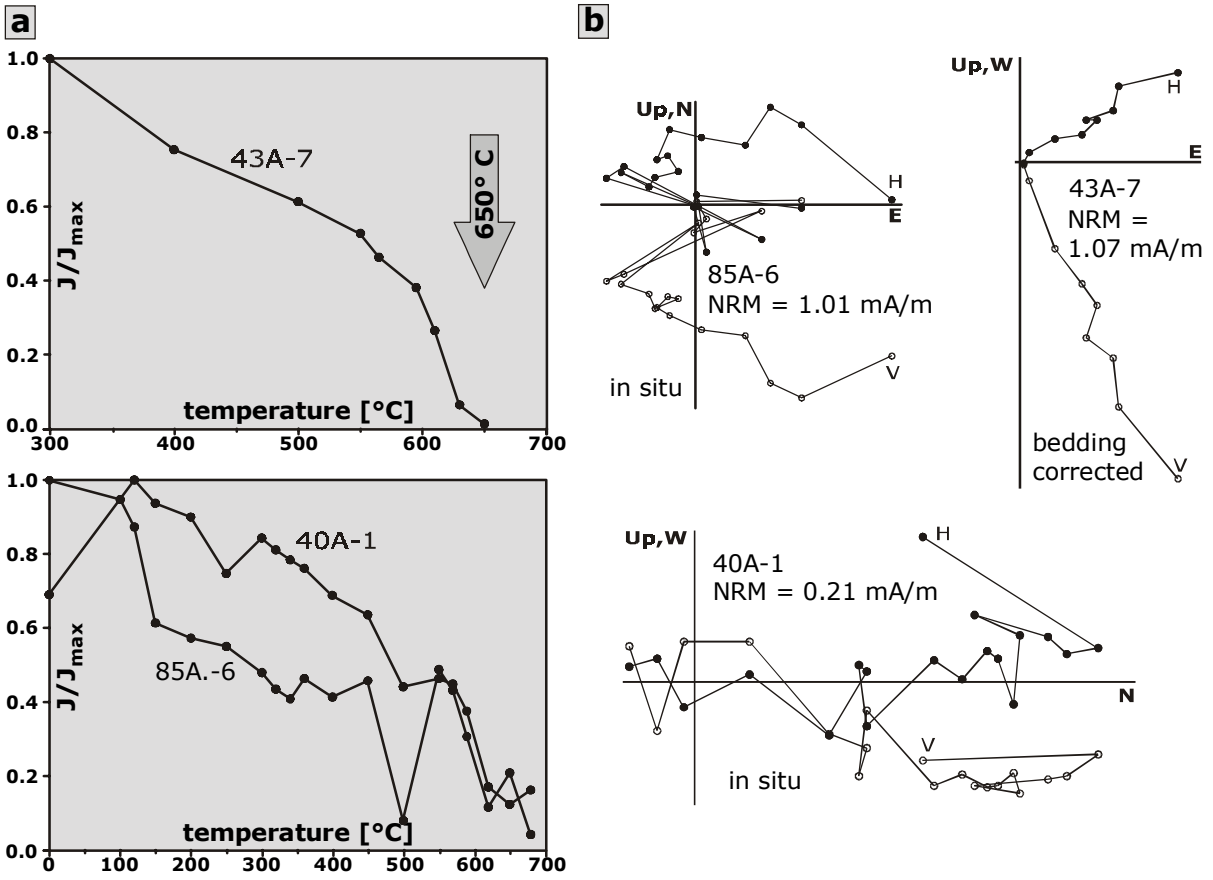

Fig. 4.2-8: *Representative examples of demagnetisation of sites from the Narmagh section. a - TH demagnetisation, b - orthogonal vector plot (Zijderveld plot) of TH demagnetisation.*

At 5 sites in the muddy limestones of supposed Cretaceous age 50 orientated core samples have been sampled for palaeomagnetic investigations. The results are not promising at all (Fig. 4.2-8). When detectable the remanences are carried by one hematite component which is demagnetised at around 680° C. The orthogonal vector plots (Zijderveld plots) of these samples with "observable" demagnetisation path do not have acceptable quality for a reliable analysis. Since the single specimen remanence directions are more than suspicious statistical methods have not been applied. It seems to be unlikely that further sampling would increase the quality of data in the Narmagh area; palaeomagnetic parameters and demagnetisation behaviour are disastrous.

4.2.3 One example from young volcanics of the Qangringngoinza range

To end up with a more encouraging detail of work in central Tibet and in the laboratory at Tübingen, one example from the Qangringngoinza range is presented last (s. Fig. 1.2-1 for locality). The site (10 orientated cores) was sampled from a trachyte that builds an impressive morphological plug near the centre of a volcanic ring structure with ~6 km in diameter. It was – future researchers be warned – the hardest drill job we had to do on the Tibetan plateau: The sampling locality lies in an area where Tuner et al. (1996) report two generations of rock ages, one at around 1 Ma, and the other from 8 to 13 Ma. Due to limitations with locating the exact spot of sampling (GPS N33°57,35'/E88°49,00') on the map by Turner et al. (1996), the age of site 17B cannot be clarified.

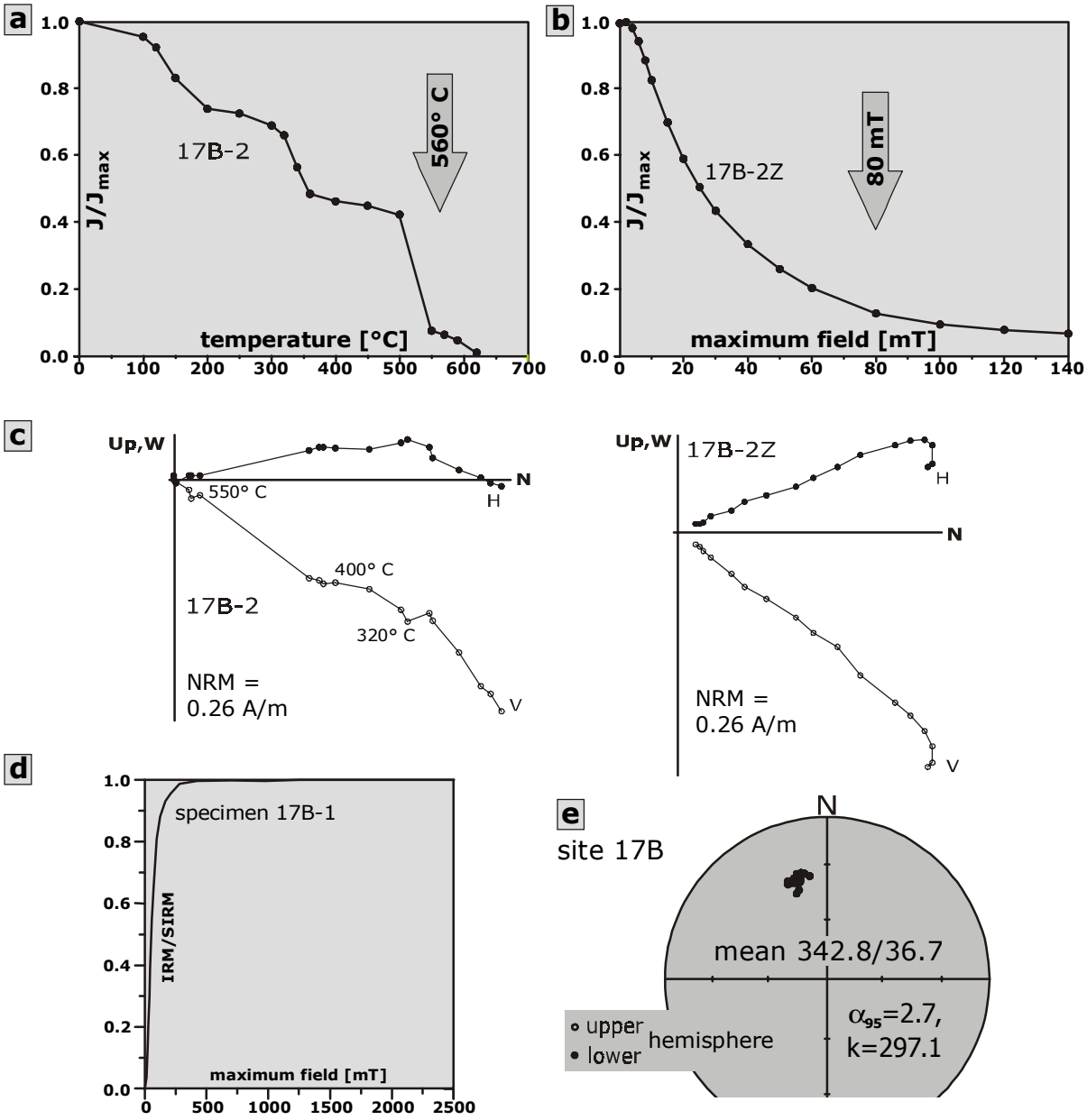

Fig. 4.2-9: *Magnetic results of Site 17B - trachyte from Qangringngoinza volcanic area. a - TH demagnetisation, unblocking of magnetite at 560° C; b - AF demagnetisation, demagnetisation of magnetite between 5 and 80 mT, 17B-2 and 17B-2Z are twin samples; c - orthogonal vectorplots (Zijderveldplots) of demagnetisation behaviour of site17B. H, V - horizontal, vertical component, in situ data; d - IRM acquisition; e - equal area stereoplot of in situ remance directions.*

The characteristic remanence is carried by magnetite as shown by TH and AF demagnetisation, and IRM acquisition respectively (Fig. 4.2-9a, b, d). Both the "undisturbed" AF measurements and the TH demagnetisation exhibit a straight demagnetisation path in the orthogonal vector plots (Zijderveld plots, Fig. 4.2-9c). Irrespective of the mode of demagnetisation the single specimen remanence directions are stable and group perfectly with k=297 (Fig. 4.2-9e).

Of course, a conclusion on local or regional rotations cannot be deduced from one measurement. But it would be an interesting future project to sample more intensively and increase the data set in the Qangringngoinza range. Depending on weather und surface conditions the area can be reached within one and a half day from Shuang Hu. Outcrops are frequent and relatively easy accessible but lie mostly above 5200 m.

5 Summary

During INDEPTH 3/GeoDepth field geology campaigns 1998 and 1999 palaeomagnetic sampling and structural measurements were carried out between approximately 30°30' to 35°30' N latitude and 88°30' to 90°30' E longitude. Because many of the reached areas had not been visited for scientific purposes before some investigations could be only taken as pioneering attempts on the base of little precognition. The work was frequently compromised by difficult surface and weather conditions but despite some drawbacks a total of 742 orientated core samples was obtained at 73 palaeomagnetic drilling sites.

In some parts of the working area a too small number of sites, deficiencies in grouping of remanences, or inadequate rock-magnetic properties prevented more advanced interpretations of results. This concerns the following sub-areas:

In the Baoji section (~N31°00', E90°10') hematite carries the ChRM in red beds of probably Cretaceous age. The directions of internally well-grouped site means are dispersed and abscond from a simple explanation. A syn-orogenic character and therefore different remagnetisation age of the separated remanences is assumed.

On the flanks of the Shiagar mountains (Shuang Hu dome, ~N33°15', E88°45') red beds of maximum Cretaceous age were sampled. Remanences are dominated by hematite but single specimen directions are scattered and precision parameter k is below 10 for most sites. Therefore the geological development cannot be identified with adequate reliability on base of the data set.

In the fold-and-thrust Narmagh section (~N32°45', E89°00') palaeomagnetic parameters and demagnetisation behaviour measured in samples from muddy limestones of supposed Cretaceous age do not have acceptable quality for a reliable analysis.

The investigation of one single trachyte example (< 13 Ma; N33°57,35', E88°49,00') from the Qangringngoinza range revealed a stable ChRM carried by magnetite and a grouping with k=297.

A detailed and complete palaeomagnetic evaluation was possible for the Zagaya section in the northernmost Lhasa block within the Upper Jurassic to Lower Cretaceous Bangong-Nujiang suture zone (~N32°15', E89°30').

Reddish sandstones interbedded with coarse conglomerates, both of Eocene age, are dominating the sequence which also comprises an ophiolite and Eocene tectonic imbricate. Structurally, sharp and steeply west-dipping normal faults building the western boundary of two characteristic blocks and a left-lateral EW-trending strike-slip fault limiting these two blocks to the north are most striking in the TM image. A polyharmonic, EW-trending governing folding with the fold axis plunging moderately around 40° to the west clearly predates faulting because the folded sequence is part of the blocks which are cut by far reaching normal and strike-slip faults. About 60% shortening is represented by the large governing fold. Fault-slip data shows (sub-) horizontally ENE-WSW- and NNE-SSW-trending compression and EW-trending extension.

Palaeomagnetic investigations were carried out on samples from 15 sites of mostly Eocene strata. Hematite was identified as main remanence carrier and single specimen directions with well-grouping site means and k-values between 9 and 62 are achieved. The fold test applied on 8 sites from the NS-trending central section of the Zagaya area is significantly positive, showing that remanence acquisition happened prior to folding. The calculation of stepwise unfolding revealed best grouping of directions at 93 % of unfolding. In order to investigate the spatial distribution of rotations, declinations were projected into a straight N-S-line. The detected trend is linear and shows increasing counterclockwise rotation of declinations to the north and thereby with proximity to the shear zone. A maximum relative rotation of 55° and a rotation of 8.1 °/km when proceeding north is determined. The linear trend of declinations demonstrates that folding predates block rotation because folding that happened after block rotation would have spread the declinations.

Among different theoretical tectonic models none resembles the characteristic distribution of declinations and the correct structural pattern of the Zagaya section at the same time. The post-folding deformation in the Zagaya section is interpreted as two-phase: Internal small-scaled left-lateral brittle shear is followed by normal faulting with the break-up of blocks as youngest stage. This means that pre-existing structures within the Bangong-Nujiang suture zone respond with left-lateral reactivation and eastward lateral extrusion to frontal compression.

The extensive study of the Dogai Coring Tso fold-and-thrust belt in the northern Qiangtang block (~N34°45', E89°00') showcases consistency between structural and palaeomagnetic investigations.

The clastic sedimentary sequence is subdivided in a basal green unit and conformably overlaying red beds which consists of reddish medium to coarse grained sandstones and conglomerates. The clastic series of the DGC, both red beds and green unit probably correspond to the Fenghuoshan Niubao Group and are likely of Tertiary age. All structural analyses lead to a model that explains the DGC as a sinistral transpressional fold-and-thrust belt in which fault-bound blocks rotated counterclockwise in domino-style in response to NE-SW compression. The dextral strike-slip faults bounding the blocks were formed syn- to post-folding and pre- to syn-kinematic with respect to thrusting because they always offset the folds and never cut across thrusts, respectively. Estimations of N-S shortening enforced by folding are assumed to range from 25 to 58 %. Counterclockwise rotation of 35° detected from the trend of dextral faulting can account for about 20 % of N-S shortening.

Palaeomagnetic investigations identified a stable ChRM carried by hematite in 11 sites from the red beds. Single specimen remanence directions group very well within sites and reach k-values between 11 and 443. The fold test is significantly positive and indicates a pre-folding acquisition of the ChRM. Calculation of stepwise unfolding for a structurally homogeneous area between large thrusts reveals best grouping of directions at 82 % of unfolding. It is assumed that remagnetisation occurred during an early stage of the tectonic development. That could mean that analysed ChRM directions represent exactly the characteristic steps of the deformation history of the DGC. There is a discrepancy of 7° between the overall mean declination and the clockwise rotation determined from the dextral wrench faults in the structural pattern. It might be possible that the target area rotated clockwise about 7° before the break-up of blocks. But since remagnetisation is younger than 40 Ma the clockwise rotation of Eurasia is smaller than 10° and thus too small to affect the result of block rotation significantly.

The palaeomagnetic results are consistent with the tectonic interpretation of domino-style blocks and prove a minimum of ~28° counterclockwise rotation resulting from NE-SW compression.

Local and regional processes reflect large-scale tectonic activity. Nevertheless, it often defies a simple explanation how features clearly detected on a local scale could be assigned to large-scale interpretations. Especially when results stem from geographically isolated areas with little geological background information it is difficult to contribute to a global scheme.

Nevertheless, findings from the Zagaya section and from the Dogai Coring Tso fold-and-thrust belt support two major ideas on Tibetan tectonics: (1) Structures within the Bangong-Nujiang suture are reactivated in left-lateral style and allow therefore eastward extrusion due to frontal compression and (2) deformation in northern Central Tibet gives evidence for NE-SW compression and northeastward growth of the plateau already in the Tertiary.

A reliable data base for future palaeomagnetic research on block rotations and crustal shortening in Central Tibet need to be supplied by continued geological mapping with stratigraphic work and structural measurements. Beginning with areas of easier accessibility sampling should then be advanced from profiles to a more equidistant grid to test whether results of local significance also hold over larger areas. All this needs outstanding logistic efficiency and scientific commitment otherwise progresses will be impeded.

Compared to traditional fields and regions of geological investigations the Tibetan plateau with both special demands and chances stands in a juvenile phase of exploration and is worth some effort – the starting-points are just defined.

6 References

Allègre, C.J., Courtillot, V., Tapponnier, P., Hirn, A., Mattauer, M., Coulon, C., Jaeger, J.J., Achache, J., Schärer, U., Marcoux, J., Burg, J.P., Girardeau, J., Armijo, J., Gariepy, C., Göpel, C., Li Tindong, Xiao Xuchang, Chang Chenfa, Li Guanggin, Lin Baoyu, Teng Ji Wen, Wang Naiwen, Chen Guoming, Han Tonglin, Wang Xibin, Den Wanming, Sheng Huaibin, Cao Yougong, Zhou Ji, Qiu Hongrong, Bao Peisheng, Wang Songchan, Wang Bixiang, Zhou Yaoxiu & Ronghua Xu (1984): Structure and evolution of the Himalaya Tibet orogenic belt, Nature, 307, 17-22.

Armijo, R., Tapponnier, P., Mercier, J. and Han Tonglin (1986): Quaternary extension in southern Tibet: field observations and tectonic implications. J. Geophys. Res., 91, 13,803-13,872.

Armijo, R., Tapponnier, P. and Han Tonglin (1989): Late Cenozoic right-lateral strike-slip faulting in southern Tibet. J. Geophys. Res., 94, 2,787-2,838.

Besse, J. and Courtillot, V. (1988): Paleogeographic maps of the continents bordering the Indian Ocean since the Early Jurassic. J. Geophys. Res., 93, 11,791- 11,808.

Besse, J. and Courtillot, V. (1991): Revised and Synthetic Apparent Polar Wander Paths of the African, Eurasian, North American and Indian Plates and True Polar Wander Since 200 Ma. J. Geophys. Res., 96, 4029-4050.

Blisniuk, P.M., Hacker, B.R., Glodny, J., Ratschbacher, L., Bi, S., Wu, Z., McWilliams, M.O. and Calvert, A. (2001): Normal faulting in central Tibet since at least 13.5 Myr ago. Nature, 412, 628-632.

Blumenwitz, M.-L. (2001): Rock- and Palaeomagnetic investigation of a pilot section across the Bangong-Nujiang Suture zone (Central Tibet). Diplomarbeit, Eberhard-Karls-Universität Tübingen, 59pp.

Chang, C., Chen, N., Coward, M.P., Deng, W., Dewey, J.F., Gansser, A., Harris, N.B.W., Jin, C., Kidd, W.S.F., Leeder, M.R., Li, H., Lin, J., Liu, C., Mei, H., Molnar, P., Pan, Yun, Pan, Yusheng, Pearce, J.A., Shackleton, R.M., Smith, A.B., Sun, Y., Ward, M., Watts, D.R., Xu, J., Xu, R., Yin, J., and Zhang, Y. (1986): Preliminary conclusions of the Royal Society and Academia Sinica 1985 geotraverse of Tibet. Nature, 323, 501-507.

Chemenda, A., Burg, J.-P. and Mattauer, M. (2000): Evolutionary model of the Himalaya-Tibet system: geopoem based on new modelling, geological and geophysical data. Earth Planet. Sci. Lett., 174, 397-409.

Chen, Y., Courtillot, V., Cogné, J.-P., Besse, J., Yang, Z. and Enkin, R. (1993a): The Configuration of Asia Prior to the Collision of India: Cretaceous Paleomagnetic Constraints. J. Geophys. Res., 98, 21,927-21,941.

Chen, Y., Cogné, J.-P., Courtillot, V., Tapponnier, P. and Zhu, X.Y. (1993b): Cretaceous Paleomagnetic Results From Western Tibet and Tectonic Implications. J. Geophys. Res., 98, 17,981-17,999.

Cogné, J., Halim, N. and Chen, Y. (1999): Resolving the problem of shallow magnetizations of Tertiary age in Asia: insights from paleomagnetic data from the Qiangtang, Kunlun, and Qaidam blocks (Tibet, China), and a new hypothesis. J. Geophys. Res., 104, 17,715-17,734.

Coward, M.P., Kidd, W.s.F., Yun, P., Shackleton, R.M. and Hu, Z. (1988): The structure of the 1985 Tibet Geotraverse, Lhasa to Golmud. Phil. Trans. R. Soc. Lond., A 327, 307-336.

Daßinnies, M. (2001): Tectonic interpretation of the Dogai-Coring thrust-fold belt, Central Tibet, based on a remote sensing study. Unpl. Diploma thesis, Technische Universität, Bergakademie Freiberg, 49 pp.

DeMets, C., Gordon, R.G., Argus, D.F. and Stein, S. (1990): Current plate motions. Geophys. J. Int., 101, 425-478.

Dewey, J.F., Shackleton, R.M., Chengfa, C. and Yiyin, S. (1988): The tectonic evolution of the Tibetan Plateau. Phil. Trans. R. Soc. Lond., A 327, 379-413.

Enkin, R., Yang, Z., Chen, Y. and Courtillot, V. (1992): Paleomagnetic constraints on the geodynamic history of the major blocks of China from the Permian to the present. J. Geophys. Res., 97, 13,953-13,989.

Gapais, D., Cobbold, P.R., Bourgeois, O., Rouby, D. and de Urreiztieta, M. (2000): Tectonic significance of fault-slip data. J. Struc. Geol., 22, 881-888.

Gilder, S., Coe, R. and Wu, H. (1993): Cretaceous and Tertiary paleomagnetic results from Southeast China and their Tectonic implications. Earth Planet. Sci. Lett., 117, 637-652.

Gilder, S.A., Zhao, X., Coe, R.S., Meng, Z., Courtillot, V. and Besse, J. (1996): Paleomagnetism and tectonics of the southern Tarim basin, northwestern China. J. Geophys. Res., 101, 22,015-22,031.

Girardeau, J., Marcoux, J., Fourcade, E., Bassoullet, J.P., and Tang, Y. (1985): Xainxa ultramafic rocks, central Tibet, China; tectonic environment and geodynamic significance. Geology, 13, 330-333.

Halim, N., Cogné, J. and Chen, Y. (1998): New Cretaceous and Early Tertiary paleomagnetic results from Xining-Lanzhou basin, Kunlun and Qiangtang blocks, China: Implications on the geodynamic evolution of Asia. J. Geophys. Res., 103, 21,035-21,045.

Harris, N.B.W., Xu, R., Lewis, C.L. and Jin, C. (1988): Plutonic rocks of the 1985 Tibet Geotraverse, Lhasa to Golmud. Phil. Trans. R. Soc. Lond., A 327, 145-168.

Huang, K., Opdyke, N. and Peng, X. (1992): Paleomagnetic results from the Upper Permian of the eastern Qiangtang Terrane of Tibet and their tectonic implications. Earth Planet. Sci. Lett., 111, 1-10.

Jelínek, V. (1981): Characterization of the magnetic fabrics of rocks. Tectonophysics, 79, 63–67.

Kapp, P., Yin, A., Manning, C., Murphy, M., Harrison, T.M., Spurlin, M., Ding, L., Deng, X.-G. and Wu, C.-M. (2000): Blueschist-bearing metamorphic core complexes in the Qiangtang block reveal deep crustal structure of northern Tibet. Geology, 28, 19-22.

Kidd, W., Yusheng, P. and Chengfa, C. (1988): Geological mapping of the 1985 Chinese-British Tibetan (Xizang-Qinghai) Plateau Geotraverse route. Phil. Trans. R. Soc. Lond., A 327, 287-305.

Klootwijk, C.T., Gee, J.S., Peirce, J.W. and Smith, G.M., 1991. Constraints on the India-Asia Convergence: Paleomagnetic results from Ninetyeast ridge. In: J. Weissel, J. Peirce, E. Taylor, J. Alt et al. (Editors), Proc. ODP, Sci. Results.,121, 777-881.

Lin, J. and Watts, D. (1988): Paleomagnetic results from the Tibetan Plateau. Phil. Trans. R. Soc. Lond., A 327, 239-262.

Maier, F. and Bachtadse, V. (1995): PALMAG - Softwarepaket zur Darstellung und Anwendung paläomagnetischer Datensätze. Universität München.

Makovsky, Y., Klemperer, S.L., Huang, L. and Lu, D. (1996): Structural elements of the southern Tethyan Himalaya crust from wide-angle seismic data. Tectonics, 15, 997-1005.

Matte, P., Tapponnier, P., Arnaud, N., Bourjot, L., Avouac, J.P., Vidal, P., Qing, L., Pan, Y. and Wang, Y. (1996): Tectonics of Western Tibet, between the Tarim and the Indus. Earth Planet. Sci. Lett., 142, 311-330.

McElhinny, M. (1963): Statistical Significance of the Fold Test in Palaeomagnetism. Geophys. J. R. Astron. Soc., 8, 338-340.

McFadden, P.L. (1990): A new fold test for palaeomagnetic studies. Geophys. J. Intern., 103, 163-169.

McKenzie, D. & Jackson, J. (1983): The relationship between strain rates, crustal thickening, palaeomagnetism, finite strain and fault movements within a deforming zone. Earth Planet. Sci. Lett., 65, 182-202.

McKenzie, D. & Jackson, J. (1986): A block model of distributed deformation by faulting. J. Geol. Soc. Lond., 143, 349-353.

Metcalfe, I. (1988): Origin and assembly of southeast Asian continental terranes. Geol. Soc. Lon. Spec. Publ., 37, 101-118.

Meyer, B., Tapponnier, P. and Bourjot, L. (1998): Crustal thickening in Gansu-Quinghai, lithospheric mantle subduction, and oblique, strike-slip controlled growth of the Tibetan plateau. Geophys. J. Int., 135, 1-47.

Murphy, M.A., Yin, An, Harrison, T.M., Dürr S.B., Chen, Z., Ryerson, F.J., Kidd, W.S.F., Wang, X. and Zhou, X,. (1997): Did the Indo-Asian collision alone create the Tibetan plateau? Geology, 25, 719-722.

Nelson, K.D., Zhao, W., Brown, L.D., Kuo, J., Che, J., Liu, X., Klemperer, S.L., Makovsky, Y., Meissner, R., Mechie, J., Kind, R., Wenzel, F., Ni,J., Nabelek, J., Chen, L., Tan, H., Wei, W., Jones, A.G., Booker, J., Unsworth, M., Kidd, W.S.F., Hauck, M., Alsdorf, D., Ross, A., Cogan, M., Wu. C., Sandvol, E.A. and Edwards, M. (1996): Partially molten middle crust beneath southern Tibet; synthesis of Project INDEPTH results. Science, 274, 1,684-1,688.

Nelson, M.R. and Jones, C.H. (1987): Paleomagnetism and crustal rotations along a shear zone, Las Vegas Range, southern Nevada. Tectonics, 6, 13-33.

Patriat, P. and Achache, J. (1984): India-Eurasia collision chronology has implications for crustal shortenings and driving mechanism of plates. Nature, 311, 615-621.

Peltzer, G. and Tapponnier, P. (1988): Formation and evolution of strike-slip faults, rifts, and basins during the India-Asia collision: an experimental approach. J. Geophys. Res., 93, 15,085-15117.

Phartiyal, B., Appel, E., Blaha, U., Hoffmann, V. and Kotlia B.S. (2003): Palaeoclimatic significance of magnetic properties from Late Quaternary lacustrine sediments at Pithoragarh, Kumaun Lesser Himalaya, India. Quat. Intern., 108, 51-62.

Powell, C., Roots, S. and Veevers, J. (1988): Pre-breakup continental extension in East Gondwanaland and the early opening of the eastern Indian Ocean. Tectonophysics, 155, 261-283.

Pozzi, J.-P., Westphal, M., Zhou, Y.X., Xing, L.S. and Chen, X.Y. (1982): Position of the Lhasa block, South Tibet, during the Late Cretaceous. Nature, 297, 319-321.

Ratschbacher, L., Sperner, B., Meschede, M. and Frisch, W. (1994): Computer techniques and applications: A programm library for stress and strain analysis. Tüb. Geow. Arb., A, University of Tübingen, 21, 62pp.

Schärer, U., Xu, R. and Allègre, C. (1984): U-Pb geochronology of Gangdese (Transhimalaya) plutonism in the Lhasa-Xigaze region, Tibet. Earth Planet. Sci. Lett., 69, 311-320.

Scotese, C.R., and McKerrow, W.S. (1990): Revised world maps and introduction. Palaeozoic Palaeogeography and Biogeography, Geol. Soc. Lon. Mem., 12, 1-21.

Sengör, A.M.C. (1984): The Cimmeride orogenic system and the tectonics of Eurasia. Geol. Soc. Am. Spec. Paper, 195, 85pp.

Smith, A.B. and Xu, J. (1988): Palaeontology of the 1985 Tibet Geotraverse, Lhasa to Golmud. Phil. Trans. R. Soc. Lond., A 327, 53-105.

Tapponnier, P., Mercier, J., Armijo, R., Tonglin, H. and Ji, Z. (1981): Field evidence for active normal faulting in Tibet. Nature, 294, 410-414.

Tapponnier, P., Peltzer, G., Le Dain, A., Armijo, R. and Cobbold, P. (1982): Propagating extrusion tectonics in Asia: New insights from simple experiments with plasticine. Geology, 10, 611-616.

Tapponnier, P., Peltzer, G. and Armijo, R. (1986): On the mechanics of the collision between India and Asia. Geol. Soc. Spec. Publ., 19, 115-157.

Thomas, J.-C., Perroud, H., Cobbold, P., Bazhenov, M.L., Burtman, V.S., Chauvin, A., and Sadybakasov, E. (1993): A paleomagnetic study of Tertiary formations from the Kyrgyz Tien-Shan and its tectonic implications. J. Geophys. Res., 98, 9571-9589.

Thomas, J.-C., Perroud, H., Cobbold, P., Bazhenov, M.L., Burtman, V.S., Chauvin, A., and Sadybakasov, E. (1993): A paleomagnetic study of Tertiary formations from the Kyrgyz Tien-Shan and its tectonic implications. J. Geophys. Res., 98, 9571-9589.

Turner, S., Arnaud, N., Liu, J., Rogers, N., Hawkesworth, C., Harris, N., Kelley, S., van Calsteren, P., and Deng, W. (1996): Post-collision, Shoshonitic Volcanism on the Tibetan Plateau: Implications for Convective Thinning of the Lithosphere and the Source of Ocean Island Basalts. J. Petrology, 37, 45-71.

Van der Voo, R. (1993): Paleomagnetism of the Atlantic, Tethys and Iapetus Oceans. University Press, Cambridge, 411pp.

Waldhör, M, Appel, E. Frisch, W. and Patzelt.A. (2001): Palaeomagnetic investigation in the Pamirs and its tectonic implications. J. of Asian Earth Sciences, 19, 429-451.

Westphal, M., Pozzi, J.-P., Zhou, Y., Xing, L. and Chen, X.Y. (1983): Palaeomagnetic data about southern Tibet (Xizang); I. The Cretaceous formations of the Lhasa block. Geophys. J. R. astr. Soc., 73, 507-521.

Xu, Z., Jiang, M., Zhao, G., Cui, J., Li, H., Lu, Q. and Xue, G. (1999): Mantle diapir and inward intracontinental subduction; a discussion on the mechanism of uplift of the Qinghai-Tibet Plateau. Geol. Soc. Am. Spec. Paper, 328, 19-31.

Yin, A., Kapp, P. and Murphy, M. (1999): Significant late Neogene east-west extension in northern Tibet. Geology, 27, 787-790.

Zhao, W., Nelson, K.D., Che, J., Guo, J., Lu, D., Wu, C., Liu, X., Brown, L.D., Hauck, M.L., Kuo, J.T., Klemperer, S.L. and Makovsky, Y. (1993): Deep seismic reflection evidence for continental underthrusting beneath southern Tibet. Nature, 366, 557-559.

Zhao, W., Mechie, M., Brown, L.D., Guo, J., Haines, S., Hearn, T., Klemperer, S.L., Ma, Y.S., Meissner, R., Nelson, K.D., Ni, J.F., Pananont, P., Rapine, R., Ross, A. and Saul, J., (2001): Crustal structure of central Tibet as derived from project INDEPTH wide-angle seismic data. Geophys. J. Intern., 145, 486-498.

Zhao, X., Coe, R., Zhou, Y., Hu, S., Wu, H., Kuang, G., Dong, Z. and Wang, J. (1994): Tertiary paleomagnetism of North and South China and a reappraisal of late Mesozoic paleomagnetic data from Eurasia; implications for the Cenozoic tectonic history of Asia. Tectonophysics, 235, 181-203.

Acknowledgements

This doctoral thesis was completed at the Geophysics working group of the Eberhard-Karls-Universität Tübingen. The project was financed by the Deutsche Forschungsgemeinschaft.

I am thankful to Prof. Erwin Appel who persistently gave substantial comments and useful suggestions to my work. I am happy that he restricted the number of slap shots to the necessary minimum.

I am grateful to Prof. Lothar Ratschbacher (TU Bergakademie Freiberg) for all his support and that he granted independency during my employment in Würzburg. His encouragement under adverse conditions in the field is especially acknowledged.

Prof. Doug Nelson, the leading INDEPTH personality over all the years, died in August 2002. He had joined the field geology team in 1999 and made things possible which hadn't functioned without him. It was a privilege to work alongside Doug Nelson – he remains unforgettable.

Dr. Mike Edwards helped with many fruitful discussions to bring this work forward. Together with Olaf Kuchel we heard a legendary 1998 world cup final - at 3 am, at -10 °C, on short wave BBC world services.

The diploma students Matthias Daßinnies and Marli Blumenwitz provided important investigations.

Without support by the Tibetan drivers palaeomagnetic sampling at 5600 m altitude would have failed short of water.

During the time of finishing our theses, Martina Schwab, Siegfried Kraft and me had weekly meetings to keep motivation up. I am thankful for this mutual support.

Last not least, I thank all those people who never lost interest in the progress of this work, especially my parents and sisters, Dietmar and Sonja Hornung, Monika Simoneit, Klaus Greif, Rebecca Burbach, Véronique Lardeux and Sam Featherston.

Wir stolze Menschenkinder
Sind eitel arme Sünder,
Und wissen gar nicht viel;
Wir spinnen Luftgespinste,
Und suchen viele Künste,
Und kommen weiter von dem Ziel.

Matthias Claudius (1778)

Bildungsgang

Martin Staiger	geb. am 20.02.1967 in Stuttgart
7/1973 – 6/1977	Schönbuchschule, Stuttgart
7/1977 - 6/1986	Hegel-Gymnasium, Stuttgart
6/1986	Abitur
10/1988 - 9/1990	Studium Bauingenieurswesen, Universität Stuttgart
10/1990 - 7/1991	Studium Literaturwissenschaft, Universität Stuttgart
10/1991 - 6/1998	Studium Geologie, Eberhard-Karls-Universität Tübingen
6/1998	Diplom in Geologie
7-1998-2/2004	Promotion am Institut für Geowissenschaften der Eberhard-Karls-Universität Tübingen, Arbeitsbereich Geophysik (Prof. Dr. Erwin Appel)